Louisiana Tech University
Louisiana Tech Digital Commons

Doctoral Dissertations | Graduate School

Winter 2007

Modeling core generation and transport phenomena of microcapsules

Xiaoshuo Wu
Louisiana Tech University

Follow this and additional works at: https://digitalcommons.latech.edu/dissertations

 Part of the Mathematics Commons

Recommended Citation
Wu, Xiaoshuo, "" (2007). *Dissertation*. 551.
https://digitalcommons.latech.edu/dissertations/551

This Dissertation is brought to you for free and open access by the Graduate School at Louisiana Tech Digital Commons. It has been accepted for inclusion in Doctoral Dissertations by an authorized administrator of Louisiana Tech Digital Commons. For more information, please contact digitalcommons@latech.edu.

MODELING CORE GENERATION AND TRANSPORT PHENOMENA OF MICROCAPSULES

by

Xiaoshuo Wu, M. S.

A Dissertation Presented in Partial Fulfillment
of the Requirements for the Degree
Doctor of Philosophy

COLLEGE OF ENGINEERING AND SCIENCE
LOUISIANA TECH UNIVERSITY

March 2007

Reproduced with permission of the copyright owner. Further reproduction prohibited without permission.

UMI Number: 3264698

INFORMATION TO USERS

The quality of this reproduction is dependent upon the quality of the copy submitted. Broken or indistinct print, colored or poor quality illustrations and photographs, print bleed-through, substandard margins, and improper alignment can adversely affect reproduction.

In the unlikely event that the author did not send a complete manuscript and there are missing pages, these will be noted. Also, if unauthorized copyright material had to be removed, a note will indicate the deletion.

UMI®

UMI Microform 3264698

Copyright 2007 by ProQuest Information and Learning Company.

All rights reserved. This microform edition is protected against unauthorized copying under Title 17, United States Code.

ProQuest Information and Learning Company
300 North Zeeb Road
P.O. Box 1346
Ann Arbor, MI 48106-1346

Reproduced with permission of the copyright owner. Further reproduction prohibited without permission.

LOUISIANA TECH UNIVERSITY

THE GRADUATE SCHOOL

January 22, 2007
Date

We hereby recommend that the dissertation prepared under our supervision by Xiaoshuo Wu

entitled MODELING CORE GENERATION AND TRANSPORT PHENOMENA OF MICROCAPSULES

be accepted in partial fulfillment of the requirements for the Degree of Doctor of Philosophy

Raja Nassar
Supervisor of Dissertation Research

Richard J. Greechie
Head of Department

Computational Analysis & Modeling
Department

Recommendation concurred in:

Weizhong Dai

Advisory Committee

Richard J. Greechie

Approved:
Director of Graduate Studies

Approved:
Dean of the Graduate School

Stan Napper
Dean of the College

GS Form 13
(5/03)

Reproduced with permission of the copyright owner. Further reproduction prohibited without permission.

APPROVAL FOR SCHOLARLY DISSEMINATION

The author grants to the Prescott Memorial Library of Louisiana Tech University the right to reproduce, by appropriate methods, upon request, any or all portions of this Dissertation. It is understood that "proper request" consists of the agreement, on the part of the requesting party, that said reproduction is for his personal use and that subsequent reproduction will not occur without written approval of the author of this Dissertation. Further, any portions of the Dissertation used in books, papers, and other works must be appropriately referenced to this Dissertation.

Finally, the author of this Dissertation reserves the right to publish freely, in the literature, at any time, any or all portions of this Dissertation.

Author 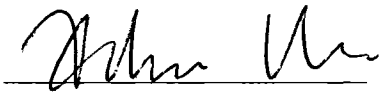

Date Feb 20, 07

GS Form 14
(5/03)

Reproduced with permission of the copyright owner. Further reproduction prohibited without permission.

ABSTRACT

Microcapsules play an important role in chemical, biomedical, and medical research. Of importance is their potential use as bio-sensors, as microreactors, and for drug delivery. In this dissertation, Computational Fluid Dynamics methodology is used to model the generation of droplets or cores (using alginate and oil) and to determine from the model process parameters needed for generating cores of homogeneous size for the manufacturing of microcapsules. Also, material diffusion through a microcapsule for controlled release is modeled based on finite difference methodology. The model was applied to experimental data on dextran release from microcapsules in order to estimate the diffusion coefficients in the core and wall of a microcapsule.

Results of the study showed that the velocities of alginate and oil and their ratio were considered as two important factors for determining droplet size. One can obtain the desired droplet size by adjusting these two factors. Also, it was observed that the properties of the two immiscible phases can influence the variance. A low viscosity of one of the phases (the non-oil phase) produced a small variance for droplet size. The flow channel was straight with a width of 100 micrometers. In future work, it would be of interest to determine if channel width and or geometry will have any effect on droplet size and variance.

Analysis of diffusivity estimates for the core and wall membrane from fitting the diffusion model to experimental data on the release of dextran from microcapsules over

Reproduced with permission of the copyright owner. Further reproduction prohibited without permission.

time revealed that only layer thickness had an effect on diffusivity in the core. The diffusivity for four layers was almost half of that for two layers of polyelectrolytes in the wall membrane. In the case of diffusivity in the microcapsule wall, both time and layer thickness had an effect. Diffusivity was larger for two layers of wall membrane thickness than for four or six layers and it was also larger for 12 hours than for 36 or 60 hours of loading time. There was no significant change in diffusivity beyond four layers or beyond 36 hours of loading time. In all cases, diffusivity in the wall membrane was considerably less than that in the core.

Reproduced with permission of the copyright owner. Further reproduction prohibited without permission.

TABLE OF CONTENTS

ABSTRACT ii

LIST OF TABLES..... vi

LIST OF FIGURES... vii

ACKNOWLEDGEMENTS..... xii

CHAPTER 1 INTRODUCTION

1.1 General Overview 1
1.2 Research Objectives 1
1.3 Organization 2

CHAPTER 2 LITERATURE REVIEW

2.1 Microcapsules 4
2.2 Droplet Generation 5
2.2.1 Microfluidic Devices 5
2.2.2 Methodologies 5
2.2.3 Alginate Microdroplets 7
2.3 Layer-by-layer Encapsulation 8
2.4 Transport Phenomena 10

CHAPTER 3 DROPLET GENERATION MODEL

3.1 Introduction 12
3.2 Experimental Procedure 13
3.2.1 Preparation of the Two Phases 14
3.2.2 Process 14
3.3 Mathematical Model 14
3.4 Simulation..... 20
3.4.1 Designing the Geometry of the Channel 20
3.4.2 Setting up the Model 23
3.4.3 Running the Model 25
3.4.4 Parrallel Computing on a Linux Cluster 25
3.4.5 Evaluating the Results 27

Reproduced with permission of the copyright owner. Further reproduction prohibited without permission.

CHAPTER 4 RESULTS AND DISCUSSION OF DROPLET GENERATION

4.1 Introduction....28
4.2 Simulation Design....28
4.3 Simulation Results....29
4.4 Results....34
4.5 Future Work....35

CHAPTER 5 MODELING OF TRANSPORT PHENOMENA

5.1 Introduction....37
5.2 Experimental Prodedure....38
5.2.1 Preparation of the Materials....38
5.2.2 Process....38
5.3 Governing Equations....39
5.4 Calculation of Transport Phenomena Based on Governing Equation....42
5.4.1 Fractional Crank-Nicholson Method....42
5.4.2 Stability Analysis....44
5.4.3 Thomas Algorithm....45
5.4.4 Inverse Problem....50
5.4.4.1 Introduction....50
5.4.4.2 Inverse Solution and Least Squares....50
5.4.4.3 Levenberg-Margquardt Method....52
5.4.4.4 The Solution Algorithm with LM....52
5.4.4.5 Check on the Diffusion Model....53

CHAPTER 6 RESULTS AND DISCUSSION OF TRANSPORT PHENOMENA

6.1 Introduction....55
6.2 Comparisons of Experimental Data and Model Results....55
6.3 Estimates of Microcapsules Core and Wall Diffusion Coefficients....80
6.4 Conclusion....87
6.5 Future Work....88

REFERENCES....89

Reproduced with permission of the copyright owner. Further reproduction prohibited without permission.

LIST OF TABLES

Table 4.1 Simulation runs for different factor combinations 29

Table 4.2 Simulation runs for different factor combinations in the vicinity of an optimum droplet size and variance 29

Table 4.3 Average and standard deviation for short and long particle droplet diameters for the different experimental runs 33

Table 6.1 Estimates of the diffusion coefficients in D1 (the core of the microcapsule) and in D2 (the wall membrane) 80

Table 6.2 Analysis of variance for D1 (the microcapsule core diffusivity) 81

Table 6.3 Pair-wise comparisons among the layer means for D1 82

Table 6.4 Analysis of variance for D2 (wall membrane diffusivity) 83

Table 6.5 Pair-wise comparisons among the layer means for D2 83

Table 6.6 Pair-wise comparisons among the loading time means for D2 84

Table 6.7 Analysis of variance for D1 of data set two 85

Table 6.8 Analysis of variance for D2 of data set two 86

Table 6.9 Pair-wise comparisons among the D2 means of data set two for loading time 86

Table 6.10 Mean diffusivity in the membrane wall for 4000 and 77000 dextran molecular weights 87

Reproduced with permission of the copyright owner. Further reproduction prohibited without permission.

LIST OF FIGURES

Figure 3.1 Enlarged T-shaped channel 12

Figure 3.2 Experimental setup 13

Figure 3.3 Two-dimensional area of the channel 21

Figure 3.4 2-D area mesh 22

Figure 3.5 Enlarged 2-D mesh 22

Figure 3.6 Boundary types of the channel sides 23

Figure 3.7 Scale grid 24

Figure 3.8 Running FLUENT on a cluster 26

Figure 3.9 Parallel computing performances of different number of processors 27

Figure 4.1 Alginate volume fraction contours 30

Figure 4.2 Exp100-1 alginate volume fraction contours 30

Figure 4.3 Exp100-2 and Exp100-3 alginate volume fraction contours 30

Figure 4.4 Exp100-4 and Exp100-5 alginate volume fraction contours 31

Figure 4.5 Exp100-11 and Exp100-12 alginate volume fraction contours 32

Figure 4.6 Exp100-13 and Exp100-14 alginate volume fraction contours 32

Figure 4.7 Exp100-15 alginate volume fraction contours 33

Figure 4.8 Exp100-15 and Exp100-16 alginate volume fraction contours 35

Figure 5.1 Five-point method 43

Figure 5.2 Total mass in the bulk over time 54

Reproduced with permission of the copyright owner. Further reproduction prohibited without permission.

Figure 6.1 Psspah41240 predicted and observed normalized concentration of dextran....56

Figure 6.2 Psspah41277 predicted and observed normalized concentration of dextran....57

Figure 6.3 Psspah43640 predicted and observed normalized concentration of dextran....57

Figure 6.4 Psspah43677 predicted and observed normalized concentration of dextran....58

Figure 6.5 Psspah46040 predicted and observed normalized concentration of dextran....58

Figure 6.6 Psspah46077 predicted and observed normalized concentration of dextran....59

Figure 6.7 Pvspah41240 predicted and observed normalized concentration of dextran....59

Figure 6.8 Pvspah43640 predicted and observed normalized concentration of dextran....60

Figure 6.9 Pvspah43677 predicted and observed normalized concentration of dextran....60

Figure 6.10 Pvspah46040 predicted and observed normalized concentration of dextran....61

Figure 6.11 Pvspah46077 predicted and observed normalized concentration of dextran....61

Figure 6.12 Psspdda41240 predicted and observed normalized concentration of dextran....62

Figure 6.13 Psspdda23640 predicted and observed normalized concentration of dextran....62

Figure 6.14 Psspdda26040 predicted and observed normalized concentration of dextran....63

Figure 6.15 Psspdda21277 predicted and observed normalized concentration of dextran....63

Reproduced with permission of the copyright owner. Further reproduction prohibited without permission.

Figure 6.16 Psspdda23677 predicted and observed normalized concentration of dextran 64

Figure 6.17 Psspdda26077 predicted and observed normalized concentration of dextran 64

Figure 6.18 Psspdda41240 predicted and observed normalized concentration of dextran 65

Figure 6.19 Psspdda43640 predicted and observed normalized concentration of dextran 65

Figure 6.20 Psspdda46040 predicted and observed normalized concentration of dextran 66

Figure 6.21 Psspdda41277 predicted and observed normalized concentration of dextran 66

Figure 6.22 Psspdda43677 predicted and observed normalized concentration of dextran 67

Figure 6.23 Psspdda46077 predicted and observed normalized concentration of dextran 67

Figure 6.24 Psspdda61240 predicted and observed normalized concentration of dextran 68

Figure 6.25 Psspdda63640 predicted and observed normalized concentration of dextran 68

Figure 6.26 Psspdda66040 predicted and observed normalized concentration of dextran 69

Figure 6.27 Psspdda61277 predicted and observed normalized concentration of dextran 69

Figure 6.28 Psspdda63677 predicted and observed normalized concentration of dextran 70

Figure 6.29 Psspdda66077 predicted and observed normalized concentration of dextran 70

Figure 6.30 Pvspdda21240 predicted and observed normalized concentration of dextran 71

Reproduced with permission of the copyright owner. Further reproduction prohibited without permission.

Figure 6.31 Pvspdda21277 predicted and observed normalized concentration of dextran 71

Figure 6.32 Pvspdda23640 predicted and observed normalized concentration of dextran 72

Figure 6.33 Pvspdda23677 predicted and observed normalized concentration of dextran 72

Figure 6.34 Pvspah26040 predicted and observed normalized concentration of dextran 73

Figure 6.35 Pvspdda26077 predicted and observed normalized concentration of dextran 73

Figure 6.36 Pvspdda41240 predicted and observed normalized concentration of dextran 74

Figure 6.37 Pvspdda43640 predicted and observed normalized concentration of dextran 74

Figure 6.38 Pvspdda46040 predicted and observed normalized concentration of dextran 75

Figure 6.39 Pvspdda41277 predicted and observed normalized concentration of dextran 75

Figure 6.40 Pvspdda43677 predicted and observed normalized concentration of dextran 76

Figure 6.41 Pvspdda46077 predicted and observed normalized concentration of dextran 76

Figure 6.42 Pvspdda61240 predicted and observed normalized concentration of dextran 77

Figure 6.43 Pvspdda61277 predicted and observed normalized concentration of dextran 77

Figure 6.44 Pvspdda63640 predicted and observed normalized concentration of dextran 78

Figure 6.45 Pvspdda63677 predicted and observed normalized concentration of dextran 78

Reproduced with permission of the copyright owner. Further reproduction prohibited without permission.

Figure 6.46 Pvspdda66040 predicted and observed normalized concentration of dextran 79

Figure 6.47 Pvspdda66077 predicted and observed normalized concentration of dextran 79

Figure 6.48 Plot of the mean of D1 against layer number 82

Figure 6.49 Plot of the mean of D2 against layer number 84

Figure 6.50 Plot of the mean of D2 against loading time 85

Figure 6.51 Plot of the mean of D2 of data set two against loading time 86

Figure 6.52 Plot of the mean of D2 of data set two against weight 87

Reproduced with permission of the copyright owner. Further reproduction prohibited without permission.

ACKNOWLEDGEMENT

I would like to thank my advisor, Dr. Raja Nassar. During the past three and a half years, he not only taught me all I know about statistics, but also showed me how to do research, how to be a consultant, how to deal with all kinds of pressure, and how to enjoy the beauty of life. I don't know if I can thank him enough, but I know I will remember him and respect him forever.

I would like to thank Dr. Dai for his help and advice with regard to the numerical analysis, Dr. Palmer for his help and guidance in the simulation of droplet generation, Dr. Greechie for his help and advice during my graduate study at Louisiana Tech University and Dr. Leangsuksun for his help with parallel computing.

Finally, I thank my parents, Shiliang Wu and Chunnan Liu. They are the closest people to me in the world. They raised me up and showed me how to be an honest and kind person. Their encouragement and care are always the best gifts I can get. I just hope that I can make them feel proud of me.

Reproduced with permission of the copyright owner. Further reproduction prohibited without permission.

CHAPTER 1

INTRODUCTION

1.1 General Overview

Microcapsules are hollow microspheres encapsulated by multilayers of polyelectrolytes. Considerable number of studies has been done on microcapsules because of its wide application. There are many applications of microcapsules in chemical, biomedical, and medical research. Interestingly they can also be used in many other areas, such as agriculture, the environment, and the automotive industry.

Various techniques and methods have been utilized in the manufacturing and applications of microcapsules. Of interest is to determine the factors that affect the size of a microcapsule during the manufacturing process as well as its characteristics for a given application process so that one can optimize both processes.

1.2 Research Objectives

Layer-by-layer adsorption of oppositely charged polyelectrolytes, poly (styrenesulfonate) PSS and poly (allylamine) PAH, is used as an encapsulating technique in the manufacturing of microcapsules. By using this kind of self-assembly technique, generated microsphere core material can be encapsulated with PSS or PAH multilayers

Reproduced with permission of the copyright owner. Further reproduction prohibited without permission.

after which the core is dissolved to obtain the hollow microcapsules. In order to study the release properties, the hollow microcapsules are loaded with fluorescein-isothiocyanate (FITC) labeled dextran of different molecular weights for different lengths of time, and then immersed into water where the concentration of dextran is measured over time. .

Generating cores of a certain homogeneous size and shape that can be dissolved after encapsulation is essential for the building of the microcapsules. Also, understanding the diffusion properties of the microcapsule is important for its use in controlled release studies for drug delivery. Hence, the objectives of this dissertation are two fold. First, to model the generation of alginate droplets or cores using Computational Fluid Dynamics (CFD) methodology in order to determine the parameters necessary for optimizing droplet size and for minimizing its variance. Second, to model the diffusion properties of microcapsules using a 3-D diffusion model in spherical coordinates and to apply the model to experimental observations on dextran release in order to estimate the diffusion coefficients in the core and wall of the microcapsules. This enables one to determine how diffusion relates to microcapsule characteristics such as wall thickness, polyelectrolyte type, loading time of dextran into the microcapsule, and the molecular weight of dextran.

1.3 Organization

Chapter One presents a brief introduction of microcapsules and the research objectives. Chapter Two gives a literature review of microcapsules, droplets or cores generation of microcapsules, and release studies of microcapsules. Chapter Three introduces the experimental procedure of droplet generation and describes the model of droplet generation, the Computational Fluid Dynamics theory behind it. Chapter Four describes results and the statistical method to optimize the simulation results. Chapter

Reproduced with permission of the copyright owner. Further reproduction prohibited without permission.

Five introduces the experimental procedure of transport phenomena, the model of release study, applied numerical analysis and model-checking methodology. Chapter Six describes simulation results and discussion.

Reproduced with permission of the copyright owner. Further reproduction prohibited without permission.

CHAPTER 2

LITERATURE REVIEW

2.1 Microcapsules

A microcapsule is generally composed of a core material encapsulated by shell material that acts as a microcapsule wall. Microencapsulation is a very useful technique because of the semi-permeability of the microcapsule wall. The wall can protect the inner material from the outer environment or can control its release. Microcapsules play an important role in chemical, biomedical, and medical research. Of importance is their potential use as bio-sensors, microreactors, microcarriers or as drug delivery vehicles (Tong, 2006; Chen, 2006). For instance, Ghan (2004) used polyelectrolyte microcapsules as reactors for synthesizing bio-polymers. Sun et al. (2003) used an ultra thin shell to encapsulate hepatocytes and showed that the obtained microcapsules had enhanced differentiated functions over cells cultured in monolayers. Microcapsules can be used also in many other areas such as bioremediation of ground water and soil, herbicides, insecticides, fertilizers (Shigemi and Yoshikawa, 1994), air bag applications in automotive, bath salt fragrance in cosmetic and personal care, and even sunscreen products containing said microcapsules (Lahmani, 1996).

Because of their wide applications, considerable research in science and engineering has been devoted to microcapsules. Thanks to the technique of layer-by-layer

Reproduced with permission of the copyright owner. Further reproduction prohibited without permission.

assembly of oppositely charged polyelectrolytes (Lvov, 1993; Hong, 1993; Decher, 1997; Sukhorukov, 2000; Lvov, 2001; Tong, 2006), multilayer microcapsules prepared by self-assembly onto removable colloidal particles have generated considerable scientific interest. These hollow capsules have shown potential applications as drug delivery vehicle, biosensors, microreactors, and microcarriers.

2.2 Droplet Generation

2.2.1 Microfluidic Devices

Because certain fluid properties, such as surface tension, wall adhesion, and energy dissipation, dominate at the microlevel, microfluidic devices are finding increasing applications as analytic systems, biomedical devices, tools for chemistry and biochemistry, and systems for fundamental research (McDonald, 2000; Thorson, 2001; Thwar, 2005). A microfluidic system was designed and fabricated by Prevot et al. (2003) to study the behavior of polyelectrolyte microcapsules flowing in microchannels. Microfluidic devices were etched in glass and silicon by using conventional methods and equipments (McDonald, 2000). Conventional equipments have a disadvantage in the sense that turbulence cannot be controlled or generated consistently throughout the volume of the liquid. Hence, compared with conventional methods and processes, microfluidic devices show superior performance. In this dissertation, a microfluidic device (capillary system) is utilized to generate alginate microdroplets.

2.2.2 Methodologies

Microdroplets are prepared by various processes. Before the wide use of microchannels, microdroplets were generated through a microporous membrane and jet pinch-off. In membrane emulsification, the droplets are formed through the pores at the

Reproduced with permission of the copyright owner. Further reproduction prohibited without permission.

surface of the membrane because of the inner and outer stress difference. Pore size of the membrane, pressure of the disperse phase, and adsorption kinetics of the emulsifier influence the results of emulsification (Schroder, 1998). Caused by the interfacial tension between two immiscible phases, microdroplets are generated by jet pinch-off technology. Variables include nozzle size, flow rate, and type and concentration of the phases (Meister, 1969; Skelland; 1989; Webster, 2001). A microcapsule generating system containing an air knife was used to form spherical microcapsules containing tissue or living cells (Dorian, 1996; Dorian, 1996). A vibrating orifice aerosol generator (VOAG) was used by Ray et al. (2005) to generate droplets with a small size variation. The droplets were dispersed in air to prevent agglomeration. The generation of tailored microspheres can be achieved using this technique. These particles are microspheres of polymeric materials manufactured by in-situ photopolymerization of droplets containing monomers and additives. The important factors using this technique are: the pressure used to generate monodisperse droplets through a VOAG, the vibration frequency of the orifice, the surrounding gas temperature, and the dispersion air.

Recently, microchannels have been used for generating microdroplets in microfluidic devices. Emulsions are formed by shearing one liquid into another immiscible liquid, often in the presence of a surfactant, to create small droplets. These droplets are formed by forces generated at the leading edge of the two liquid phases. Results of the emulsification process can be described by the mean droplet size and the variance of the droplet size. Among other parameters, flow rates of the two phases, viscosity of the two phases, and geometry of the microchannel can influence the emulsification significantly (Lister, 1998; Thorson, 2001; Tan, 2004). Droplets formed

Reproduced with permission of the copyright owner. Further reproduction prohibited without permission.

by the co-flow of oil and water through a T-shaped microchannel have been studied by several groups (Thorson, 2001; Collins, 2003). Droplet generation has been studied in Dr. Palmer's Laboratory at Louisiana Tech University. They used a T-shaped channel microfluidic device with a bifurcating junction to generate alginate droplets. Alginate is sheared by a continuing phase, vegetable oil.

2.2.3 Alginate Microdroplets

Alginate, used in the generation of microdroplets or spheres, is derived from seaweed which is a salt of alginic acid. Alginate is widely used in many areas because of its mild gelling, biocompatibility, and biodegradability. For instance, alginate is the most popular material for the formation of the polymer matrix and outer biocompatible membrane. Purified alginate was used to coat cell or tissue transplants (Dorian, 1996). Sodium alginate can be used in the food industry as an emulsifier, thickener, stabilizer, or gel-forming agent like agar and carrageenan (Ragaza, 1999). Wheatley (1991) attempted to form microparticles from sodium alginate in a 1/3 % buffered calcium chloride solution. Also, sodium alginate-chitosan (AC) microcapsules were used by Yu (2006) as immobilization carriers for cell culture. Ma et al. (2005) provided a method for preparing sodium alginate-polylysine microcapsules which contain immobilized yeast cells. Calcium alginate is a traditional method to fix bone splitters. As a general therapy, calcium alginate is administered as a nutrient additive 1-2 times a day in addition to diet. Orive et al. (2006) created alginate-PLL-alginate (APA) microcapsules using an electrostatic droplet generator. The alginate-poly-L-lysine-alginate membrane is widely used in cell encapsulation. Chen (2006) successfully used these APA microcapsules to limit the major immuno-rejection problems related to the use of live cells and bacteria in

Reproduced with permission of the copyright owner. Further reproduction prohibited without permission.

some animal models. Li et al. (2005) attempted to evaluate the function of porcine islets encapsulated by APA. APA microencapsulated porcine islets were able to secrete insulin both in vitro and under a perfusion condition. The porcine islets showed the ability to secrete insulin in a culture medium of different glucose concentrations. It was shown that both in vitro and in vivo APA microencapsulated porcine islets can maintain their function and therapeutic effect. Sun et al. (2002) used an electrostatic droplet generator (EDG) technique to prepare APA microcapsules and study the thickness of the polyelectrolyte APA microcapsule membrane. Glucose oxidase-doped alginate microspheres encapsulated with calcium chloride added for ionic gelation were produced for enzymic sensors using water-in-oil emulsion (McShane, 2005). Monodisperse calcium alginate microparticles were studied in this research. These microcapsules can be used as vehicles to carry sensing material into the human body. The optimum size of the microparticles for implanting in the transderma layer was about 40-50 μm.

2.3 Layer-by-layer Encapsulation

Microcapsules prepared by the deposition of alternate layers of crosslinked atelocollagen and polyholosides are biocompatible by virtue of the presence of atelocollagen. Atelocollagen with a very low antigenicity and a perfect biodegradability has most of the advantageous properties of collagen (Levy, 1997). Ijichi (1997) was successful in obtaining spherical gelatine/acacia microcapsules with thicker membrane by using the conventional complex coacervation method. Double layered microcapsules were made by Yamamoto and Sefton (1996) using vinyl amine copolymer films. Those microcapsules can perform polymer grafting reactions without damaging cells inside the

Reproduced with permission of the copyright owner. Further reproduction prohibited without permission.

microcapsules. Takiguchi et al. (2004) developed technology for discharging and microencapsulating minute amounts of droplets.

Polyelectrolyte multilayer microcapsules are microcapsules with the walls made of polyelectrolyte multilayers. Layer-by-layer assembly of oppositely charged polyelectrolyte onto removable colloidal particle surfaces has been used by many groups because of its potential application (Radtchenko, 2000; Antipov, 2002; Tong, 2006). Voigt (1999) reported on the use of nonsol. Polystyrene sulfate latex, solution melamine formaldehyde resin latex, and decomposable glutaraldehyde-fixed human red blood cells as target particles for layer-by-layer adsorption. Zhao et al. (2006) and Gao et al. (2006) showed how the structure and stability of polypeptide multilayer films can affect various types of noncovalent interactors. Rilling et al. (1997) used polycation/polyanion double layers to encapsulate cytochrome C. The layer-by-layer assembly technique was used to construct various types of POM-polyelectrolyte composite microcapsules because of the versatile properties of polyoxometalate (POM) (Gao, 2005). For the layer-by-layer self-assembled polyelectrolyte microcapsules, a magnetic field can be used to modulate the permeability (Lu, 2005; Prouty, 2004).

At the Institute for Micromanufacturing (IFM), Louisiana Tech University, poly (styrene sulfonate) (PSS) and poly (allylamine) (PAH) are the two polyelectrolytes used in layer-by-layer encapsulation of microsphere colloidal core material (melamine formal dehyde (MF)) to obtain multilayer microcapsules. Pargaonkar (2005) showed that the release phenomena can be controlled by the component and the number of layers. A composition of a sustained release layer and a fast release layer was also used in order to optimize microcapsules for controlled release.

Reproduced with permission of the copyright owner. Further reproduction prohibited without permission.

2.4 Transport Phenomena

"The main focus in the area of emulsion technology is to improve stability and control the release of active matter in double emulsions" (Lyon, 2002). Because of the permeability property of a microcapsule's wall, microencapsulation is an important technique used to protect the inner materials from the outer environment or to control the release of the encapsulated inner materials. Studies of mass transport in microcapsules are important for microcapsule applications. Microcapsules have potential applications in drug delivery, as biosensors, microreactors, or microcarriers.

Setterstrom et al. (1982) developed microcapsules that can maintain slow release of effective therapeutic doses of antibiotics in a wound over a 14-day period. Polk (1994) used semi-permeable biocompatible microcapsules to entrap a vaccine in order to destruct the fish digestive system. It was showed that controlled-release formulations can provide a short half-life "pulsed" plasma profile of a sedative-hypnotic compound. Research on anticancer drug doxorubicin hydrochloride (DOX) in a drug delivery system was undertaken by Yang et al. (2005), Khopade et al. (2002), and Liu et al. (2005). Benichou et al. (2004) attempted to select food-grade blends of emulsifiers to enhance emulsion stability at both inner and outer interfaces. They used new polymeric amphiphiles (carriers, complexing agents, natural polymeric emulsifiers) in order to control and reduce the reverse micellar transport phenomena and to control the transport the inventive method and associated device was used by Windhab (2005) to obtain multi-microcapsules. These microcapsules are adapted to different substance components and release conditions.

In so many applications of microcapsules, a critical question is how to control the transport phenomena. From research in the literature, it is clear that the permeability of a

Reproduced with permission of the copyright owner. Further reproduction prohibited without permission.

microcapsule depends on the type and thickness of the wall, loading time of the inner material, pH value, temperature, and molecular weight of the inner material (Takagishi, 1994; Antipov, 2002; Kim, 2004; Yang, 2005; Pargaonkar, 2005; Windhab, 2005; Tong, 2006). To determine how these factors can influence the transport phenomena, it is necessary to develop a theoretical model. The determination of the mass transfer coefficient value yields clear insight into the characterization of microcapsules with semi-permeable membranes (Lewinska, 2002; Rosinski, 2005). Due to the semipermeability of the capsule wall, Tong (2006) created a Donnan equilibrium between the inner solution within the capsules and the bulk solution. Kwok et al. (1991) developed a general diffusion model for alginate-polylysine (PLL) microcapsules which can describe mass transport phenomena and membrane diffusivities. The apparent size of the impermeable gel core and the capsule membrane permeability were used to describe the results. Factors that can affect the results are the size of the diffusing protein and the alginate-PLL reaction time. These microcapsules can be used in cell culture engineering and cell transplantation by affecting cell viability. Manca et al. (2003) modeled the release process within the human body. In that model, they showed how polymer coating can affect the transport phenomena.

Reproduced with permission of the copyright owner. Further reproduction prohibited without permission.

CHAPTER 3

DROPLET GENERATION MODEL

3.1 Introduction

For application purposes, it is desirable to produce alginate microspheres in the range of 40-50 μm in diameter. Such capsules have been produced in Dr. Palmer's laboratory at Louisiana Tech University using alginate and vegetable oil as the immiscible phase. Before the wide use of microchannels, microparticles were generated through a microporous membrane and jet pinch-off. The microchannel technique involves the use of a T-shaped channel microfluidic device with a bifurcating junction (Figure 3.1) which allows for the mixing of the two immiscible phases, alginate and vegetable oil.

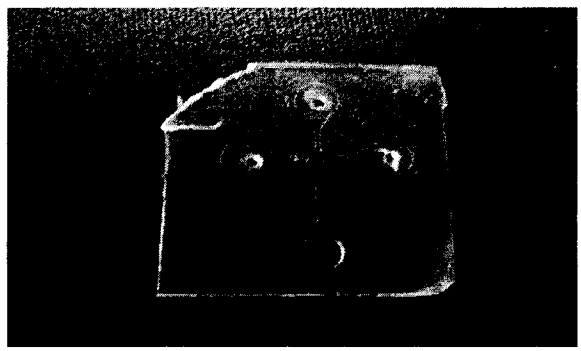

Figure 3.1. Enlarged T-shaped channel

Reproduced with permission of the copyright owner. Further reproduction prohibited without permission.

The alginate microparticles are produced due to the interfacial tension (or force) generated between the two immiscible phases. When alginate molecules at the interface are subjected to this interfacial force, they rearrange themselves in order to reduce this exerted force. This rearrangement is in the form of a spherical configuration since this reduces the surface area and produces the least strain on the system.

3.2 Experimental Procedure

The experimental setup is shown in Figure 3.2. The critical components are labeled in the diagram.

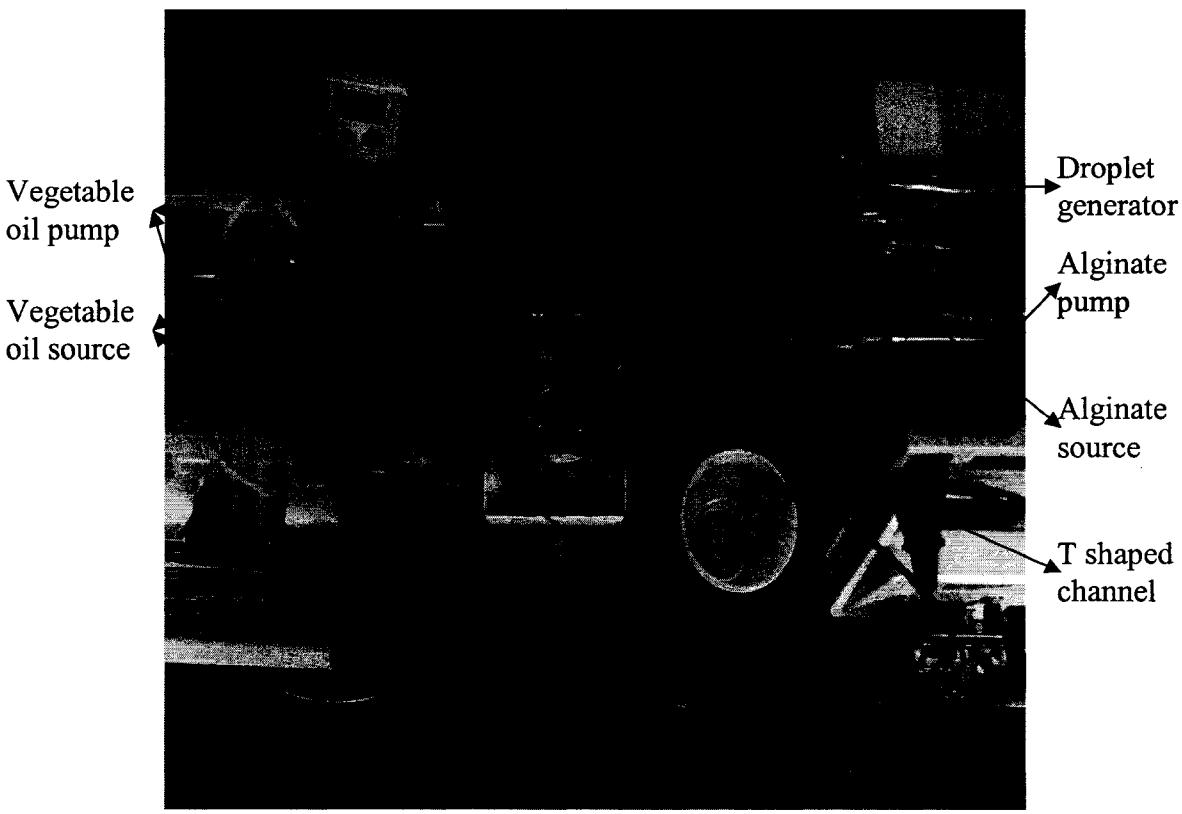

Figure 3.2. Experimental setup

Reproduced with permission of the copyright owner. Further reproduction prohibited without permission.

3.2.1 Preparation of the Two Phases

Calcium chloride solution: 10% wt of calcium chloride is made by adding 50 g of calcium chloride into 500 g of water.

Alginate solution: 2% wt alginate solution is made by adding 4 mg of FITC dextran and 0.6 g of sodium alginate into 30 g of water.

3.2.2 Process

Alginate and calcium chloride solutions are inputed into the system at the same time. After the flows are stabilized, the alginate particles sheared by the calcium chloride flow are sent into the CSTR containing the calcium chloride solution which is under constant stirring (over head stirrer). Alginate spheres tend to coagulate at the inter phase surfactants. In order to prevent coagulation, Tween 80 (2%v/v) and Span 80 (1.5%v/v) are added to the dispersed and the continuous phase.

3.3 Mathematical Model

Droplets are generated by the imbalance between the interfacial tension and the Laplace pressure. Alginate molecules arrange themselves into microspheres in order to reduce the tension by reducing their interfacial area. A spherical configuration minimizes the stain on the system.

FLUENT, a computational fluid dynamics (CFD) software, can be used to simulate complex engineering problems. We can use FLUENT to model droplet or microcapsule generation. The model can be verified by comparing predicted values to experimental results. A model that can accurately simulate the process of droplet generation would be useful for planning and design of experiments and for reducing experimental time and cost.

Reproduced with permission of the copyright owner. Further reproduction prohibited without permission.

The model chosen in FLUENT for droplet generation is the volume of fluid (VOF) model. The VOF model can simulate the behavior of two immiscible fluids by solving the momentum equation in each cell and tracking the volume fraction of each fluid throughout the domain. The volume fraction of the phase in the computational cell is introduced as a variable for each phase in the model. The volume fractions of all phases sum to unity in each cell. The whole domain is meshed into a large number of cells. For two phases, let α_q stand for the qth fluid volume fraction (q = 1,2) in a cell. It is seen that

1. $\alpha_q = 0$ implies that the cell is empty of the qth fluid.
2. $\alpha_q = 1$ implies that the cell is full of the qth fluid.
3. $0 < \alpha_q < 1$ implies that the cell contains both the qth fluid and the other fluid. A cell that conatins both fluids is at the interface.

The solution of the continuity equation, Equation 3.1, for the volume fraction is used for the tracking of the interfaces between the two phases.

$$\frac{\partial \alpha_q}{\partial t} + \vec{v} \cdot \nabla \alpha_q = 0 \tag{3.1}$$

In Equation 3.1, α_q stands for the qth fluid's volume fraction in the cell,

$\vec{v}$ stands for velocity vector of the fluid in the cell, and

t stands for time.

All phases in each cell sum to unity,

$$\sum_{q=1}^{n} \alpha_q = 1. \tag{3.2}$$

Reproduced with permission of the copyright owner. Further reproduction prohibited without permission.

Thus, the density and viscosity in a given cell can be evaluated as weighted means of the densities and viscosities of the individual phases. The weights are the volume fraction of the phases. For instance, one can use the following equations to represent the density and viscosity in each cell:

$$\rho = \sum \alpha_q \rho_q , \tag{3.3}$$

where ρ stands for the density in the cell,

α_q stands for the qth fluid's volume fraction, and

ρ_q stands for the density of the qth fluid.

Also,

$$\mu = \sum \alpha_q \rho_q \tag{3.4}$$

where μ stands for the viscosity in the cell,

α_q stands for the qth fluid's volume fraction, and

μ_q stands for the viscosity of the qth fluid.

The properties ρ and μ depend on the volume fractions of all phases. Therefore, the momentum equation in a cell, in which ρ and μ are included, is dependent on the volume fractions of all phases. The VOF model simulates the process by solving a set of momentum equations over cells and tracking the volume fraction of all the phases throughout the domain. As such, ρ and μ are the connection between the momentum equation and the volume fractions of the two phases.

The 2-D continuity equation used in this model is

Reproduced with permission of the copyright owner. Further reproduction prohibited without permission.

$$\frac{\partial \rho}{\partial t} + \frac{\partial (\rho \vec{v})}{\partial x} + \frac{\partial (\rho \vec{v})}{\partial y} = 0 \tag{3.5}$$

where ρ is the density,

$\vec{v}$ is the velocity vector for the two fluids.

Momentum is a vector quantity. It is based on Newton's second law of motion. This is expressed as

$$P = mv \tag{3.6}$$

Where P stands for momentum,

v stands for velocity of the fluid in the cell, and

m stands for mass of the fluid in the cell

Dividing the left and right hand sides of Equation 3.6 by time t, one obtains the following equation:

(output – input + accumulation) x rate of momentum = $\sum F$, (3.7)

where F is the force.

The momentum equation for every cell is:

$$\frac{\partial}{\partial t}(\rho \vec{v}) + \nabla \cdot (\rho \vec{v} \vec{v}) = -\nabla p + \nabla \cdot [\mu (\nabla \vec{v} + \nabla \vec{v}^{T})] + \rho \vec{g} + \vec{F}, \tag{3.8}$$

Where t is time,

$\vec{v}$ is the velocity of the fluid in the cell,

ρ is the density in the cell,

p stands for the pressure exerted on the fluid in the cell,

μ stands for the viscosity in the cell,

Reproduced with permission of the copyright owner. Further reproduction prohibited without permission.

$\vec{g}$ is the gravitational force exerted on the fluid in the cell, and

$\vec{F}$ is the friction force exerted on the fluid in the cell.

The first expression on the left hand side of Equation 3.8 represents the increase in momentum. The second expression on the left hand side of Equation 3.8 represents momentum input by convection. The first expression on the right hand side of Equation 3.8 represents the pressure force. The second expression on the right hand side of Equation 3.8 represents momentum input by viscous forces. The third expression on the right hand side of Equation 3.8 represents gravitational force. The fourth expression on the right hand side of Equation 3.8 represents friction force.

The boundary conditions and initial conditions for the momentum equation are:

Boundary conditions:

Alginate input and vegetable oil input are defined as velocity inlet boundaries describing flow entering the physical domain of the model. FLUENT uses the velocity inlets boundary conditions to compute the mass flow into the domain through the inlets and to compute the fluxes of momentum, energy, and species through the inlets. The mass flow rate entering a fluid cell adjacent to a velocity inlet boundary is computed as

$$\dot{m} = \int \rho \vec{v} \cdot d\vec{A}, \tag{3.9}$$

where $\dot{m}$ stands for the mass flux,

ρ stands for the density in the cell,

$\vec{v}$ stands for velocity of the fluid in the cell, and

$\vec{A}$ stands for the area.

Reproduced with permission of the copyright owner. Further reproduction prohibited without permission.

The oil/alginate interface boundary is computed as

$$\dot{m}_i = \int \rho \vec{v} \cdot d\vec{A}_i - \rho \dot{\Omega}_i \tag{3.10}$$

where $\dot{m}_i$ stands for the mass flux going through the interface area

$\vec{A}_i$ stands for the interface area

$\dot{\Omega}_i$ volume of fluid

The output boundary is defined as the outlet pressure. FLUENT uses condition pressure as the static pressure of the fluid at the outlet plane, and all other conditions are extrapolated from the interior of the domain.

The boundary condition at the wall is a fixed heat flux of zero. Walls are stationary and shear condition at the wall is no slip.

Initial conditions:

$v_a = v_1$, at the alginate input interface

$v_a = 0$, otherwise

$v_o = v_2$, at the vegetable oil input interface

$v_o = 0$, otherwise,

where v_a stands for the velocity of alginate,

v_o stands for the velocity of vegetable oil, and

v_1 and v_2 stand for the constants.

It is seen that the momentum equation Equation 3.8 and volume fraction equation Equation 3.1 are coupled equations. The velocity in Equation 3.1 is obtained from the solution of Equation 3.8. Also, the solution to the momentum equation depends on ρ and

Reproduced with permission of the copyright owner. Further reproduction prohibited without permission.

μ which in turn depend on the knowledge of the volume fraction from Equation 3.1. Hence, the VOF model simulates the process through a simultaneous solution of Eqs. 3.8 and 3.1.

3.4 Simulation

FLUENT, as a powerful CFD software, is used in this research to simulate the droplet generation process. The volume of fluid (VOF) model was chosen because it can model two immiscible fluids by solving a set of momentum equations and tracking the volume fraction of each of the fluids throughout the domain.

The simulation process includes the following steps:

- Designing the geometry of the channel
- Setting up the model
- Running the model
- Evaluating the results

3.4.1 Designing the Geometry of the Channel

Gambit 2.1 as the preprocessor for FLUENT is used to design the geometry of the channel. There are three main steps in the design of the geometry.

- Draw a 2-dimensional area to represent the channel. To draw the area, one needs to locate all the points by specifying x and y coordinates, join the points to obtain the sides (boundaries), and then connect all the sides together to get the 2-D area (Figure 3.3).

Reproduced with permission of the copyright owner. Further reproduction prohibited without permission.

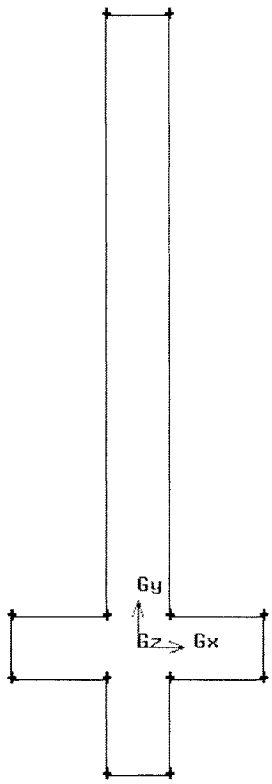

Figure 3.3. Two-dimensional area of the channel

- Mesh the 2-dimensional area (Figure 3.4), see the enlarged graph (Figure 3.5). FLUENT operates on this area using the finite volume method.

Reproduced with permission of the copyright owner. Further reproduction prohibited without permission.

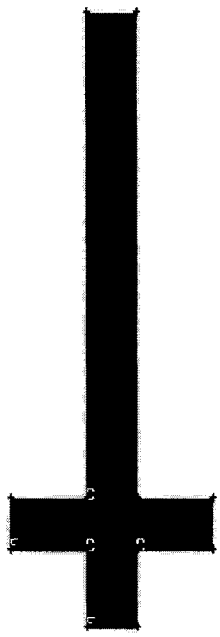

Figure 3.4. Two-D area mesh

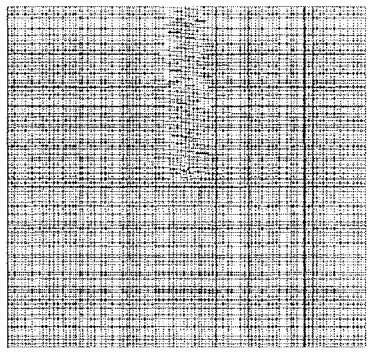

Figure 3.5. Enlarged 2-D mesh

- Set the type of boundaries. As is shown in Figure 3.6, a velocity inlet is set for the alginate input, two velocity inlets are set for vegetable oil input, and a pressure outlet is set for the output. The other boundaries are wall boundaries.

Reproduced with permission of the copyright owner. Further reproduction prohibited without permission.

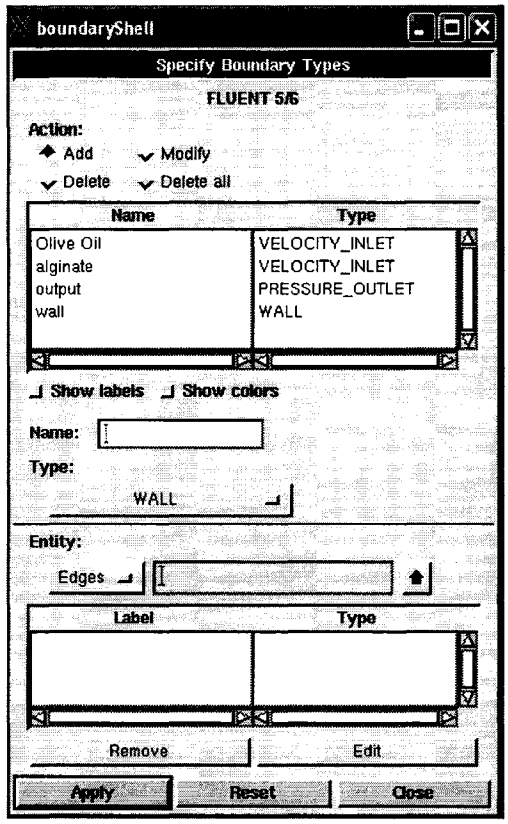

Figure 3.6. Boundary types of the channel sides

The design of the channel geometry can be saved as a mesh file which includes the channel geometry and the boundary type information.

3.4.2 Setting up the Model

A mesh file is created by Gambit with all the information about channel geometry and boundary conditions. FLUENT will take the file over from Gambit to set up the model according to the following steps:

- Import the mesh file.

  The mesh file created by Gambit is imported into FLUENT. The mesh file provides the geometry information. The next step is to specify the unit according to the experimental equipment shown in Figure 3.7.

Reproduced with permission of the copyright owner. Further reproduction prohibited without permission.

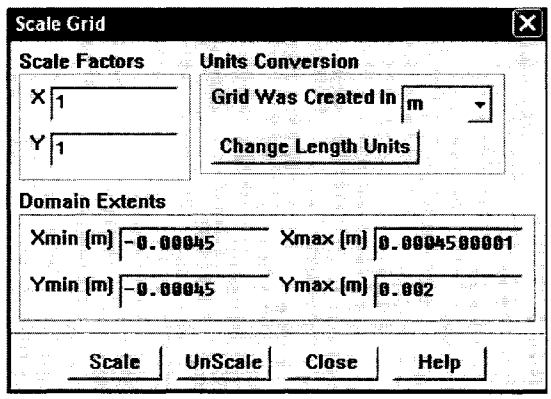

Figure 3.7. Scale grid

- Choose the solver and model.

The segregated solver is chosen. An implicit unsteady first order formulation is used in this solver. PRESTO! and PISO schemes are chosen for pressure and pressure-velocity coupling. The momentum scheme is the first order upwind. In order to specify the VOF model, one needs to set up the materials and phases.

- Materials and phases.

The two fluids, alginate and vegetable oil, are created by specifying the density and viscosity properties of the fluids. Vegetable oil is set to be the primary phase and alginate the secondary phase. Interfacial tension between the primary phase and the secondary phase is set to be 1 because the two phases are immiscible.

- Boundary conditions:

The boundary conditions need to be specified for the VOF model. Walls are stationary and shear condition is no slip as default. Output is the pressure outlet satisfying PRESTO! and PISO schemes. The vegetable oil velocity inlet

Reproduced with permission of the copyright owner. Further reproduction prohibited without permission.

is the input of the primary phase. So the phase for this boundary is the primary phase vegetable oil and the input velocity of this phase is entered here. The alginate velocity inlet is the input of the secondary phase. So the phase for this boundary has to be the secondary phase alginate and the input velocity of this phase is entered here.

3.4.3 Running the Model

The above steps are all that is needed to set up the VOF model. To run this model, the setting of the initial conditions and iteration is required.

- Initial conditions:

  The initial velocity for all the cells is zero except for the boundaries of alginate input and vegetable oil input. The initial velocity of alginate at the alginate input boundary is entered here and the direction is along the x axis. The initial velocity of vegetable oil at the vegetable oil input boundary is entered and the direction is along the y axis.

- Iteration:

  In this step, the time step and the number of sub-steps are specified. The time step is the maximum interval which can guarantee convergence and shorten the simulation time.

3.4.4 Parallel Computing on a Linux Cluster

FLUENT can work efficiently on a PC for small problems. For big problems, like the droplet simulation in this paper, we used parallel computing on a cluster to reduce calculation time. Cluster computing was considerably faster than the PC. Parallel computing is widely used in the scientific computing and engineering analysis

Reproduced with permission of the copyright owner. Further reproduction prohibited without permission.

communities. The idea is to connect several computers together to solve a single problem using their collective power. A multi-processor FLUENT job is launched from a "host node." A graphical user interface (GUI) is run on the host node. Using the Putty (a telnet/SSH client) and Cygwin (Linux-like environment for Windows), FLUENT on the cluster can be run on any PC as a terminal.

Figure 3.8 shows how the idea works in FLUENT, the communication between all nodes represents passing messages.

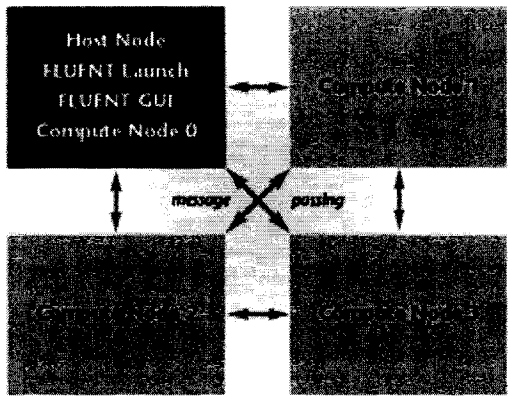

Figure 3.8. Running FLUENT on a cluster

It is seen from Figure 3.8 that all the nodes can run in parallel. This can reduce the turn-around time in computation. As is shown in Figure 3.9, computation speed as a function of project size increases with an increase in the number of processors in the cluster.

Reproduced with permission of the copyright owner. Further reproduction prohibited without permission.

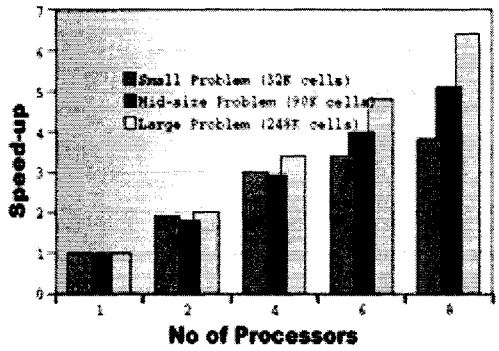

Figure 3.9. Parallel computing performances of different number of processors

Figure 3.9 represents three size groups. The droplet simulation project has 300,007 cells, which belongs to the larger size group. As such, performance was dramatically improved by parallel computing. Fourteen processors were used in the simulation because of the limitation of the license Louisiana Tech University purchased.

3.4.5 Evaluating the Results

The volume fraction distribution of the secondary phase (alginate) is captured in graphical mode every time step. All the graphs are connected into a video to show how alginate is sheared by the vegetable oil flow. The droplet size and its variance can be used to describe the results. In Chapter 4, comparison of the simulation results and experimental results is studied in detail.

Reproduced with permission of the copyright owner. Further reproduction prohibited without permission.

CHAPTER 4

RESULTS AND DISCUSSION OF DROPLET GENERATION

4.1 Introduction

This chapter deals with the simulation of a two phase flow process in a 100 micron width channel for the generation of droplets. The geometry in Figure 3.3 is used with proper boundary conditions. Comparisons between the theoretical results from simulation and experimental results are presented.

4.2 Simulation Design

A factorial experiment at two levels with a center point (Table 4.1) was used in order to obtain an optimum factor combination that gave the desired particle size with minimum variance. The velocity of the vegetable oil and the velocity ratio of vegetable oil to alginate were considered as the two quantitative continuous factors. The idea used is based on response surface methodology. It involves collecting observations at each location on a grid of treatment combinations spanning the entire simulation region, and then estimating the response surface in the vicinity of the optimum response. Based on the responses obtained from the first design in Table 4.1, an optimum was selected and a second factorial experiment (Table 4.2) was run in the vicinity of this optimum.

Reproduced with permission of the copyright owner. Further reproduction prohibited without permission.

Table 4.1. Simulation runs for different factor combinations

	Vegetable Oil		Ratio	
Model	Coded	Uncoded	Coded	Uncoded
Exp100-1	-1	0.05	-1	5
Exp100-2	-1	0.05	1	25
Exp100-3	1	0.2	-1	5
Exp100-4	1	0.2	1	25
Exp100-5	0	0.125	0	15

Table 4.2. Simulation runs for different factor combinations in the vicinity of an optimum droplet size and variance

	Vegetable Oil		Ratio	
Model	Coded	Uncoded	Coded	Uncoded
Exp100-11	-1	0.08	-1	8
Exp100-12	-1	0.08	1	12
Exp100-13	1	0.12	-1	8
Exp100-14	1	0.12	1	12
Exp100-15	0	0.1	0	10

4.3 Simulation Results

In running the simulation, the alginate volume fraction contours, as shown in Figure 4.1 were used to represent the alginate phase distribution which ranges from 1 (red color) to 0 (blue color). For the runs in Table 4.1, Exp100-1 and Exp100-2 did not generate any droplets (Figures. 4.2 and 4.3a). This was attributed to the low velocity of the vegetable oil. In Exp100-3, alginate was distributed as a stream because of the low ratio (Figure 4.3b). Particles or droplets were generated in the case of the two runs, Exp100-4 and Exp100-5 (Figure 4.4 a, b). However, the particle size was too small in both of these runs, but in Exp100-5, the particle size was much larger than in the case of Exp100-4. As a result, the experimental runs in Table 4.2 were designed in a new region with center point at 0.1 m/s for the vegetable oil velocity and 10 for the ratio.

Reproduced with permission of the copyright owner. Further reproduction prohibited without permission.

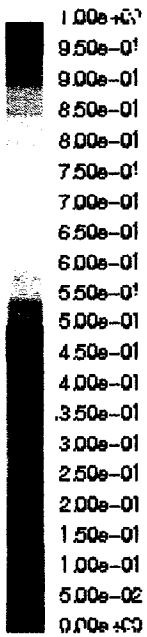

Figure 4.1. Alginate volume fraction contours

Figure 4.2. Exp100-1 alginate volume fraction contours

Figure 4.3. (a) Exp100-2 and (b) Exp100-3 alginate volume fraction contours

Reproduced with permission of the copyright owner. Further reproduction prohibited without permission.

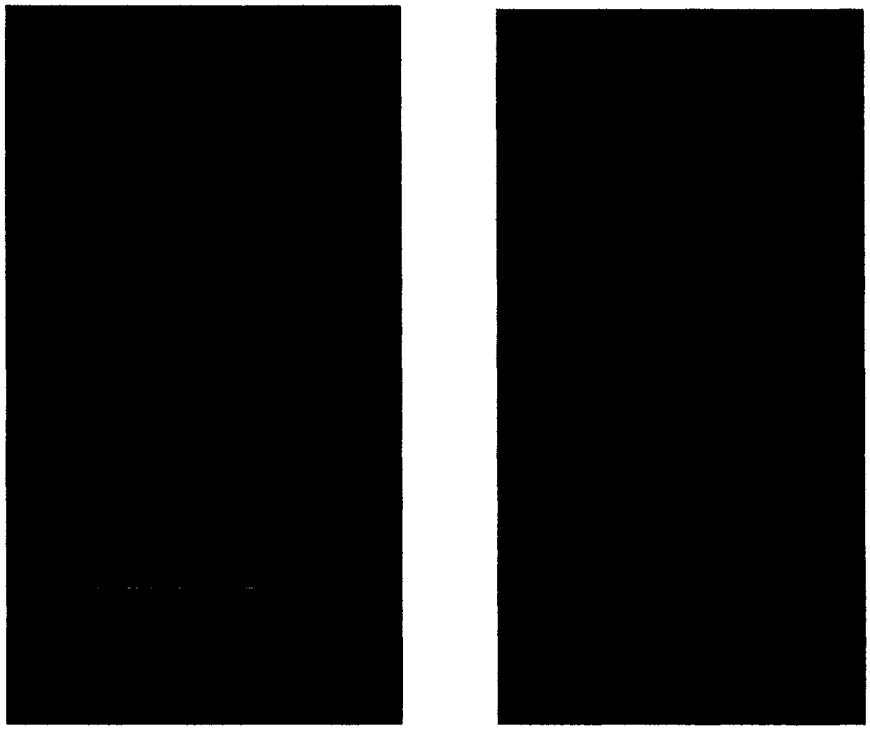

Figure 4.4. (a) Exp100-4 and (b) Exp100-5 alginate volume fraction contours

In Exp100-11 and Exp100-13 of Table 4.2, alginate was distributed as a stream because of the low ratio (Figures 4.5a, 4.6a). Particles were produced in the cases of Exp100-12 (Figure 4.5b), Exp100-14 (Figure 4.6b), and Exp100-15 (Figure 4.7). The Exp100-15 run gave the largest particle size and the largest variance. The means and standard deviations for the short and long droplet diameters are presented in Table 4.3.

Reproduced with permission of the copyright owner. Further reproduction prohibited without permission.

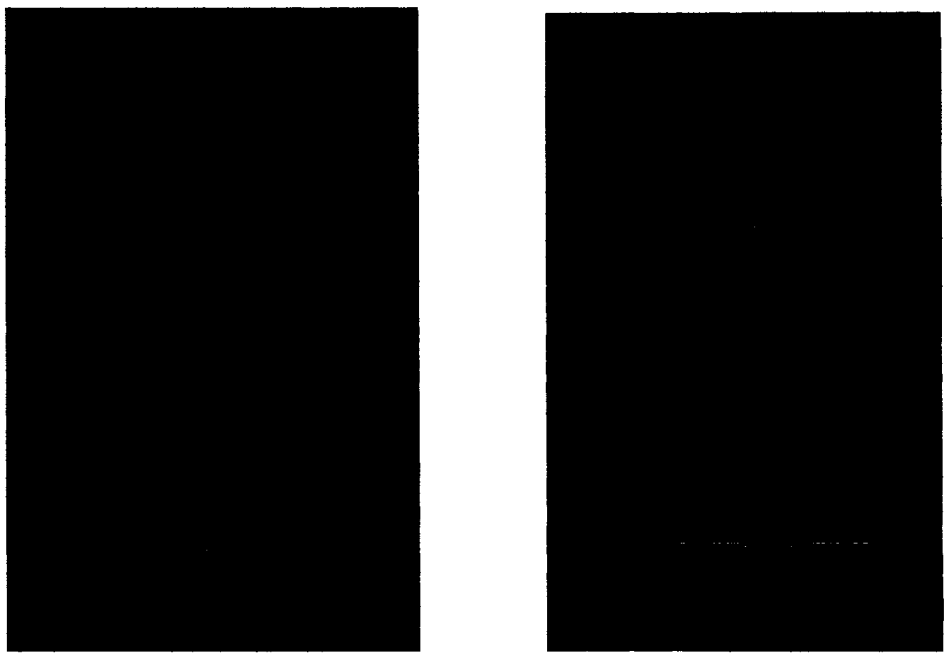

Figure 4.5. (a) Exp100-11 and (b) Exp100-12 alginate volume fraction contours

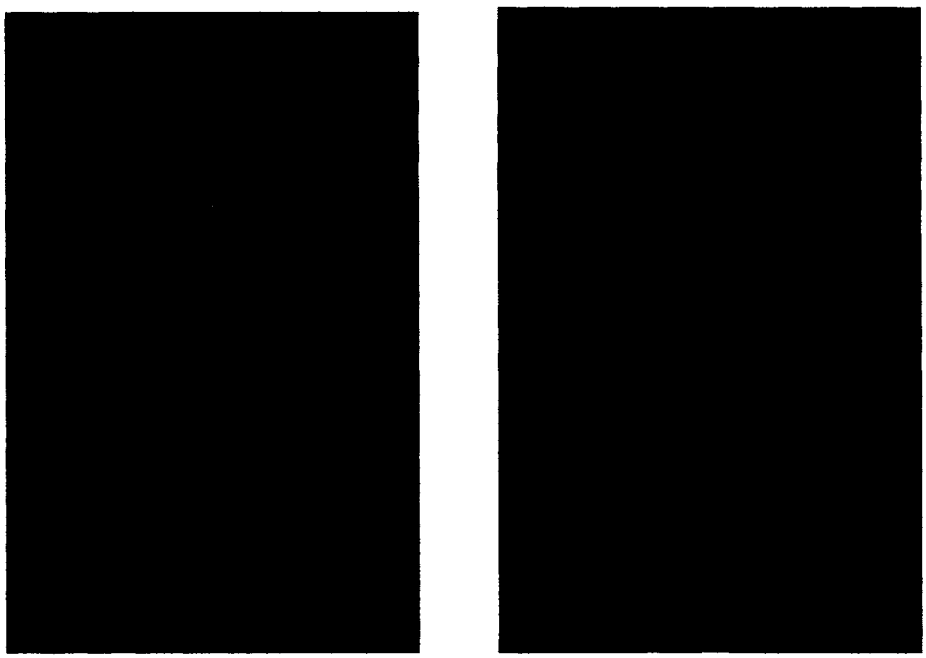

Figure 4.6. (a) Exp100-13 and (b) Exp100-14 alginate volume fraction contours

Reproduced with permission of the copyright owner. Further reproduction prohibited without permission.

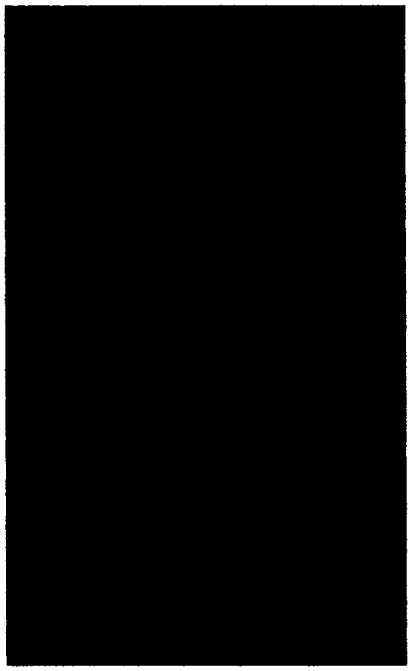

Figure 4.7. Exp100-15 alginate volume fraction contours

Table 4.3. Average and standard deviation for short and long particle droplet diameters for the different experimental runs

Case #	Alginate flow rate (m/s)	Oil flow (m/s)	Ratio	Average short particle diameter (μm)	Standard deviation of short diameter	Average long particle diameter (μm)	Standard deviation of long diameter
Exp100-11	0.01	0.08	8	No D.F.			
Exp100-12	0.0067	0.08	12	21.7	8.1	25.1	8.6
Exp100-13	0.015	0.12	8	No D.F.			
Exp100-14	0.01	0.12	12	22.9	7.2	24.8	8.5
Exp100-15	0.01	0.1	10	22.7	11.3	26.9	17.5

Reproduced with permission of the copyright owner. Further reproduction prohibited without permission.

4.4 Results

As it is shown in Table 4.3, the coefficient of variation (standard deviation/mean) of the short diameter ranges from 0.314 to 0.498 and that of the long diameter ranges from 0.342 to 0.65. Exp100-15 has the largest coefficients of variation (0.498 for the short diameter and 0.65 for the long diameter). Considering the mean and coefficient of variation for droplet size, it would seem that the factor combination in Exp100-14 gives a relatively large mean diameter and small coefficient of variation and is to be preferred to the other experimental runs.

For all the simulation in this study, the following properties for oil and alginate were used.

Olive oil: Density 930 kg/m3

Viscosity 0.03 kg/m-s

Alginate: Density 1012 kg/m3

Viscosity 0.21372 kg/m-s

In order to determine if changing the properties would decrease the variance from that observed in Table 4.3, we changed, for simulation purpose, the properties of oil and alginate as follows:

Olive oil: Density 918 kg/m3

Viscosity 0.084 kg/m-s

Alginate: Density 998.2 kg/m3

Viscosity 0.001003 kg/m-s

The biggest change was in the viscosity of alginate which made it closer to water. Run Exp100-16 represented the low viscosity of alginate. Comparisons of the mean and

Reproduced with permission of the copyright owner. Further reproduction prohibited without permission.

standard deviation for Exp100-15 and Exp100-16 show that the means are almost the same, but the variance for the low viscosity (Exp100-16 run) was much smaller than that for Exp100-15. The variance changed from 11.3 to 7.97 for the short diameter and from 17.5 to 9.18 for the long diameter. It should be noted that since density and viscosity for oil and alginate are what they are, changing the viscosity or density for simulation purposes would imply that in practice one should use other materials for generating a droplet size with low variance or coefficient of variation.

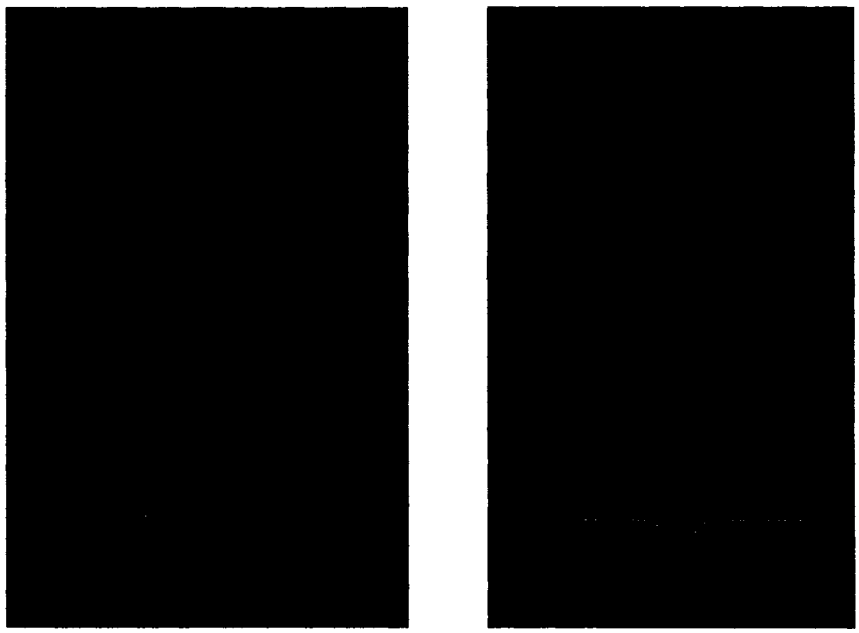

Figure 4.8. (a) Exp100-15 and (b) Exp100-16 alginate volume fraction contours.

4.5 Future Work

In this research, the velocity and ratio were considered as two factors. One can obtain the desired particle size by adjusting these two factors affecting the size of generated microcapsules. Also, it was observed that the properties of the two immiscible phases can influence the variance. In all the above simulations, the channel was straight with the width fixed at 100 micrometers. In future work, it would be of interest to

Reproduced with permission of the copyright owner. Further reproduction prohibited without permission.

determine if channel width and or geometry will have any effect on droplet size and variance.

Reproduced with permission of the copyright owner. Further reproduction prohibited without permission.

CHAPTER 5

MODELING OF TRANSPORT PHENOMENA

5.1 Introduction

"The main focus in the area of emulsion technology is to improve stability and control the release of active matter in double emulsions" (Lyon, 2002). Because of the permeability property of a microcapsule's wall, microencapsulation is an important technique used to protect the inner materials from the outer materials or to control the release of the encapsulated inner materials. In so many applications of microcapsules, a critical question is how to control the transport phenomena. To develop a theoretical model, it is necessary to determine how different factors can influence the transport phenomena. These factors include type and thickness of the wall, loading time of the inner material, pH value, temperature, and molecular weight of the inner material (Takagishi, 1994; Antipov, 2002; Kim, 2004; Yang, 2005; Pargaonkar, 2005; Windhab, 2005; Tong, 2006).

Due to the semipermeability of the capsule wall, Tong (2006) created a Donnan equilibrium between the inner solution within the capsules and the bulk solution. Kwok et al. (1991) developed a general diffusion model for alginate-polylysine (PLL) microcapsules which can describe mass transport phenomena and membrane diffusivities.

Reproduced with permission of the copyright owner. Further reproduction prohibited without permission.

In this chapter, the finite difference method is applied to model the transport phenomena of microcapsules.

5.2 Experimental Procedure

Layer-by-layer assembly of oppositely charged polyelectrolyte onto removable colloidal particle surfaces has been used by many groups because of its potential application (Radtchenko, 2000; Antipov, 2002; Tong, 2006). At the Institute for Micromanufacturing (IFM), Louisiana Tech University, poly (styrene sulfonate) (PSS), poly (vinylsulfat) (PVS), poly (allylamine) (PAH) and poly (diallyldimethylammonium chloride) (PDDA) are the four polyelectrolytes used in layer-by-layer encapsulation of microsphere colloidal core material (melamine formal dehyde (MF)) to obtain multilayer microcapsules.

5.2.1 Preparation of the Materials

Polyelectrolyte solutions: 1 mg/ml PSS or PAH with 20 mM of Tris-buffer and 0.5 M NaCl.

Solvent solution: 0.1 MHCI.

Dextran solution: 0.15 mg/ml of 4000MW FITC-dextran or 0.14 mg/ml of 77,000 MW FITC-dextran.

Core particles: melamine formaldehyde (MF) colloidal core particles of 5.3 μm in diameter.

5.2.2 Process

- Layer deposition: Polyelectrolyte PSS or PAH layer is deposited onto the MF core material by incubation for 15 min in the polyelectrolyte solution sequentially. After depositing every layer, the particles are washed three

Reproduced with permission of the copyright owner. Further reproduction prohibited without permission.

times in a 121 mM Tris-buffer solution and centrifuged at 6000 rpm for 5 min to remove the wash.

- Dissolving the melamine formaldehyde core: A 0.1 MHCI solution is used to dissolve the core after depositing the desired layers. Centrifugation during the wash after core removal is performed at 3000 rpm for 8 min to minimize damage to the resultant shells.
- Loading dextran: 0.15 mg/ml of 4000MW FITC-dextran or 0.14 mg/ml of 77,000 MW FITC-dextran is loaded into the hollow microcapsules from the above procedure for 12, 36, and 60 h at a pH of 7. Seven washes are performed with 20 mM Tris-buffer to remove loosely associated FITC labeled dextran.
- Transport phenomena: The prepared FITC labeled dextran microcapsules are immersed into the mother-liquor (or bulk) to study the transport phenomena. A Quanta Master TM Model QM-2000-4 excitation/emission spectrofluorometer is used to quantify the concentration of FITC labeled dextran in the mother-liquor of the sample.

5.3 Governing Equations

$$\frac{\partial C}{\partial t} = D_i \frac{1}{r^2} \frac{\partial}{\partial r}\left(r^2 \frac{\partial C}{\partial r}\right) \tag{5.1}$$

where C stands for the concentration.

t stands for the loading time,

Di stands for the ith diffusion coefficient, in the core (i=1), wall membrane (i=2), and bulk liquid (i=3),

Reproduced with permission of the copyright owner. Further reproduction prohibited without permission.

r stands for the radial distance from the center.

In this model, we assume that the core diffusion coefficient (D_1) and the membrane diffusion coefficient (D_2) and outside medium diffusion coefficient (D_3) are constant and not a function of distance or time.

In all experiments, dextran was first allowed to diffuse into the microcapsules for a certain length of time (loading period). After the loading was complete, the microcapsules were immersed in a water medium where dextran was released to the outside. Both loading and release are transfer phenomena and can be simulated by the diffusion model in Equation 5.1 with different initial and boundary conditions.

Loading Initial Conditions:

$$C(r,0) = 0,\ 0 \le r < R_2 \tag{5.2.1}$$

$$C(r,0) = C_{out}, R_2 \le r < R_3, \tag{5.2.2}$$

where R_2 stands for the radius of the microcapsule.

R_3 stands for the radius of the total area, microcapsule and outside medium

$C(r,0)$ stands for the concentration of dextran at position r at time 0.

C_{out} stands for the concentration of dextran in the outside medium and was equal to 0.14 mg/ml.

Initial conditions are the conditions at t = 0. So at time 0, the dextran concentrations in the core and in the membrane were 0. In the outside medium, the concentration was 0.14.

Loading Boundary Conditions:

Reproduced with permission of the copyright owner. Further reproduction prohibited without permission.

$$\frac{\partial C_1}{\partial r} = 0, r = 0 \tag{5.3.1}$$

$$D_1 \frac{\partial C_1}{\partial r} = D_2 \frac{\partial C_2}{\partial r}, r = R_1 \tag{5.3.2}$$

$$C_1 = C_2, r = R_1 \tag{5.3.3}$$

$$D_2 \frac{\partial C_2}{\partial r} = D_3 \frac{\partial C_3}{\partial r}, r = R_2 \tag{5.3.4}$$

$$C_2 = C_3, r = R_2 \tag{5.3.5}$$

$$\frac{\partial C_3}{\partial r} = 0, r = R_3 \tag{5.3.6}$$

where C_1 stands for the dextran concentration in the core.

C_2 stands for the dextran concentration in the membrane.

C_3 stands for the dextran concentration in the outside medium.

D_1, D_2, and D_3 are the diffusion coefficients of core material, membrane and liquid bulk (outside medium).

Release Initial Conditions

$$C(r,0) = C(r,t), \ 0 \le r < R_2 \tag{5.4.1}$$

$$C(r,0) = 0, R_2 \le r < R_3, \tag{5.4.2}$$

where R_2 stands for the radius of the microcapsule.

$C(r,0)$ stands for the concentration of dextran at position r at time 0.

$C(r,t)$ stands for the concentration of dextran at position r at time t,

where t is the loading time.

Initial conditions are the conditions at time 0. As is known from the experimental conditions, the microcapsules were loaded with dextran for a certain time, t. So the initial

Reproduced with permission of the copyright owner. Further reproduction prohibited without permission.

condition for the release process is $C(r,t)$, which is the dextran concentration at position r at time t. C(r,t) is obtained from the diffusion model during loading time.

Release Boundary Conditions:

$$\frac{\partial C_1}{\partial r} = 0, r = 0 \tag{5.5.1}$$

$$D_1 \frac{\partial C_1}{\partial r} = D_2 \frac{\partial C_2}{\partial r}, r = R_1 \tag{5.5.2}$$

$$C_1 = C_2, r = R_1 \tag{5.5.3}$$

$$D_2 \frac{\partial C_2}{\partial r} = D_3 \frac{\partial C_3}{\partial r}, r = R_2 \tag{5.5.4}$$

$$C_2 = C_3, r = R_2 \tag{5.5.5}$$

$$\frac{\partial C_3}{\partial r} = 0, r = R_3 \tag{5.5.6}$$

where C_1 stands for the dextran concentration in the core.

C_2 stands for the dextran concentration in the membrane.

C_3 stands for the dextran concentration in the bulk.

D_1, D_2, and D_3 are the diffusion coefficients of core material, membrane and bulk.

5.4 Calculation of Transport Phenomena Based on Governing Equations

5.4.1 Fractional Crank-Nicholson Method

More and more scientific and engineering problems involve fractional calculus. Recently, Metzler et al. (1999), Barkai et al. (2000), Metzler et al. (2000) proposed a fractional Fokker-Planck equation to describe subdiffusive anomalous transport in the

Reproduced with permission of the copyright owner. Further reproduction prohibited without permission.

presence of an external field. This equation becomes the fractional partial differential equation for the force-free case (Balakrishnan, 1985; Scalas et al., 2004; Metzler et al., 2000; Schneider et al., 1988).

The Crank-Nicholson method is applied for solving the governing spherical finite difference equations. This method uses central differences rather than the forward difference of the Euler method or the backward difference of the backward Euler. The Crank-Nicholson method is also called the 5-point method. Every point is related to the adjacent five points as shown in Figure 5.1.

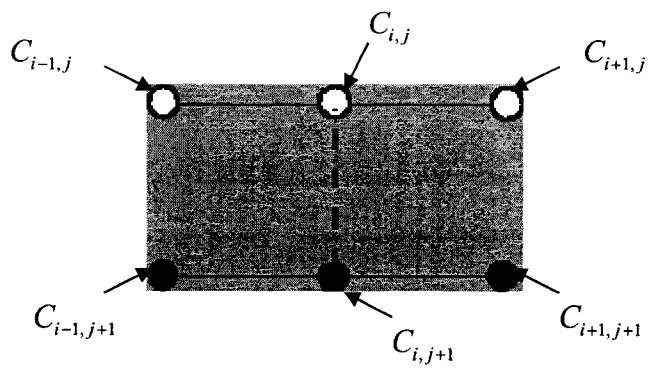

Figure 5.1. Five-point method

$C_{i,j}$ represents the dextran concentration at position i at time j. In the Crank-Nicholson method, the calculation of a value at a given point depends on the five adjacent points.

Crank-Nicholson method:

$$\frac{C_{i,j+1}-C_{i,j}}{\Delta t}=\theta\frac{D}{r_i^2}\frac{1}{2\Delta r^2}[r^2_{j+\frac{1}{2}}(C_{i+1,j+1}-C_{i,j+1})-r^2_{j-\frac{1}{2}}(C_{i,j+1}-C_{i-1,j+1})]$$
$$+(1-\theta)\frac{D}{r_i^2}\frac{1}{2\Delta r^2}[r^2_{j+\frac{1}{2}}(C_{i+1,j}-C_{i,j})-r^2_{j-\frac{1}{2}}(C_{i,j}-C_{i-1,j})] \quad (5.6.1)$$

Reproduced with permission of the copyright owner. Further reproduction prohibited without permission.

where θ is the weight factor,

If θ=1, Equation 5.6.1 gives rise to the fractional explicit method (Yuste et al., 2003; Yuste et al., 2004).

If θ is not equal to 1, the method is implicit.

If θ=0, the method is fully implicit.

If θ=1/2, Equation 5.6.1 is the fractional Crank-Nicholson method.

For θ=1/2 and $\mu = \frac{D}{r_i^2}\frac{1}{2\Delta r^2}$, Equation 5.6.1 is re-written as follows:

$$\begin{aligned} &\mu r^2_{j+\frac{1}{2}} C_{i+1,j+1} + (-\mu r^2_{j+\frac{1}{2}} - \mu r^2_{j-\frac{1}{2}} - 1) C_{i,j+1} + \mu r^2_{j-\frac{1}{2}} C_{i-1,j+1} \\ &= -\mu r^2_{j+\frac{1}{2}} C_{i+1,j} + (\mu r^2_{j+\frac{1}{2}} + \mu r^2_{j-\frac{1}{2}} - 1) C_{i,j} - \mu r^2_{j-\frac{1}{2}} C_{i-1,j} \end{aligned} \tag{5.6.2}$$

5.4.2 Stability Analysis

It is known that the exact solution of the differential equation can be expressed as a Fourier series. The Fourier mode of the fractional Crank-Nicholson method is as follows:

$$C_{i,j} = (\lambda)^n e^{ik(j\Delta x)} \tag{5.7.1}$$

where $\lambda = \dfrac{1 - 2D\sin^2\frac{1}{2}k\Delta x}{1 + 2D\sin^2\frac{1}{2}k\Delta x}$ (5.7.2)

λ is called the amplification factor for the mode. This mode will be stable as long as $(\lambda)^n$ is bounded as $n \to \infty$. In other words, $0 < \lambda <= 1$ is the requirement if the mode is to be stable. The diffusion coefficient D is larger than 0. As a result, λ cannot be larger than 1. Since this is a three-region diffusion model, D has different values for different regions. D_{mem} stands for the diffusion coefficient of the membrane. D_{core} and D_{out} stand

Reproduced with permission of the copyright owner. Further reproduction prohibited without permission.

for the diffusion coefficients in the core and bulk or outside solution. The diffusion coefficients in the core and bulk can be large enough to cause λ to become negative, which leads to an unstable mode. In order to attain stability, the fully implicit scheme was used in the core and bulk regions.

5.4.3 Thomas Algorithm

Concentrations C at different positions at different times are the variables in Equation 5.6.2. $C_{i-1,j}$, $C_{i,j}$, and $C_{i+1,j}$ on the right hand side of the equation are the concentrations at positions i-1, i, and i+1 at the previous time step j. We can consider these three variables as known. $C_{i-1,j+1}$, $C_{i,j+1}$, and $C_{i+1,j+1}$ on the right hand of the equation are the concentrations at positions i-1, i, and i+1 at the new time step j+1, which are considered as unknown. Equation 5.6.2 can be simplified as follows:

$$\begin{aligned} &-b_i C_{i-1,j+1} + a_i C_{i,j+1} - c_i C_{i+1,j+1} = d_i, i = 1,.....,n \\ &C_{o,j+1} = C_{1,j+1}, C_{n-1,j+1} = C_{n,j+1} \end{aligned} \tag{5.8}$$

Here, a_i, b_i, c_i are the coefficients corresponding to Equation 5.6.2 and d_i is a term related to $C_{i-1,j}, C_{i,j}, C_{i+1,j}$. In other words, when the new time step i+1 is calculated, d_i can be considered as known from the previous time step. For every three adjacent points, we can get an equation like Equation 5.8. So for all the n+1 points in the domain, we can get n-1 schemes like the above one. All the schemes can be written in matrix form as follows:

Reproduced with permission of the copyright owner. Further reproduction prohibited without permission.

$$\begin{bmatrix} a_1 - b_1 & -c_1 & & & & & & \\ -b_2 & a_2 & -c_2 & & & & & \\ & \cdot & \cdot & \cdot & & & & \\ & & \cdot & \cdot & \cdot & & & \\ & & & -b_i & a_i & -c_i & & \\ & & & & \cdot & \cdot & \cdot & \\ & & & & & \cdot & \cdot & \cdot \\ & & & & & & -b_{n-1} & a_{n-1} & c_{n-1} \\ & & & & & & & -b_n & a_n - c_n \end{bmatrix} \begin{bmatrix} C_{1,j+1} \\ C_{2,j+1} \\ \cdot \\ \cdot \\ C_{i,j+1} \\ \cdot \\ \cdot \\ C_{n-1,j+1} \\ C_{n,j+1} \end{bmatrix} = \begin{bmatrix} d_1 \\ d_2 \\ \cdot \\ \cdot \\ d_i \\ \cdot \\ \cdot \\ d_{n-1} \\ d_n \end{bmatrix}$$

(5.9)

The usual approach to solve tridiagonal linear systems is the Thomas algorithm (William, 1941). The forward Thomas algorithm is shown as follows:

- When $i = 1$, Equation 5.8 is applied to give

$$-b_1 C_{0,j+1} + a_1 C_{1,j+1} - c_1 C_{2,j+1} = d_1 \tag{5.10.1}$$

At the boundary condition, $C_{o,j+1} = C_{1,j+1}$, so the terms are combined to give Equation 5.10.2.

$$(a_1 - b_1) C_{1,j+1} - c_1 C_{2,j+1} = d_1 \tag{5.10.2}$$

Both sides are divided by $(a_1 - b_1)$ to give

$$C_{1,j+1} = \frac{d_1}{a_1 - b_1} + \frac{c_1}{a_1 - b_1} C_{2,j+1} = f_1 + e_1 C_{2,j+1} \tag{5.10.3}$$

- When $i = 2$, Equation 5.8 becomes

$$-b_2 C_{1,j+1} + a_2 C_{2,j+1} - c_2 C_{3,j+1} = d_2 \tag{5.10.4}$$

Equation 5.10.4 is simplified by applying Equation 5.10.3 to obtain Equation 5.10.5.

$$C_{2,j+1} = \frac{d_2 + b_2 f_1}{a_2 - b_2 e_1} + \frac{c_2}{a_2 - b_2 e_1} C_{3,j+1} = f_2 + e_2 C_{3,j+1} \tag{5.10.5}$$

Reproduced with permission of the copyright owner. Further reproduction prohibited without permission.

- When i=1,….., n, the general equation is

$$C_{i,j+1} = f_i + e_i C_{i+1,j+1}, i = 1,....,n \tag{5.10.6}$$

$$e_i = \frac{c_i}{a_i - b_i e_{i-1}}, i = 1,...., n, e_0 = 0 \tag{5.10.7}$$

$$f_i = \frac{d_i + b_i f_{i-1}}{a_i - b_i e_{i-1}}, i = 1,...., n, f_0 = 0 \tag{5.10.8}$$

Using the same approach, the backward Thomas algorithm can be obtained. The general equation is as follows:

$$C_{i+1,j+1} = fb_{i+1} + eb_{i+1} C_{i,j+1}, i = 0,....., n-1 \tag{5.10.9}$$

$$eb_i = \frac{b_i}{a_i - b_i eb_{i+1}}, i = 1,...., n-1, eb_n = 0 \tag{5.10.10}$$

$$fb_i = \frac{d_i + c_i fb_{i+1}}{a_i - c_i eb_{i+1}}, i = 1,...., n-1, fb_n = 0 \tag{5.10.11}$$

The algorithm introduced above is easy to use in a SIMD (Single Instruction, Multiple Data). A new parallel method was introduced by Dai (2000) for time saving. The problem can be decomposed into a number of independent sub-problems and all the sub-problems can be preceded independently. Later on, the solutions of all the independent sub-problems can be combined to obtain the solution of the original problem. The parallel application for this research is shown as follows:

- $0 \le r < R_1$, the core material. The forward Thomas algorithm is applied as in Equation 5.10.6. At the inside of the membrane, the concentrations satisfy the following conditions.

$$C_{R_1-1,j+1} = f_{R_1-1} + e_{R_1-1} C_{R_1,j+1} \tag{5.11.1}$$

$$D_1(C_{R_1,j+1} - C_{R_1-1,j+1}) = D_2(C_{R_1+1} - C_{R_1}) \tag{5.11.2}$$

Reproduced with permission of the copyright owner. Further reproduction prohibited without permission.

Equations 5.11.1 and 5.11.2 are combined to eliminate the variable $C_{R_1-1,j+1}$. This gives

$$C_{R_1+1,j+1} = (\frac{D_1}{D_2} + \frac{D_1}{D_2} e_{R_1-1} + 1)C_{R_1,j+1} - \frac{D_1}{D_2} f_{R_1-1} \tag{5.11.3}$$

- $R_2 \le r$, the liquid bulk. The backward Thomas algorithm is applied as in Equation 5.10.9. At the outside of the membrane, the concentrations need to satisfy the following conditions.

$$C_{R_2+1,j+1} = fb_{R_2+1} + eb_{R_2+1} C_{R_2,j+1} \tag{5.11.4}$$

$$D_2(C_{R_2,j+1} - C_{R_2-1,j+1}) = D_2(C_{R_2+1} - C_{R_2}) \tag{5.11.5}$$

Equations 5.11.4 and 5.11.5 are combined to obtain Equation 5.11.6.

$$C_{R_2-1,j+1} = (\frac{D_3}{D_2} - \frac{D_3}{D_2} eb_{R_2+1} + 1)C_{R_2,j+1} - \frac{D_3}{D_2} fb_{R_2+1} \tag{5.11.6}$$

- $R_1 \le r < R_2$, the membrane material. The following equations are applied in that region.

$$C_{R_1+1,j+1} = \tilde{f}_{R_1+1} + \tilde{e}_{R_1+1} C_{R_1,j+1} + g_{R_1+1} C_{R_2,j+1} \tag{5.11.7}$$

$$C_{R_2-1,j+1} = \tilde{f}b_{R_2-1} + \tilde{e}b_{R_2-1} C_{R_2,j+1} + gb_{R_2-1} C_{R_1,j+1}, \tag{5.11.8}$$

where $$\tilde{e}_{R_1+1} = \frac{c_{R_1+1}}{a_{R_1+1} - b_{R_1+1}\tilde{e}_{R_1}}, \tilde{e}_{R_1} = 0 \tag{5.11.9}$$

$$\tilde{f}_{R_1+1} = \frac{d_{R_1+1} + b_{R_1+1}\tilde{f}_{R_1}}{a_{R_1+1} - b_{R_1+1}\tilde{e}_{R_1}}, \tilde{f}_{R_1} = 0 \tag{5.11.10}$$

$$g_{R_1+1} = \frac{b_{R_1+1} g_{R_1}}{a_{R_1+1} - \tilde{e}_{R_1} b_{R_1+1}}, g_{R_1} = 1 \tag{5.11.11}$$

Reproduced with permission of the copyright owner. Further reproduction prohibited without permission.

$$\tilde{e}b_{R_2-1} = \frac{b_{R_2-1}}{a_{R_2-1} - c_{R_2-1}\tilde{e}_{R_2}}, \tilde{e}_{R_2} = 0 \tag{5.11.12}$$

$$\tilde{f}b_{R_2-1} = \frac{d_{R_2-1} + c_{R_2-1}\tilde{f}b_{R_2}}{a_{R_2-1} - c_{R_2-1}\tilde{e}b_{R_2}}, \tilde{f}b_{R_2} = 0 \tag{5.11.13}$$

$$gb_{R_2-1} = \frac{c_{R_2-1}gb_{R_2}}{a_{R_2-1} - \tilde{e}b_{R_2}c_{R_2-1}}, gb_{R_2} = 1 \tag{5.11.14}$$

Equations 5.11.3, 5.11.6, 5.11.7 and 5.11.8 can be used to solve for $C_{R_1,j+1}$ and $C_{R_2,j+1}$, which are used to calculate all the concentrations at any position at the new time step.

The parallel procedure is as follows:

- Calculate e_i and $f_i, i = 0,....,R_1$, and calculate Equation 5.11.3.

$$C_{R_1+1,j+1} = (\frac{D_1}{D_2} + \frac{D_1}{D_2}e_{R_1-1} + 1)C_{R_1,j+1} - \frac{D_1}{D_2}f_{R_1-1}$$

- Calculate $\tilde{e}_{R_1+1}, \tilde{f}_{R_1+1}$ and g_{R_1+1} to obtain Equation 5.11.7.

$$C_{R_1+1,j+1} = \tilde{f}_{R_1+1} + \tilde{e}_{R_1+1}C_{R_1,j+1} + g_{R_1+1}C_{R_2,j+1}$$

- Calculate $\tilde{e}b_{R_2-1}, \tilde{f}b_{R_2-1}$ and gb_{R_2-1} to obtain Equation 5.11.8.

$$C_{R_2-1,j+1} = \tilde{f}b_{R_2-1} + \tilde{e}b_{R_2-1}C_{R_2,j+1} + gb_{R_2-1}C_{R_1,j+1}$$

- Calculate eb_i and fb_i, $i = R_2,.....N$, and calculate Equation 5.11.6.

$$C_{R_2-1,j+1} = (\frac{D_3}{D_2} - \frac{D_3}{D_2}eb_{R_2+1} + 1)C_{R_2,j+1} - \frac{D_3}{D_2}fb_{R_2+1}$$

- Solve for $C_{R_1,j+1}$ and $C_{R_2,j+1}$ using the above four equations.

Reproduced with permission of the copyright owner. Further reproduction prohibited without permission.

- Calculate all concentrations at any position at the new time step using Eqs. 5.11.1 and 5.11.4.

5.4.4 Inverse Problem

5.4.4.1 Introduction. Inverse analyses have many applications in various branches of science and engineering such as that of chemical engineering, geophysics and statistics. Difficulties arise with the implementation of an inverse analysis. The main difficulty is that the inverse solution may not be unique, because it is very sensitive to the changes in input data resulting from measurement and modeling errors. Inverse problems cannot satisfy the general requirement of existence, uniqueness, and stability under small changes in the data, so they belong to the ill-posed problems mathematically.

Inverse problems have attracted the interests of many scientists and engineers. Many analytic and numerical approaches have applied to inverse problems. The Duhamel method was utilized by Stoltz (2004) to develop an analytic solution for a linear inverse heat conduction problem. As one of the earliest investigators, Stoltz offered us a good insight into the problem. Stolz's solution, however, was found to be unstable for small time steps. In the nonlinear case, the finite difference method (FDM) and the finite element method (FEM) were used to solve the inverse heat conduction problems (IHCP).

5.4.4.2 Inverse Solution and Least Squares. In this research, a diffusion formulation and solution is presented to simultaneously estimate the unknown diffusion coefficients. Because the inverse solution can minimize the least squares norm, the existence of the inverse solution is guaranteed.

$$S(\hat{p}) = \sum_{i=1}^{\Omega} [Y_i - \hat{T}_i(p_j)]^2 \,, \quad j = 1,2 \tag{5.12.1}$$

Reproduced with permission of the copyright owner. Further reproduction prohibited without permission.

where Y_i stands for the measured concentration,

$\hat{T}_i(\hat{p}_j)$ stands for the estimated concentration obtained from the solution of the direct problem by using the estimated values of the unknown parameters,

$\hat{p}_j$ stands for the elements of the unknown parameter vector $\hat{p} = \{D_1, D_2\}^T$, and Ω stands for the total number of the measurements.

The sum of squares can be minimized by differentiating it with respect to each of the unknown parameters $\hat{p}_j$ (j=1, 2) and then setting the resulting expression equal to zero.

$$\frac{\partial S}{\partial \hat{p}_j} = 2\sum_{i=1}^{\Omega}\left(\frac{\partial \hat{T}_i}{\partial \hat{p}_j}\right)(\hat{T}_i(\hat{p}) - Y_i) = 0, j = 1,2 \qquad (5.12.2)$$

Equation 5.13.2 is written in matrix form as

$$\frac{\partial S}{\partial \hat{p}} = 2X^T(T - Y) = 0, \qquad (5.12.3)$$

where $T = \begin{bmatrix} T_1 \\ T_2 \\ \cdots \\ T_\Omega \end{bmatrix}, Y = \begin{bmatrix} Y_1 \\ Y_2 \\ \cdots \\ Y_\Omega \end{bmatrix}, \hat{p} = \begin{bmatrix} \hat{p}_1 \\ \hat{p}_2 \end{bmatrix}$, and $X = \frac{\partial T}{\partial \hat{p}^T} = \begin{bmatrix} \frac{\partial \hat{T}_1}{\partial \hat{p}_1} & \frac{\partial \hat{T}_1}{\partial \hat{p}_2} \\ \frac{\partial \hat{T}_2}{\partial \hat{p}_1} & \frac{\partial \hat{T}_2}{\partial \hat{p}_2} \\ \\ \frac{\partial \hat{T}_\Omega}{\partial \hat{p}_1} & \frac{\partial \hat{T}_\Omega}{\partial \hat{p}_2} \end{bmatrix}$

X is the sensitivity coefficient matrix with respect to p.

Reproduced with permission of the copyright owner. Further reproduction prohibited without permission.

5.4.4.3 Levenberg-Margquardt Method. We can see that the system of equations in Equation 5.12.3 is nonlinear, so an iterative technique is required here to get the solution. The modified Levenberg-Marquardt (LM) algorithm, a combination of the Newton method and the steepest descent method, can be used to solve the nonlinear least squares equations by iteration (Ozisik, 1993).

$$\hat{p}^{k+1} = \hat{p}^{k} + (J^T J + \mu_k I)^{-1} J^T (Y - T), k = 1,2,3,.... \qquad (5.12.4)$$

where $\hat{p} = \{D_1, D_2\}^T$ = estimated parameter vector,

Y stands for the measured concentration,

μ_k stands for damping parameters, and

$J = X$ = the sensitivity coefficient matrix with respect to p.

The speed of the Levenberg-Marquardt (LM) iterative least-squares method for the nonlinear problem depends upon the choice of the damping parameters. To solve difficult problems efficiently, LM requires additive damping with small damping increments and large damping decrements, Lampton (1997).

5.4.4.4 The Solution Algorithm with LM. The following is the solution algorithm with the LM method.

1. Solve Equation 5.1 with the FDM using the estimated values of $\hat{p} = \{D_1, D_2\}^T$ and compute T, the estimated concentration obtained from the solution of the direct problem by using the estimated values of the unknown parameters.

Reproduced with permission of the copyright owner. Further reproduction prohibited without permission.

2. Solve Equation 5.1 with the FDM two more times with different parameters

$$T(D_1 + \Delta D_1, D_2)$$
$$T(D_1, D_2 + \Delta D_2)$$

3. Compute the sensitivity coefficients matrix J using the solution from step 1 and 2. For example, with respect to D_1 we have

$$\frac{\partial T_i}{\partial D_1} = \frac{T(D_1 + \Delta D_1, D_2) - T(D_1, D_2)}{\Delta D_1}$$

4. Calculate $(J^T J + \mu_k I)^{-1} J^T (Y - T)$

5. Calculate $\hat{p}^{k+1}$

6. Restart from step 1 until the following criterion is satisfied

$$\frac{\left|S^{k+1} - S^k\right|}{S^{k+1}} < 1E-5$$

5.4.4.5 <u>Check on the Diffusion Model.</u> Mass balance was applied to check on the accuracy of the diffusion model. The estimation of core diffusivity and membrane diffusivity were obtained from the diffusion model. Using these estimates the total mass in the whole bulk area was calculated at different time steps. If the model is correct, one expects the total mass to remain constant over time. The Figure 5.1 is the total mass over time when I specify $D_1 = 18.7 \mu m^2/hr, D_2 = 5.9 \times 10^{-6} \mu m^2/hr$. It is seen from Figure 5.2 that, in fact, the total mass remains constant which indicates that the model is accurate.

Reproduced with permission of the copyright owner. Further reproduction prohibited without permission.

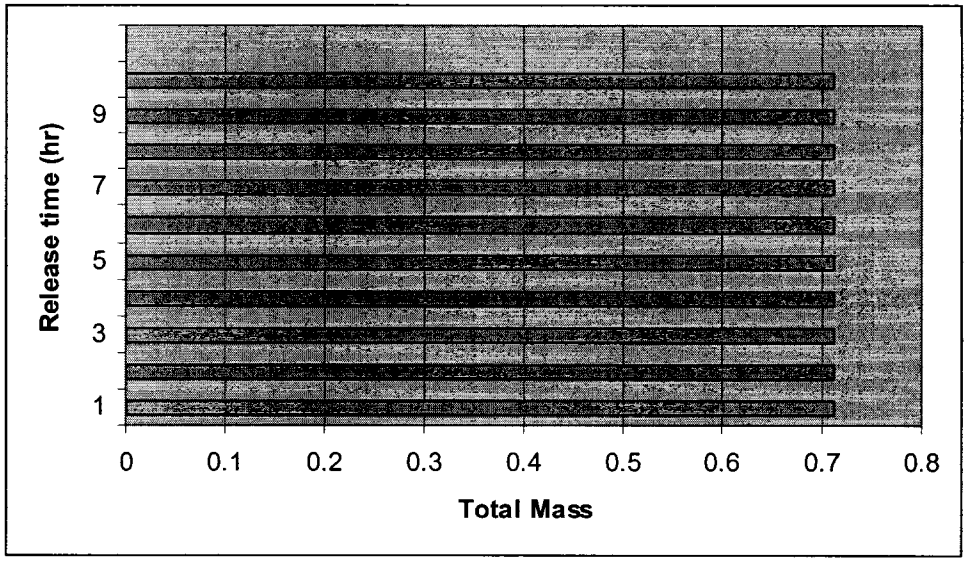

Figure 5.2. Total mass in the bulk over time

Reproduced with permission of the copyright owner. Further reproduction prohibited without permission.

CHAPTER 6

RESULTS AND DISCUSSION OF TRANSPORT PHENOMENA

6.1 Introduction

At the Institute for Micromanufacturing (IfM), Louisiana Tech University, poly (styrene sulfonate) (PSS), poly (vinylsulfat) (PVS), poly (allylamine) (PAH) and poly (diallyldimethylammonium) (PDDA) are the four polyelectrolytes used in layer-by-layer encapsulation of microsphere colloidal core material (melamine formal dehyde (MF)) to obtain multilayer microcapsules. A permeability comparison for different layers of PSS/PAH, PVS/PAH, PSS/PDDA and PVS/PDDA was made using 4000 MW or 7700 MW FITC-dextran loaded for 12h, 36h or 60h.

6.2 Comparisons of Experimental Data and Model Results

In fitting the model to the experimental observations, the radius of the bulk liquid, R, was taken to be 18.6 μm. This was determined from the ratio of the volume of the microcapsules in solution to the volume of the bulk solution. This ratio (estimated as 0.002439 from experimental conditions) is equal to

Reproduced with permission of the copyright owner. Further reproduction prohibited without permission.

$$Ratio = \frac{\frac{4}{3}\pi R_s^3}{\frac{4}{3}\pi R^3 - \frac{4}{3}\pi R_s^3} \tag{6.1}$$

where R_s is the radius of the microcapsule and is equal to 2.5 μm.

Comparisons of the experimental data and model results are shown in Figures. 6.1-6.47. The experimental data are the normalized concentration of dextran in the bulk liquid over time, recorded as the average of three measurements. The model results are the predicted values from the finite difference release phenomena model. It is seen from these figures that, in general, there is a very good fit of the model to the experimental observations.

The parameters D_1 and D_2 were estimated from fitting the model to the experimental data. The parameter D_3, is known and represents the diffusivity of dextran in water which was taken to be $6.28 \times 10^5 \mu m^2 / hr$.

Figure 6.1 shows that predicted (■) and observed (♦) normalized concentration of dextran released into the bulk liquid over time. Microcapsule wall is four layers of PSS/PAH. Loading time=12h, MW=4000. Sum of square error, SSE=0.067.

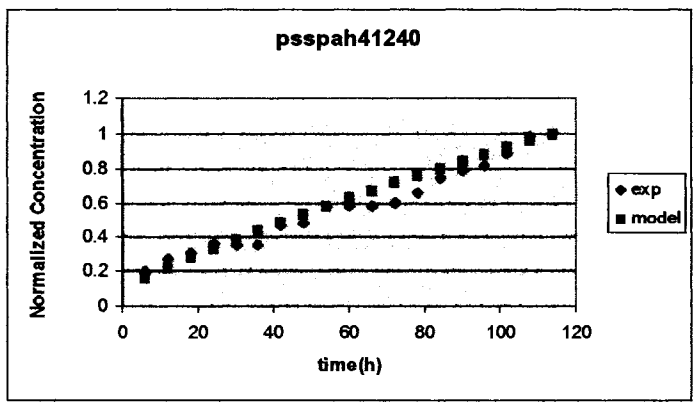

Figure 6.1. Psspah41240 predicted and observed normalized concentration of dextran

Reproduced with permission of the copyright owner. Further reproduction prohibited without permission.

Figure 6.2 shows that predicted (■) and observed (♦) normalized concentration of dextran released into the bulk liquid over time. Microcapsule wall is four layers of PSS/PAH. Loading time=12h, MW=77000. Sum of square error, SSE=0.056.

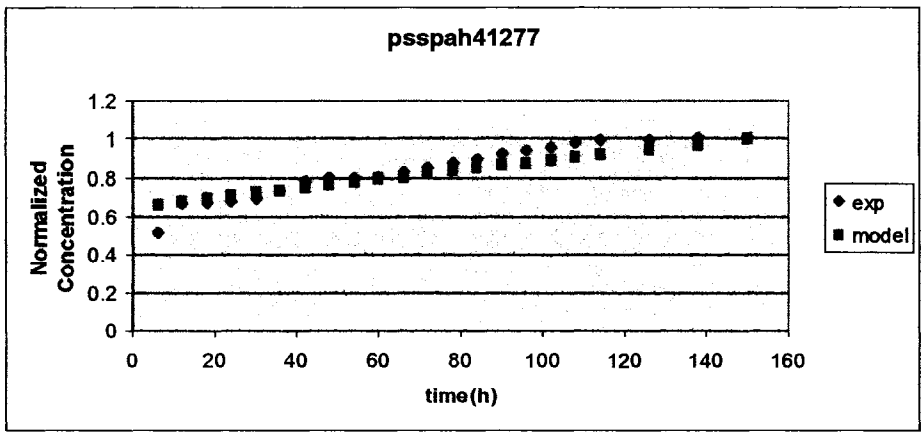

Figure 6.2. Psspah41277 predicted and observed normalized concentration of dextran

Figure 6.3 shows that predicted (■) and observed (♦) normalized concentration of dextran released into the bulk liquid over time. Microcapsule wall is four layers of PSS/PAH. Loading time=36h, MW=4000. Sum of square error, SSE=0.059625.

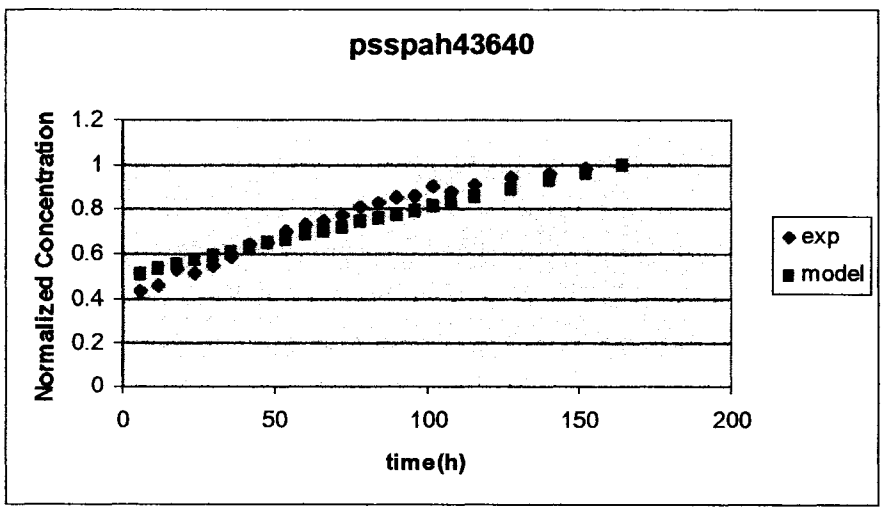

Figure 6.3. Psspah43640 predicted and observed normalized concentration of dextran

Reproduced with permission of the copyright owner. Further reproduction prohibited without permission.

Figure 6.4 shows that predicted (■) and observed (♦) normalized concentration of dextran released into the bulk liquid over time. Microcapsule wall is four layers of PSS/PAH. Loading time=36h, MW=77000. Sum of square error, SSE=0.03471.

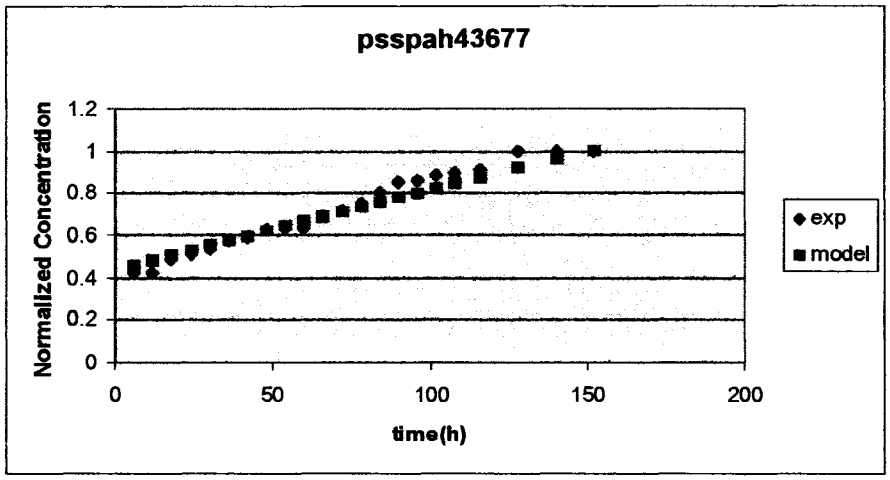

Figure 6.4. Psspah43677 predicted and observed normalized concentration of dextran

Figure 6.5 shows that predicted (■) and observed (♦) normalized concentration of dextran released into the bulk liquid over time. Microcapsule wall is four layers of PSS/PAH. Loading time=60h, MW=4000. Sum of square error, SSE=0.004871.

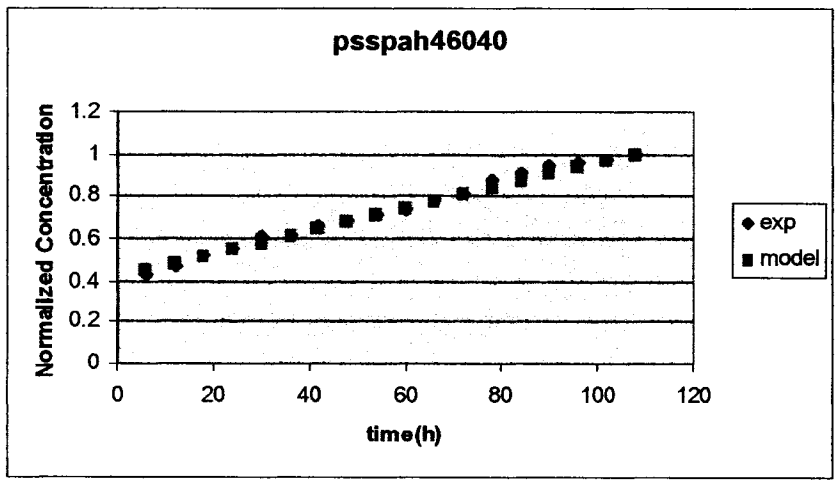

Figure 6.5. Psspah46040 predicted and observed normalized concentration of dextran

Reproduced with permission of the copyright owner. Further reproduction prohibited without permission.

Figure 6.6 shows that predicted (■) and observed (♦) normalized concentration of dextran released into the bulk liquid over time. Microcapsule wall is four layers of PSS/PAH. Loading time=60h, MW=77000. Sum of square error, SSE=0.002657.

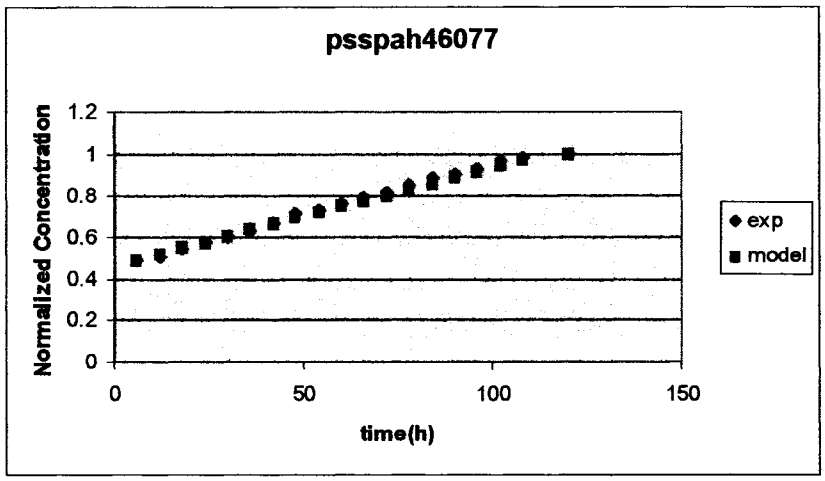

Figure 6.6. Psspah46-77 predicted and observed normalized concentration of dextran

Figure 6.7 shows that predicted (■) and observed (♦) normalized concentration of dextran released into the bulk liquid over time. Microcapsule wall is four layers of PVS/PAH. Loading time=12h, MW=4000. Sum of square error, SSE=0.007494.

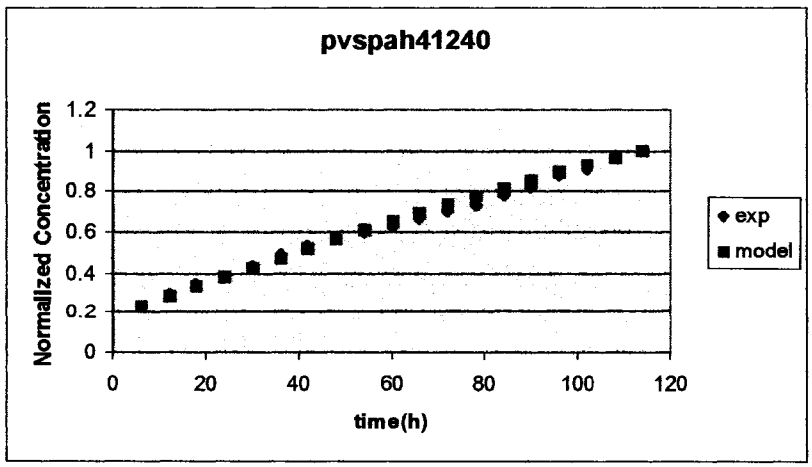

Figure 6.7. Pvspah41240 predicted and observed normalized concentration of dextran

Reproduced with permission of the copyright owner. Further reproduction prohibited without permission.

Figure 6.8 shows that predicted (■) and observed (♦) normalized concentration of dextran released into the bulk liquid over time. Microcapsule wall is four layers of PVS/PAH. Loading time=36h, MW=4000. Sum of square error, SSE=0.0757.

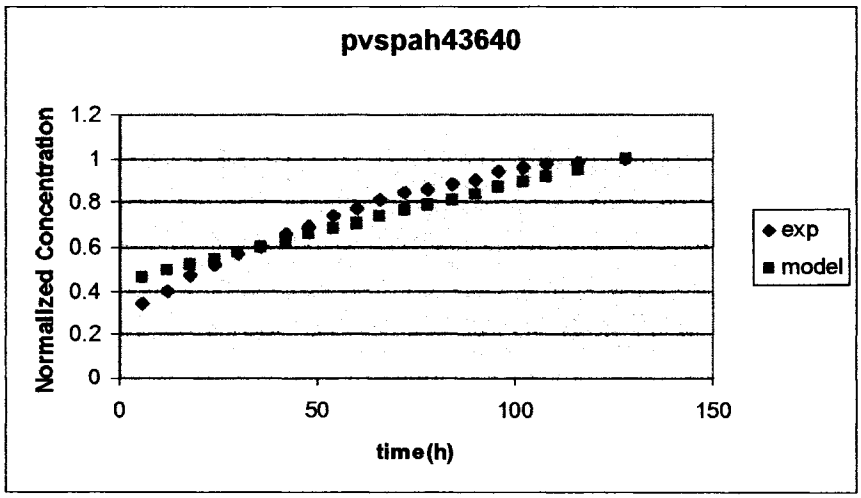

Figure 6.8. Pvspah43640 predicted and observed normalized concentration of dextran

Figure 6.9 shows that predicted (■) and observed (♦) normalized concentration of dextran released into the bulk liquid over time. Microcapsule wall is four layers of PVS/PAH. Loading time=36h, MW=77000. Sum of square error, SSE=0.002008.

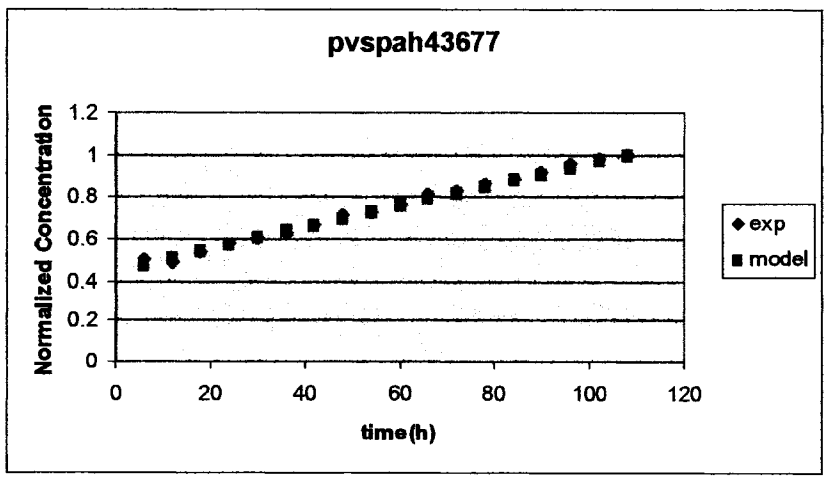

Figure 6.9. Pvspah43677 predicted and observed normalized concentration of dextran

Reproduced with permission of the copyright owner. Further reproduction prohibited without permission.

Figure 6.10 shows that predicted (■) and observed (♦) normalized concentration of dextran released into the bulk liquid over time. Microcapsule wall is four layers of PVS/PAH. Loading time=60h, MW=4000. Sum of square error, SSE=0.04956.

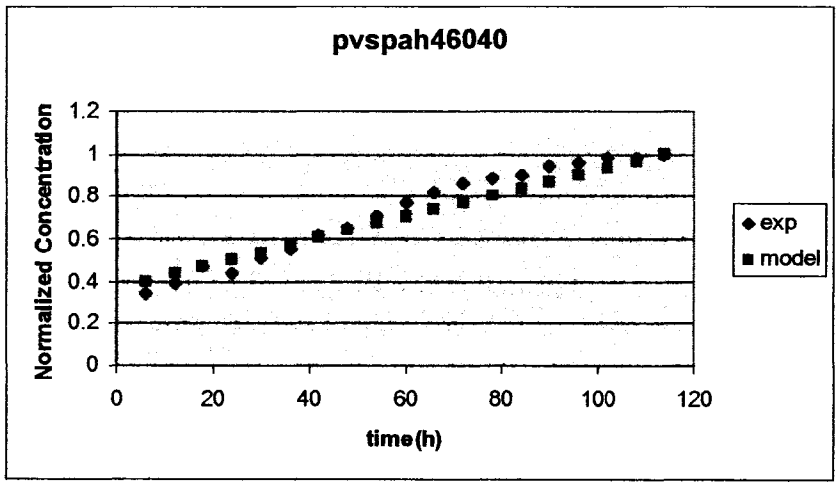

Figure 6.10. Pvspah46040 predicted and observed normalized concentration of dextran

Figure 6.11 shows that predicted (■) and observed (♦) normalized concentration of dextran released into the bulk liquid over time. Microcapsule wall is four layers of PVS/PAH. Loading time=60h, MW=77000. Sum of square error, SSE=0.030535.

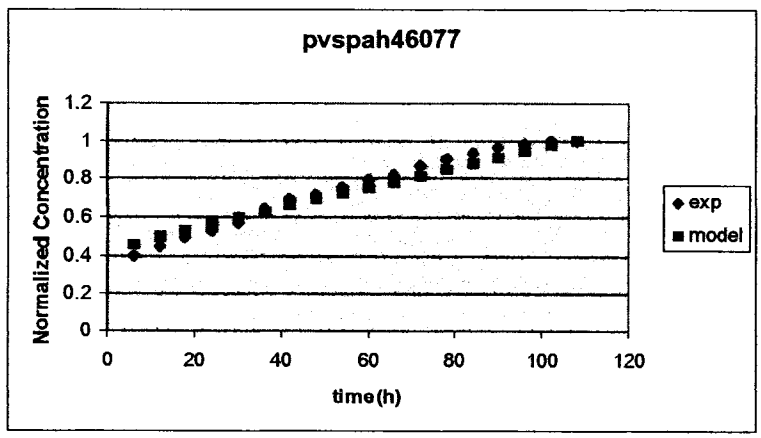

Figure 6.11. Pvspah46077 predicted and observed normalized concentration of dextran

Reproduced with permission of the copyright owner. Further reproduction prohibited without permission.

Figure 6.12 shows that predicted (■) and observed (♦) normalized concentration of dextran released into the bulk liquid over time. Microcapsule wall is two layers of PSS/PDDA. Loading time=12h, MW=4000. Sum of square error, SSE=0.00247.

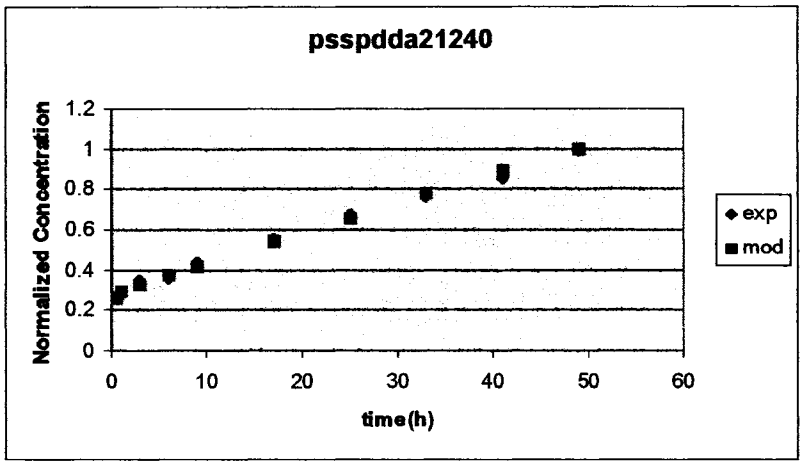

Figure 6.12. Psspdda41240 predicted and observed normalized concentration of dextran

Figure 6.13 shows that predicted (■) and observed (♦) normalized concentration of dextran released into the bulk liquid over time. Microcapsule wall is two layers of PSS/PDDA. Loading time=36h, MW=4000. Sum of square error, SSE=0.054048.

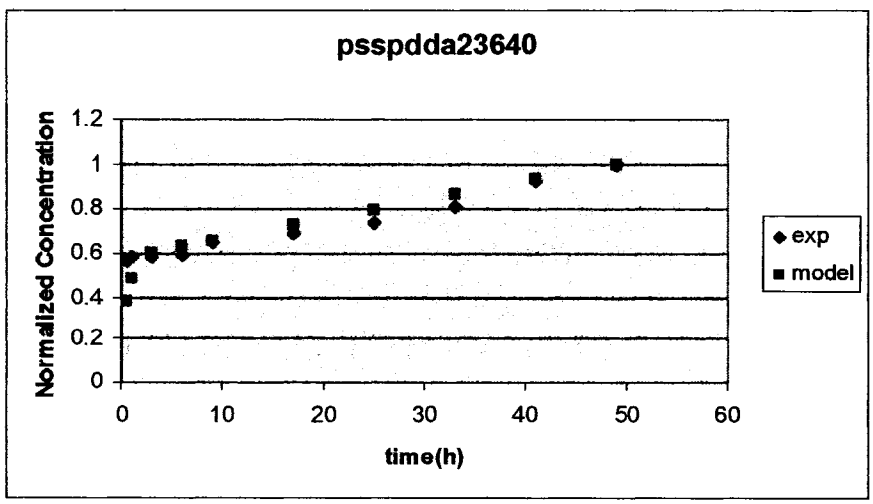

Figure 6.13. Psspdda23640 predicted and observed normalized concentration of dextran

Reproduced with permission of the copyright owner. Further reproduction prohibited without permission.

Figure 6.14 shows that predicted (■) and observed (♦) normalized concentration of dextran released into the bulk liquid over time. Microcapsule wall is two layers of PSS/PDDA. Loading time=60h, MW=4000. Sum of square error, SSE=0.032675.

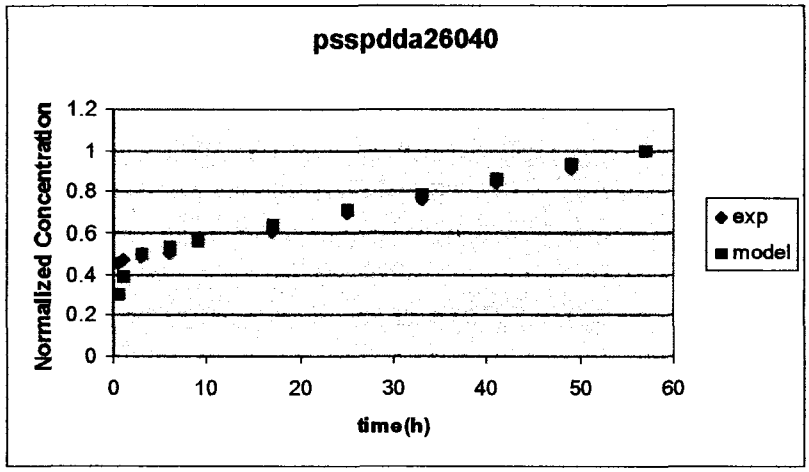

Figure 6.14. Psspdda26040 predicted and observed normalized concentration of dextran

Figure 6.15 shows that predicted (■) and observed (♦) normalized concentration of dextran released into the bulk liquid over time. Microcapsule wall is two layers of PSS/PDDA. Loading time=12h, MW=77000. Sum of square error, SSE=0.018417.

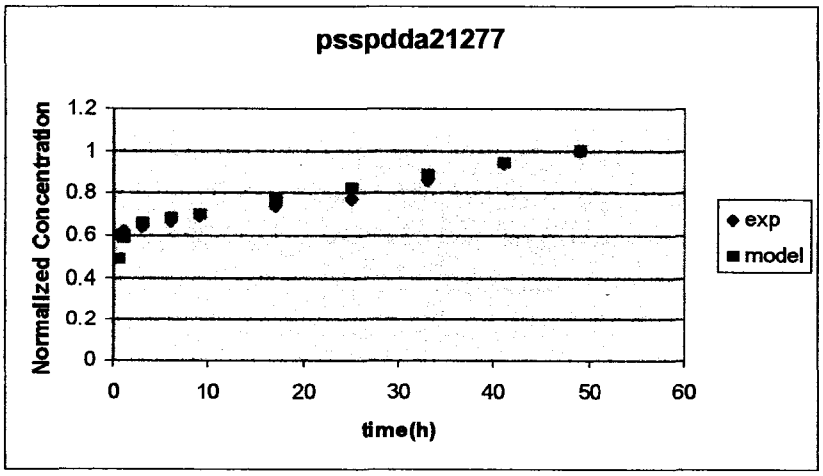

Figure 6.15. Psspdda21277 predicted and observed normalized concentration of dextran

Reproduced with permission of the copyright owner. Further reproduction prohibited without permission.

Figure 6.16 shows that predicted (■) and observed (♦) normalized concentration of dextran released into the bulk liquid over time. Microcapsule wall is two layers of PSS/PDDA. Loading time=36h, MW=77000. Sum of square error, SSE=0.057577.

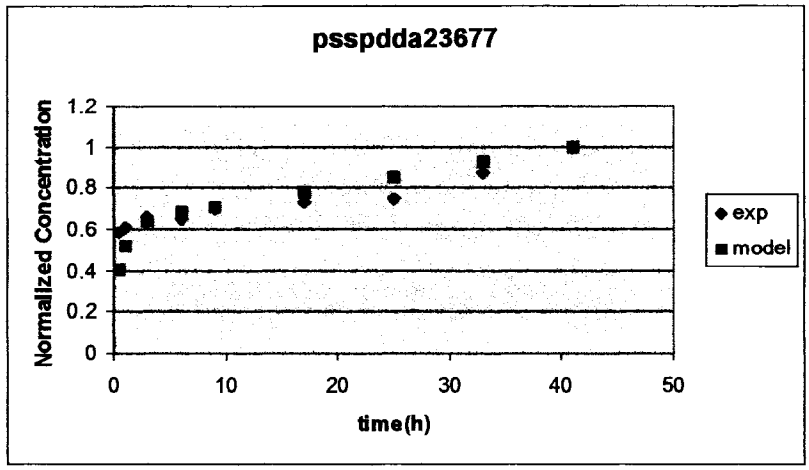

Figure 6.16. Psspdda23677 predicted and observed normalized concentration of dextran

Figure 6.17 shows that predicted (■) and observed (♦) normalized concentration of dextran released into the bulk liquid over time. Microcapsule wall is two layers of PSS/PDDA. Loading time=60h, MW=77000. Sum of square error, SSE=0.049597.

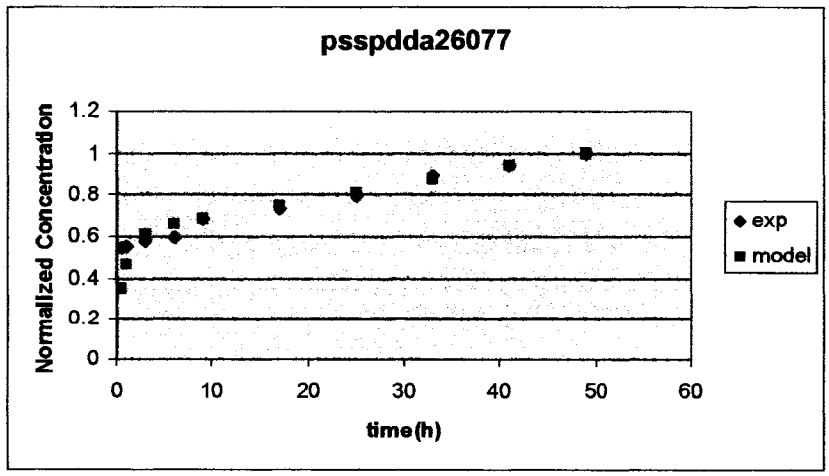

Figure 6.17. Psspdda26077 predicted and observed normalized concentration of dextran

Reproduced with permission of the copyright owner. Further reproduction prohibited without permission.

Figure 6.18 shows that predicted (■) and observed (♦) normalized concentration of dextran released into the bulk liquid over time. Microcapsule wall is four layers of PSS/PDDA. Loading time=12h, MW=4000. Sum of square error, SSE=0.009251.

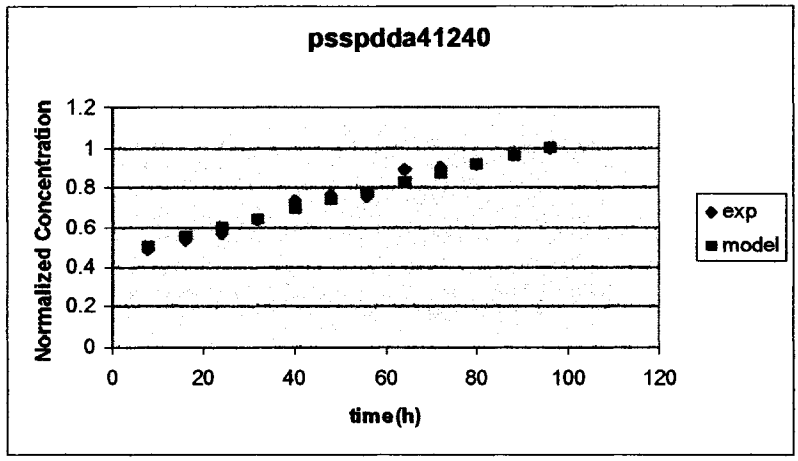

Figure 6.18. Psspdda41240 predicted and observed normalized concentration of dextran

Figure 6.19 shows that predicted (■) and observed (♦) normalized concentration of dextran released into the bulk liquid over time. Microcapsule wall is four layers of PSS/PDDA. Loading time=36h, MW=4000. Sum of square error, SSE=0.015766.

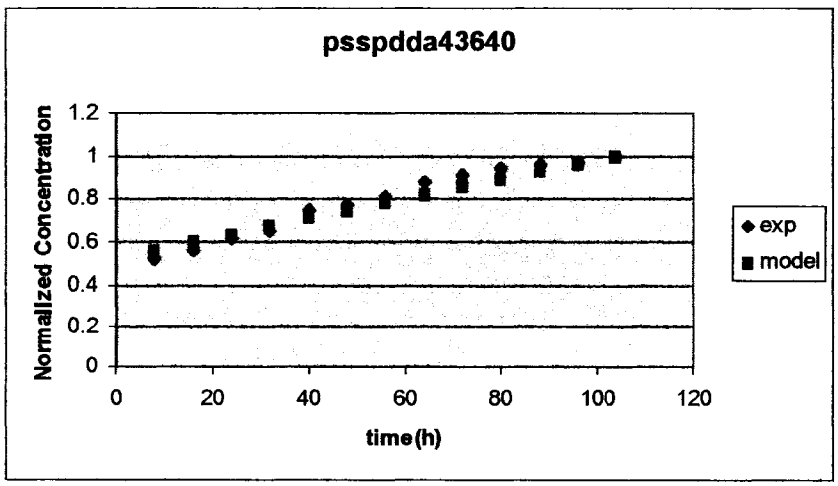

Figure 6.19. Psspdda43640 predicted and observed normalized concentration of dextran

Reproduced with permission of the copyright owner. Further reproduction prohibited without permission.

Figure 6.20 shows predicted (■) and observed (♦) normalized concentration of dextran released into the bulk liquid over time. Microcapsule wall is four layers of PSS/PDDA. Loading time=60h, MW=4000. Sum of square error, SSE=0.238115.

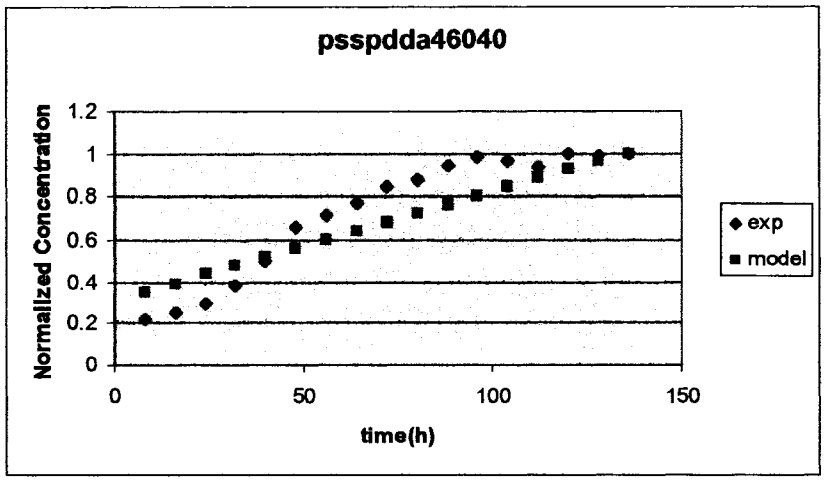

Figure 6.20. Psspdda46040 predicted and observed normalized concentration of dextran

Figure 6.21 shows that predicted (■) and observed (♦) normalized concentration of dextran released into the bulk liquid over time. Microcapsule wall is four layers of PSS/PDDA. Loading time=12h, MW=77000. Sum of square error, SSE=0.014435.

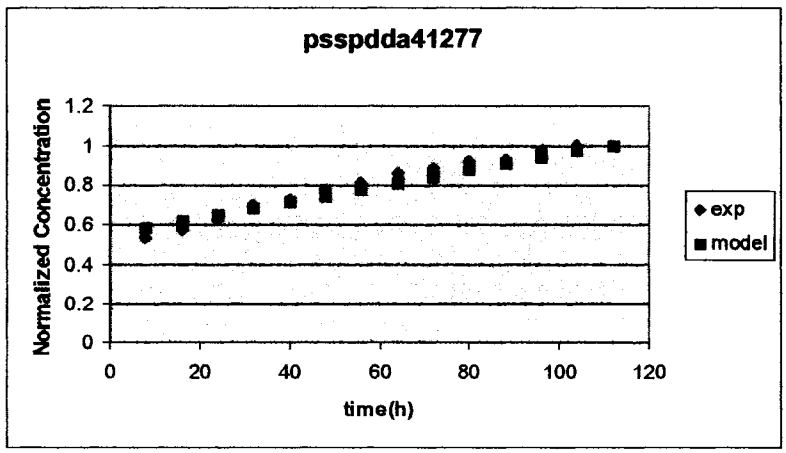

Figure 6.21. Psspdda41277 predicted and observed normalized concentration of dextran

Reproduced with permission of the copyright owner. Further reproduction prohibited without permission.

Figure 6.22 shows that predicted (■) and observed (♦) normalized concentration of dextran released into the bulk liquid over time. Microcapsule wall is four layers of PSS/PDDA. Loading time=36h, MW=77000. Sum of square error, SSE=0.012.

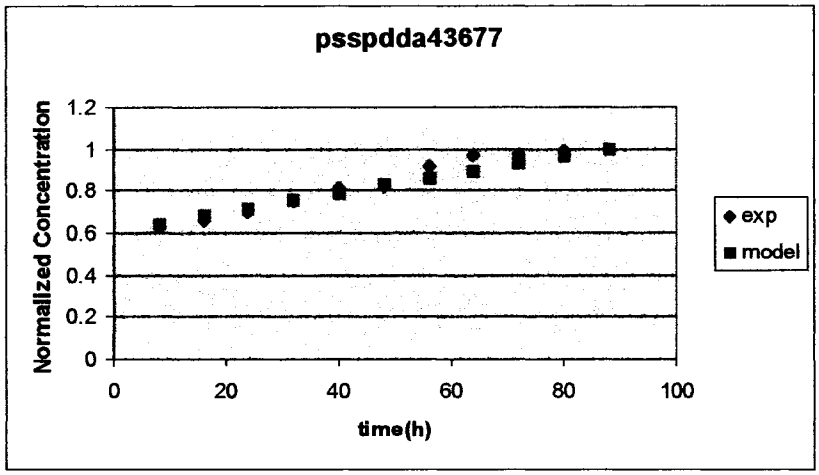

Figure 6.22. Psspdda43677 predicted and observed normalized concentration of dextran

Figure 6.23 shows that predicted (■) and observed (♦) normalized concentration of dextran released into the bulk liquid over time. Microcapsule wall is four layers of PSS/PDDA. Loading time=60h, MW=77000. Sum of square error, SSE=0.026.

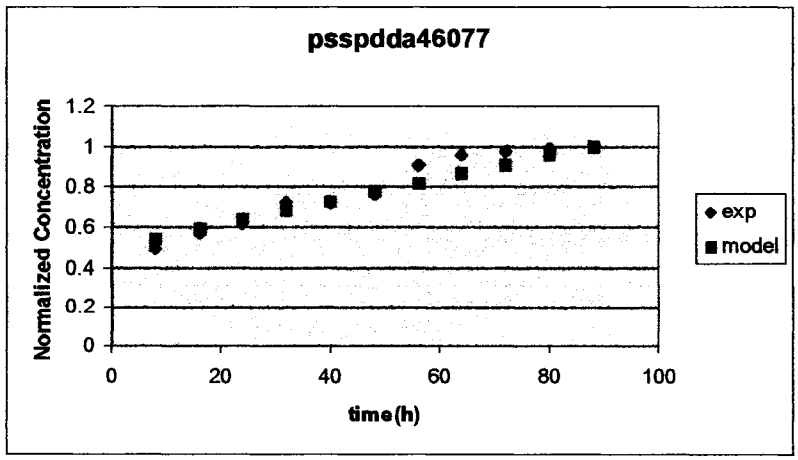

Figure 6.23. Psspdda46077 predicted and observed normalized concentration of dextran

Reproduced with permission of the copyright owner. Further reproduction prohibited without permission.

Figure 6.24 shows that predicted (■) and observed (♦) normalized concentration of dextran released into the bulk liquid over time. Microcapsule wall is six layers of PSS/PDDA. Loading time=12h, MW=4000. Sum of square error, SSE=0.025808.

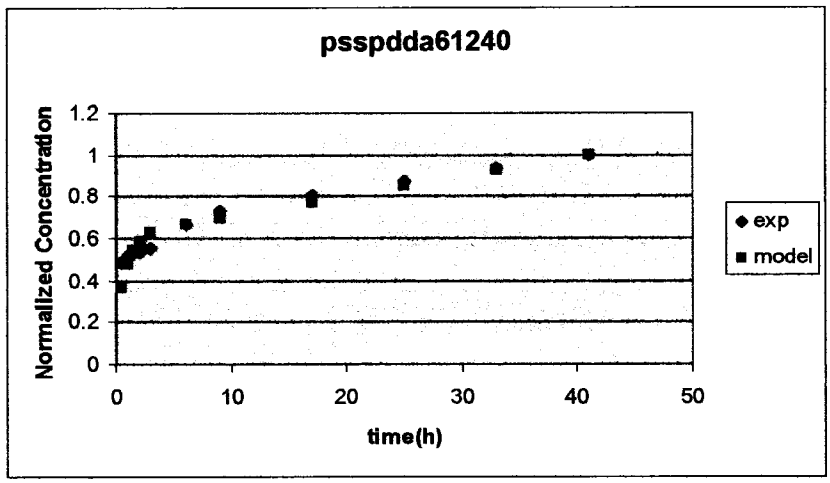

Figure 6.24. Psspdda61240 predicted and observed normalized concentration of dextran

Figure 6.25 shows that predicted (■) and observed (♦) normalized concentration of dextran released into the bulk liquid over time. Microcapsule wall is six layers of PSS/PDDA. Loading time=36h, MW=4000. Sum of square error, SSE=0.024.

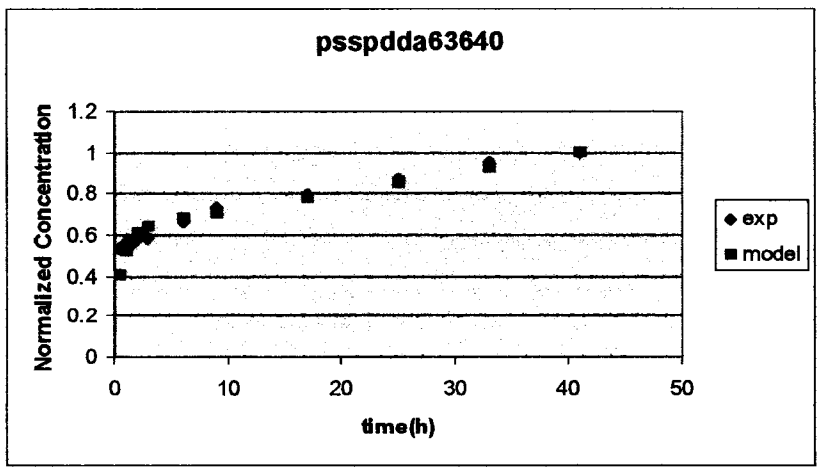

Figure 6.25. Psspdda63640 predicted and observed normalized concentration of dextran

Reproduced with permission of the copyright owner. Further reproduction prohibited without permission.

Figure 6.26 shows that predicted (■) and observed (♦) normalized concentration of dextran released into the bulk liquid over time. Microcapsule wall is six layers of PSS/PDDA. Loading time=60h, MW=4000. Sum of square error, SSE=0.036.

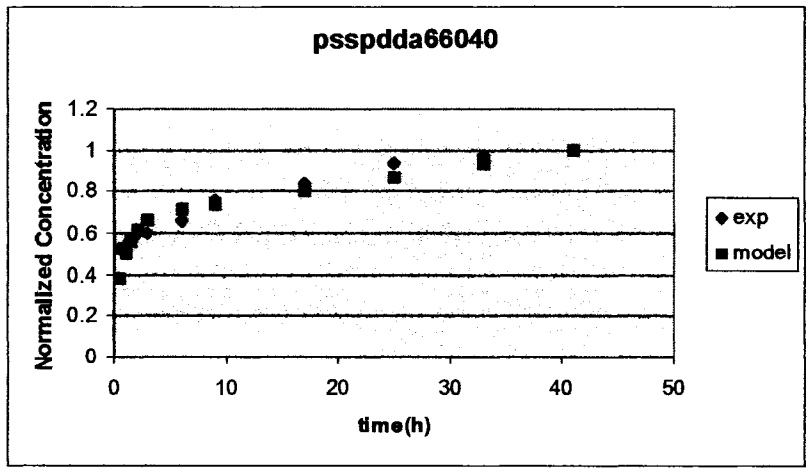

Figure 6.26. Psspdda66040 predicted and observed normalized concentration of dextran

Figure 6.27 shows that predicted (■) and observed (♦) normalized concentration of dextran released into the bulk liquid over time. Microcapsule wall is six layers of PSS/PDDA. Loading time=12h, MW=77000. Sum of square error, SSE=0.014997.

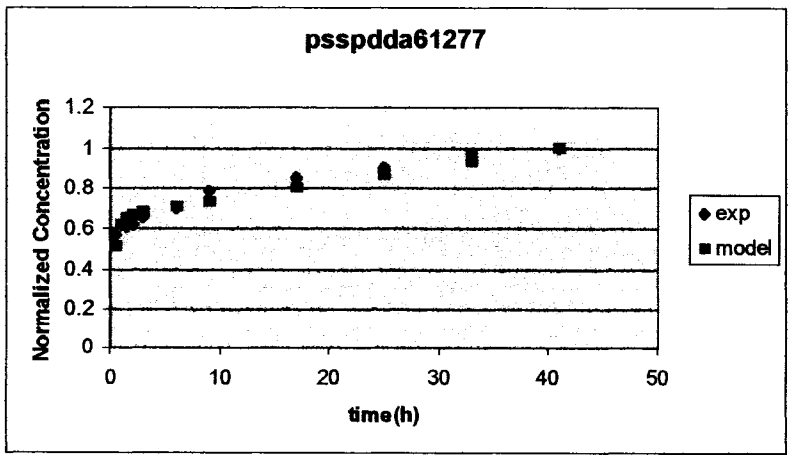

Figure 6.27. Psspdda61277 predicted and observed normalized concentration of dextran

Reproduced with permission of the copyright owner. Further reproduction prohibited without permission.

Figure 6.28 shows that predicted (■) and observed (♦) normalized concentration of dextran released into the bulk liquid over time. Microcapsule wall is six layers of PSS/PDDA. Loading time=36h, MW=77000. Sum of square error, SSE=0.034.

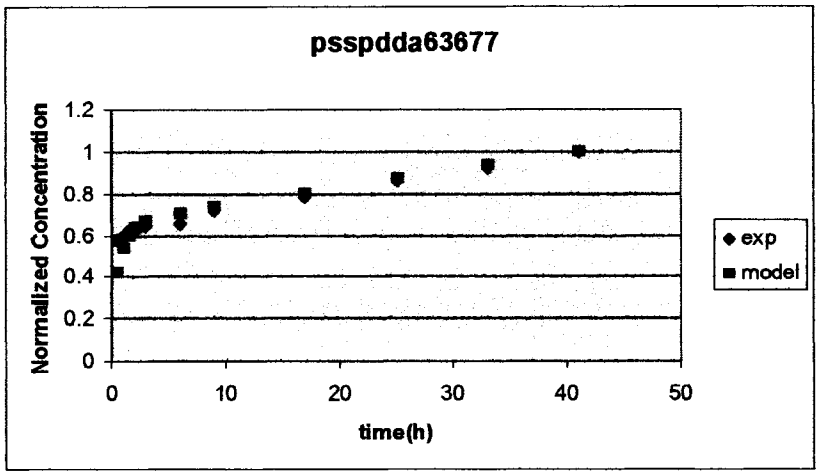

Figure 6.28. Psspdda63677 predicted and observed normalized concentration of dextran

Figure 6.29 shows that predicted (■) and observed (♦) normalized concentration of dextran released into the bulk liquid over time. Microcapsule wall is six layers of PSS/PDDA. Loading time=60h, MW=77000. Sum of square error, SSE=0.36.

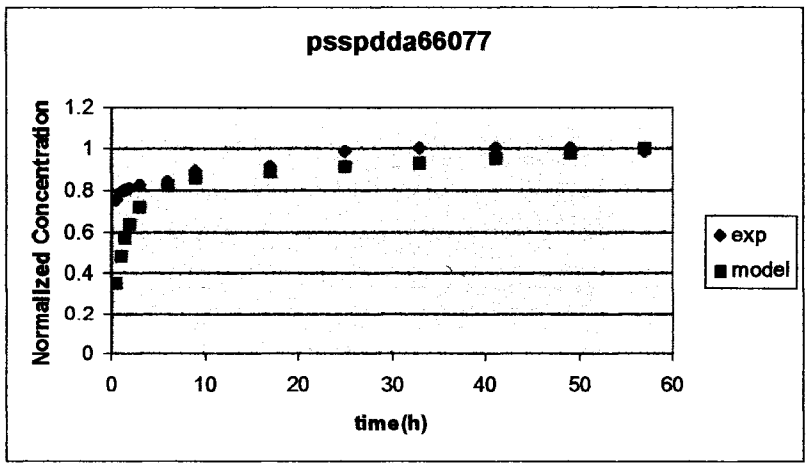

Figure 6.29. Psspdda66077 predicted and observed normalized concentration of dextran

Reproduced with permission of the copyright owner. Further reproduction prohibited without permission.

Figure 6.30 shows that predicted (■) and observed (♦) normalized concentration of dextran released into the bulk liquid over time. Microcapsule wall is two layers of PVS/PDDA. Loading time=12h, MW=4000. Sum of square error, SSE=0.010652.

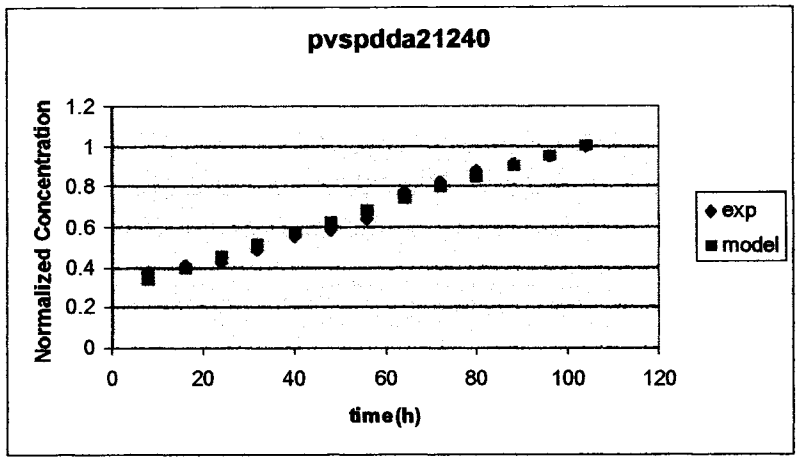

Figure 6.30. Pvspdda21240 predicted and observed normalized concentration of dextran

Figure 6.31 shows that predicted (■) and observed (♦) normalized concentration of dextran released into the bulk liquid over time. Microcapsule wall is two layers of PVS/PDDA. Loading time=12h, MW=77000. Sum of square error, SSE=0.065815.

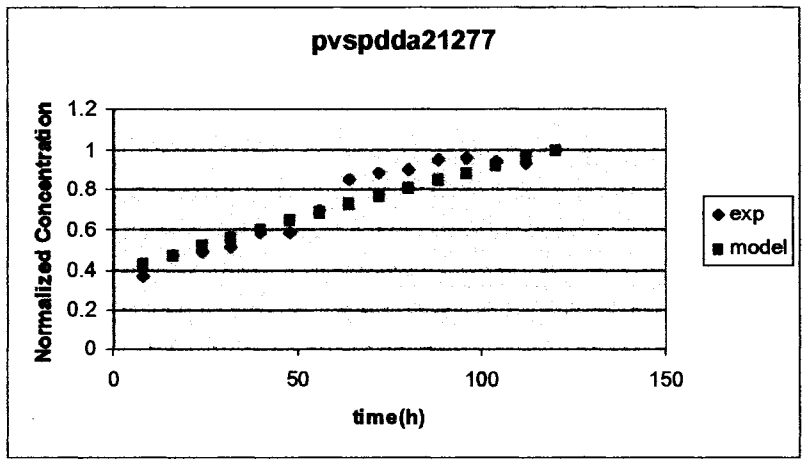

Figure 6.31. Pvspdda21277 predicted and observed normalized concentration of dextran

Reproduced with permission of the copyright owner. Further reproduction prohibited without permission.

Figure 6.32 shows that predicted (■) and observed (♦) normalized concentration of dextran released into the bulk liquid over time. Microcapsule wall is two layers of PVS/PDDA. Loading time=36h, MW=4000. Sum of square error, SSE=0.003324.

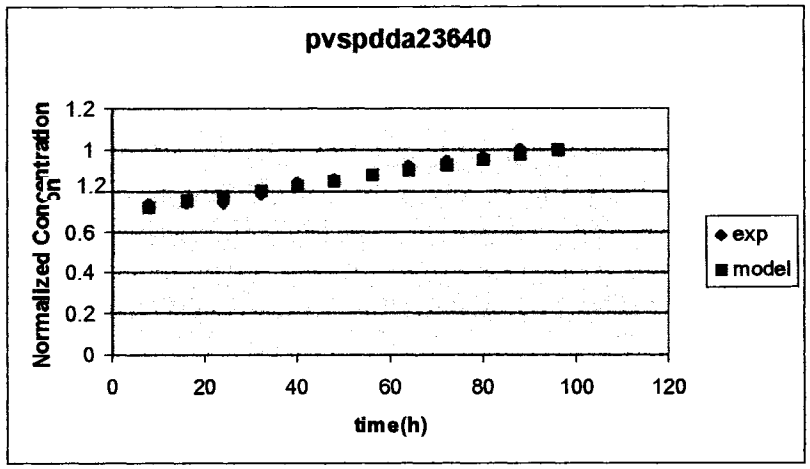

Figure 6.32. Pvspdda23640 predicted and observed normalized concentration of dextran

Figure 6.33 shows that predicted (■) and observed (♦) normalized concentration of dextran released into the bulk liquid over time. Microcapsule wall is two layers of PVS/PDDA. Loading time=36h, MW=77000. Sum of square error, SSE=0.011105.

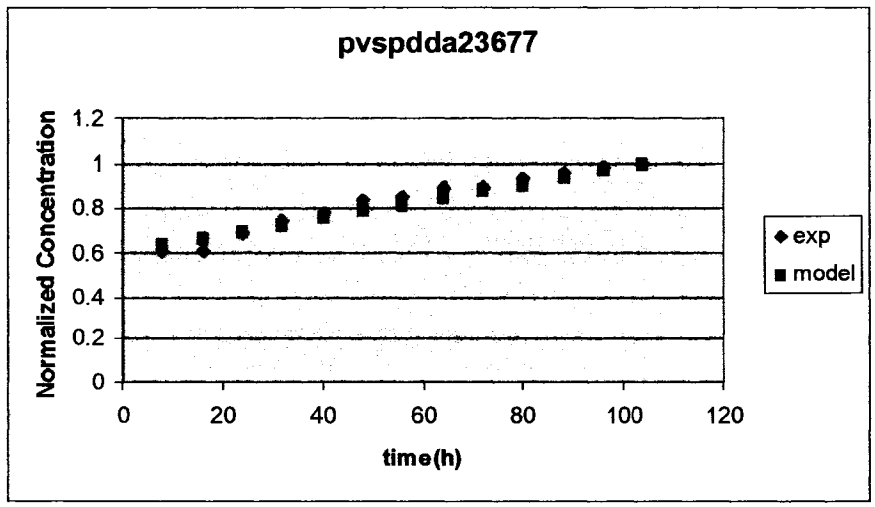

Figure 6.33. Pvspdda23677 predicted and observed normalized concentration of dextran

Reproduced with permission of the copyright owner. Further reproduction prohibited without permission.

Figure 6.34 shows that predicted (■) and observed (♦) normalized concentration of dextran released into the bulk liquid over time. Microcapsule wall is two layers of PVS/PDDA. Loading time=60h, MW=4000. Sum of square error, SSE=0.015402.

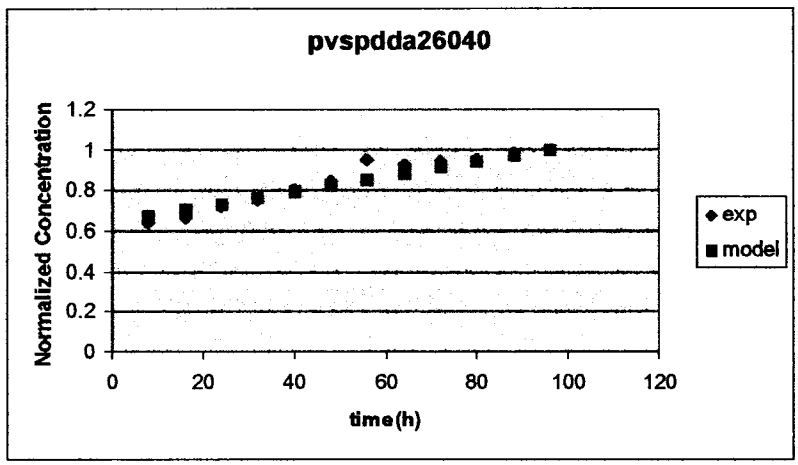

Figure 6.34. Pvspah26040 predicted and observed normalized concentration of dextran

Figure 6.35 shows that predicted (■) and observed (♦) normalized concentration of dextran released into the bulk liquid over time. Microcapsule wall is two layers of PVS/PDDA. Loading time=60h, MW=77000. Sum of square error, SSE=0.034494.

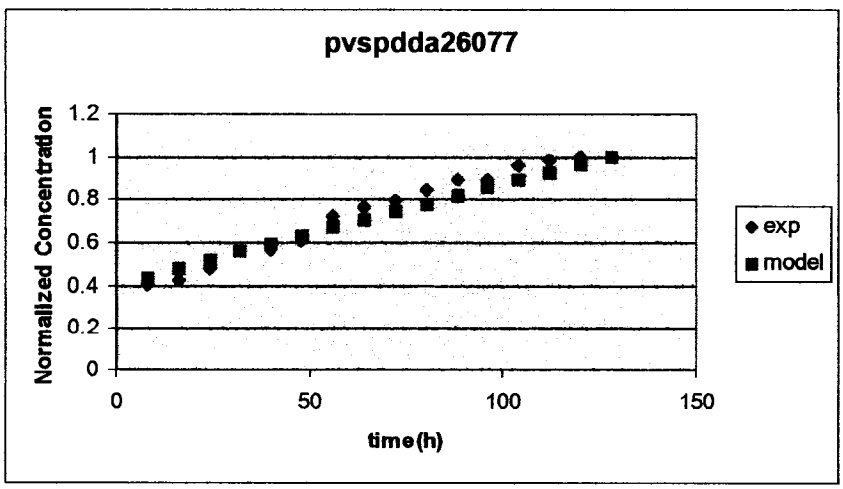

Figure 6.35. Pvspdda26077 predicted and observed normalized concentration of dextran

Reproduced with permission of the copyright owner. Further reproduction prohibited without permission.

Figure 6.36 shows that predicted (■) and observed (♦) normalized concentration of dextran released into the bulk liquid over time. Microcapsule wall is four layers of PVS/PDDA. Loading time=12h, MW=4000. Sum of square error, SSE=0.00472.

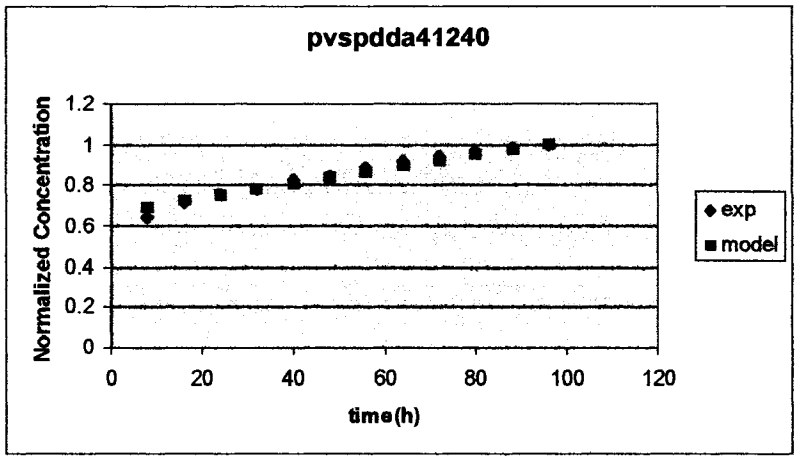

Figure 6.36. Pvspdda41240 predicted and observed normalized concentration of dextran

Figure 6.37 shows that predicted (■) and observed (♦) normalized concentration of dextran released into the bulk liquid over time. Microcapsule wall is four layers of PVS/PDDA. Loading time=36h, MW=4000. Sum of square error, SSE=0.004604.

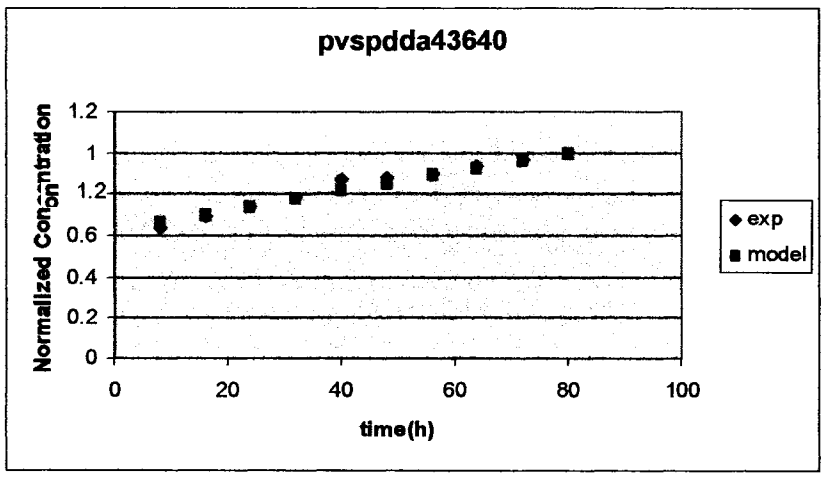

Figure 6.37. Pvspdda43640 predicted and observed normalized concentration of dextran

Reproduced with permission of the copyright owner. Further reproduction prohibited without permission.

Figure 6.38 shows that predicted (■) and observed (♦) normalized concentration of dextran released into the bulk liquid over time. Microcapsule wall is four layers of PVS/PDDA. Loading time=60h, MW=4000. Sum of square error, SSE=0.011997.

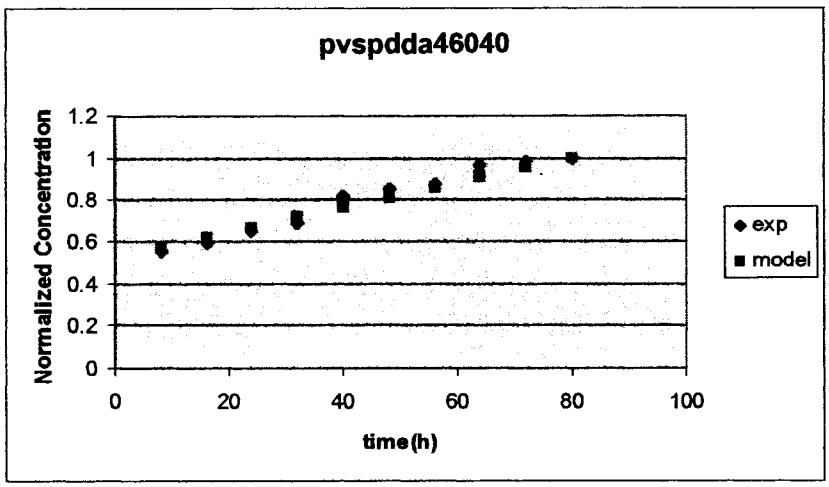

Figure 6.38. Pvspdda46040 predicted and observed normalized concentration of dextran

Figure 6.39 shows that predicted (■) and observed (♦) normalized concentration of dextran released into the bulk liquid over time. Microcapsule wall is four layers of PVS/PDDA. Loading time=12h, MW=77000. Sum of square error, SSE=0.022496.

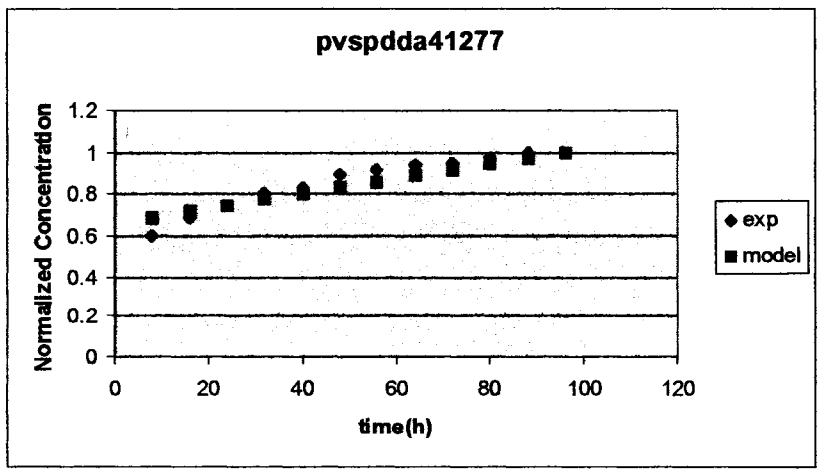

Figure 6.39. Pvspdda41277 predicted and observed normalized concentration of dextran

Reproduced with permission of the copyright owner. Further reproduction prohibited without permission.

Figure 6.40 shows that predicted (■) and observed (♦) normalized concentration of dextran released into the bulk liquid over time. Microcapsule wall is four layers of PVS/PDDA. Loading time=36h, MW=77000. Sum of square error, SSE=0.014.

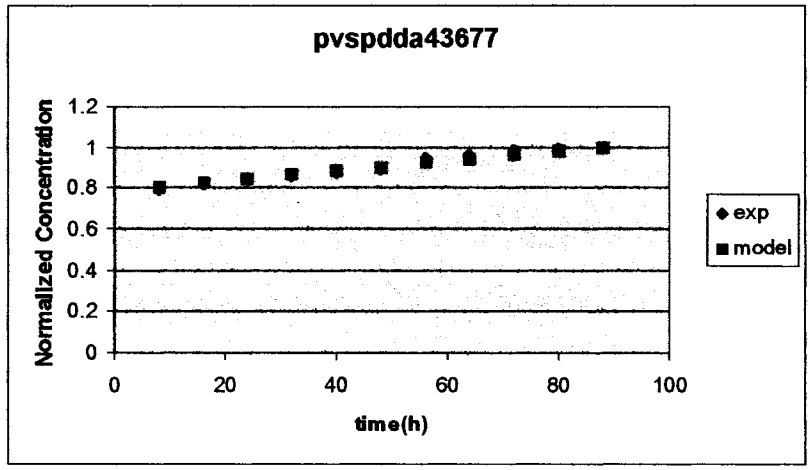

Figure 6.40. Pvspdda43677 predicted and observed normalized concentration of dextran

Figure 6.41 shows that predicted (■) and observed (♦) normalized concentration of dextran released into the bulk liquid over time. Microcapsule wall is four layers of PVS/PDDA. Loading time=60h, MW=77000. Sum of square error, SSE=0.003661.

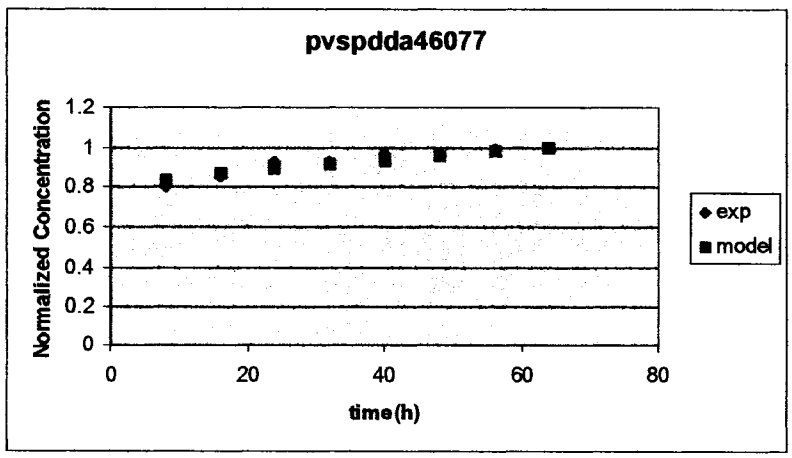

Figure 6.41. Pvspdda46077 predicted and observed normalized concentration of dextran

Reproduced with permission of the copyright owner. Further reproduction prohibited without permission.

Figure 6.42 shows that predicted (■) and observed (♦) normalized concentration of dextran released into the bulk liquid over time. Microcapsule wall is six layers of PVS/PDDA. Loading time=12h, MW=4000. Sum of square error, SSE=0.04102.

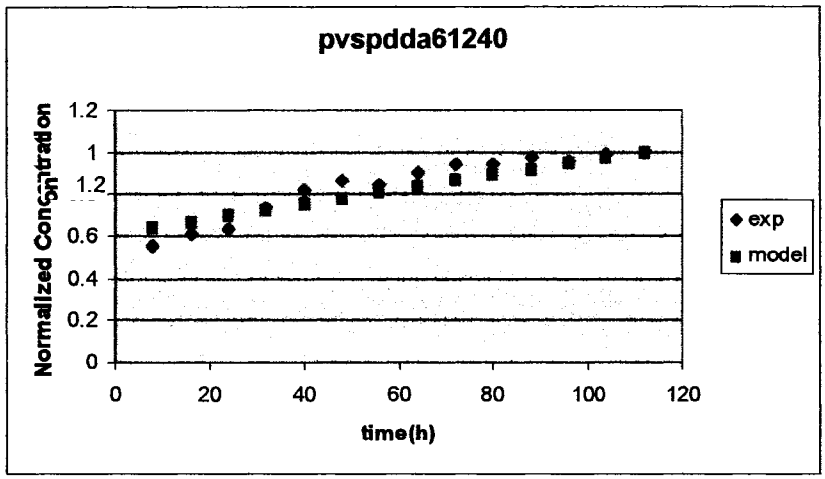

Figure 6.42. Pvspdda61240 predicted and observed normalized concentration of dextran

Figure 6.43 shows that predicted (■) and observed (♦) normalized concentration of dextran released into the bulk liquid over time. Microcapsule wall is six layers of PVS/PDDA. Loading time=12h, MW=77000. Sum of square error, SSE=0.013186.

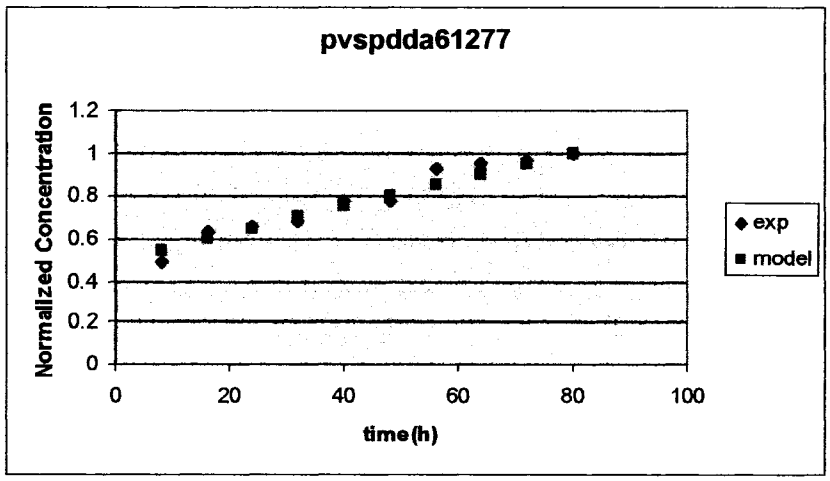

Figure 6.43. Pvspdda61277 predicted and observed normalized concentration of dextran

Reproduced with permission of the copyright owner. Further reproduction prohibited without permission.

Figure 6.44 shows that predicted (■) and observed (♦) normalized concentration of dextran released into the bulk liquid over time. Microcapsule wall is six layers of PVS/PDDA. Loading time=36h, MW=4000. Sum of square error, SSE=0.008347.

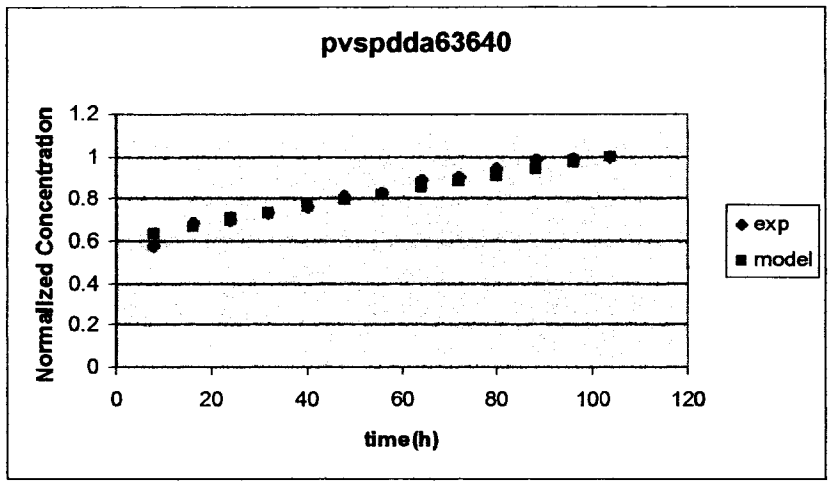

Figure 6.44. Pvspdda63640 predicted and observed normalized concentration of dextran

Figure 6.45 shows that predicted (■) and observed (♦) normalized concentration of dextran released into the bulk liquid over time. Microcapsule wall is six layers of PVS/PDDA. Loading time=36h, MW=77000. Sum of square error, SSE=0.038904.

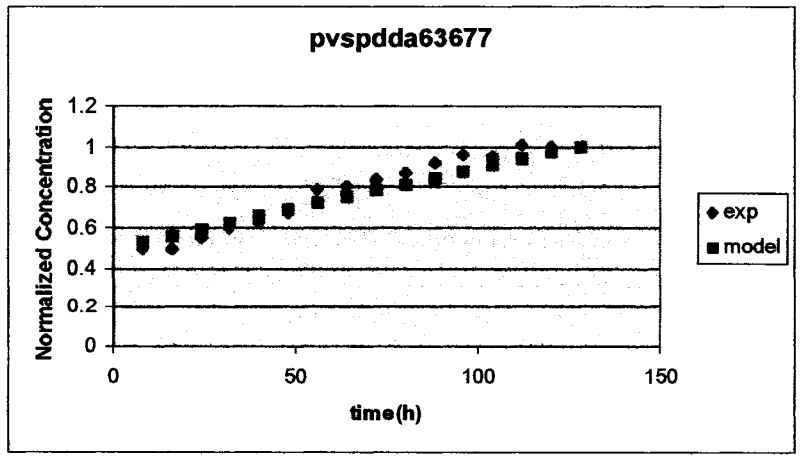

Figure 6.45. Pvspdda63677 predicted and observed normalized concentration of dextran

Reproduced with permission of the copyright owner. Further reproduction prohibited without permission.

Figure 6.46 shows that predicted (■) and observed (♦) normalized concentration of dextran released into the bulk liquid over time. Microcapsule wall is six layers of PVS/PDDA. Loading time=60h, MW=4000. Sum of square error, SSE=0.00288.

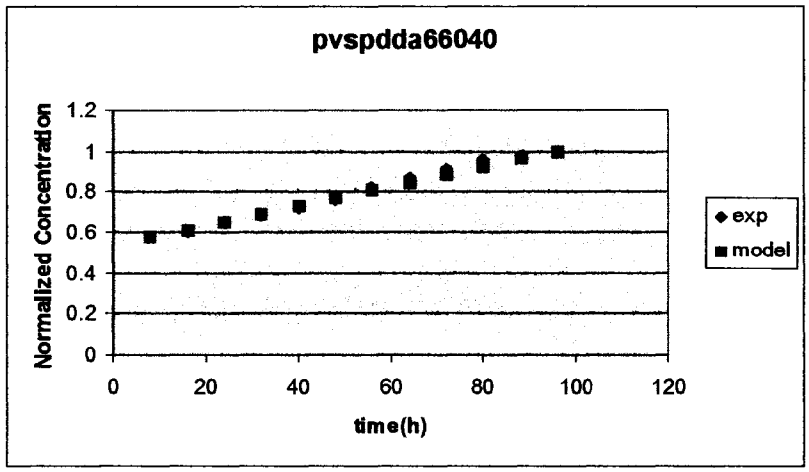

Figure 6.46. Pvspdda66040 predicted and observed normalized concentration of dextran

Figure 6.47 shows that predicted (■) and observed (♦) normalized concentration of dextran released into the bulk liquid over time. Microcapsule wall is six layers of PVS/PDDA. Loading time=60h, MW=77000. Sum of square error, SSE=0.022259.

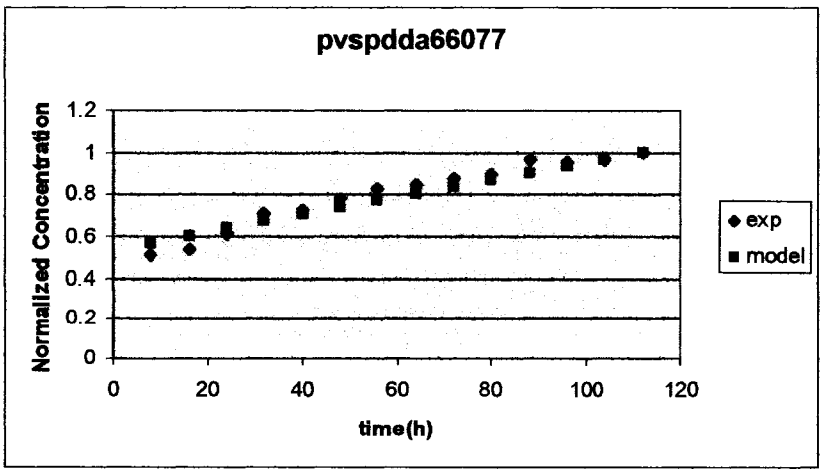

Figure 6.47. Pvspdda66077 predicted and observed normalized concentration of dextran

Reproduced with permission of the copyright owner. Further reproduction prohibited without permission.

6.3 Estimates of Microcapsule Core and Wall Membrane Diffusion Coefficients

Estimates of the diffusivity in the core of the microcapsule (D1) and in the wall membrane (D2) were obtained from fitting the model to the experimental data as shown in Figures. 6.1-6.47. Table 6.1 gives these estimates for different types of membranes, loading times, molecular weights, and layer thickness. The unit of the diffusion coefficient (D1 and D2) is in μm^2 per hour.

Table 6.1. Estimates of the diffusion coefficients in D1 (the core of the microcapsule) and in D2 (the wall membrane)

psspdda	21240	23640	26040	21277	23677	26077
D1=	10.168659	24.8381887	18.562249	23.951496	24.900449	20.509278
D2=	1.64E-05	4.82E-06	4.20E-06	7.50E-06	4.79E-06	3.53E-06
SSE=	0.0024743	0.0540485	0.0326746	0.0184165	0.0575772	0.0495965
psspdda	41240	43640	46040	41277	43677	46077
D1=	8.5991903	6.04202352	8.0807803	9.5221096	4.8	4.7
D2=	7.89E-06	3.73E-06	4.02E-06	5.99E-06	3.40E-06	3.30E-06
SSE=	0.0092506	0.01576627	0.2381145	0.0144352	0.012	0.026
psspdda	61240	63640	66040	61277	63677	66077
D1=	13.591459	10.2	10.5	15.199701	11.4	11
D2=	3.81E-06	4.80E-06	3.40E-06	7.75E-06	4.50E-06	1.80E-06
SSE=	0.0258080	0.024	0.036	0.0149972	0.034	0.36
pvspdda	21240	23640	26040	21277	23677	26077
D1=	13.288079	11.0090987	10.688615	18.676951	10.709831	9.8895273
D2=	1.17E-05	2.67E-06	2.32E-06	8.22E-06	3.13E-06	3.34E-06
SSE=	0.0106521	0.00332407	0.0154420	0.0658148	0.0111052	0.0344934
pvspdda	41240	43640	46040	41277	43677	46077
D1=	10.671604	10.9032036	10.806467	10.224095	10.968331	10.461454
D2=	5.05E-06	3.43E-06	3.29E-06	5.06E-06	2.19E-06	1.75E-06
SSE=	0.0047195	0.00460433	0.0119969	0.0224955	0.0013996	0.0036612
pvspdda	61240	63640	66040	61277	63677	66077
D1=	9.3441210	10.7027215	10.964211	10.142274	10.248225	10.486949
D2=	5.27E-06	3.14E-06	2.94E-06	7.95E-06	3.60E-06	2.70E-06
SSE=	0.0410197	0.00834733	0.0028802	0.0131864	0.0389037	0.0222586

Reproduced with permission of the copyright owner. Further reproduction prohibited without permission.

psspah	41240	43640	46040	41277	43677	46077
D1=	1.94E+02	6.553579	6.423386	6.70E+00	7.574897	6.388522
D2=	2.10E-05	3.15E-06	3.50E-06	4.20E-06	3.74E-06	3.11E-06
SSE=	0.067	0.059625	0.004871	0.056	0.03471	0.002657
pvspah	41240	43640	46040	41277	43677	46077
D1=	18.42723	9.060798	7.467331		6.792011	4.64723
D2=	1.46E-05	4.02E-06	3.82E-06		4.28E-06	3.46E-06
SSE=	0.007494	0.075704	0.04956		0.002008	0.030535

In order to determine the main effects of membrane type, loading time, dextran molecular weight, and number of layers in the wall membrane on the diffusivity coeffiecients D1 and D2, an anlysis of variance was performed on the portion of the data in Table 6.1 that includes psspdda and pvspdda. This excluded psspah and pvspah since this data set was only for four layers. Results of the analysis of variance for D1 are presented in Table 6.2.

Table 6.2. Analysis of variance for D1 (the microcapsule core diffusivity)

Source	DF	Type III SS	Mean Square	F Value	Pr > F
type	1	36.7636534	36.7636534	2.39	0.1330
layer	2	365.5990966	182.7995483	11.88	0.0002
time	2	11.8244606	5.9122303	0.38	0.6844
mw	1	9.8491392	9.8491392	0.64	0.4302

From the p values in Table 6.2, it is seen that only layer number has a significant effect on D1. Table 6.3 gives pair-wise mean comparisons among the layer means. It is seen from the p values in the table that D1 is significantly larger for two layers than for four layers. However, there is no difference in the D1 diffusivity between four and six layers.

Reproduced with permission of the copyright owner. Further reproduction prohibited without permission.

Table 6.3. Pair-wise comparisons among the layer means for D1

layer	D1 MEAN	Number
2	16.4327021E-6	1
4	8.8149383E-6	2
6	11.1483054E-6	3

Dependent Variable: D1

i/j	1	2	3
1		0.0001	0.0070
2	0.0001		0.3259
3	0.0070	0.3259	

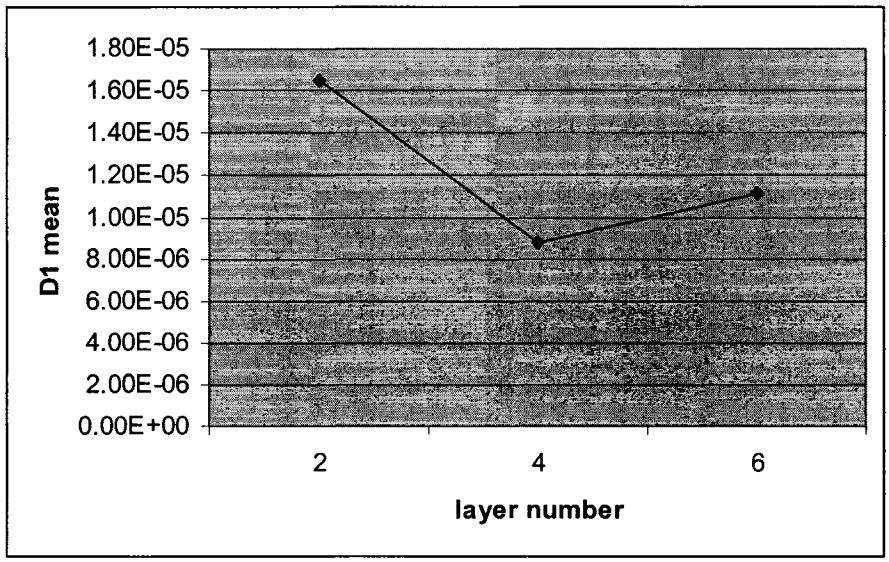

Figure 6.48. Plot of the mean of D1 against layer number

The plot in Figure 6.48 shows that the mean diffusivity in the core decreases from two to four layers, but the difference between four and six is not significant as indicated in Table 6.3.

The same analysis of variance for diffusivity (D2) in the wall membrane is presented in Table 6.4.

Reproduced with permission of the copyright owner. Further reproduction prohibited without permission.

Table 6.4. Analysis of variance for D2 (wall membrane diffusivity)

Source	DF	Type III SS	Mean Square	F Value	Pr > F
type	1	8.8804E-12	8.8804E-12	2.47	0.1270
layer	2	2.7751E-11	1.387591E-11	3.86	0.0327
time	2	1.53764E-10	7.6882E-11	21.37	<.0001
mw	1	4.257344E-12	4.257344E-12	1.18	0.2857

It is seen from the p values in the table that both layer and time have significant effects on D2. The pair-wise mean comparisons in Table 6.5 show that D2 decreased significantly with an increase in the number of layers from two to four. However, the difference in diffusivity between four and six layers was not significant. These results are shown graphically in Figure 6.49. From the pair-wise mean comparisons among the D2 means for the different loading times (Table 6.6), it is seen that D2 decreased significantly from two to four layers. However, the decrease in D2 as the number of layers increased from four to six was not significant. These results are shown graphically in Figure 6.50.

Table 6.5. Pair-wise comparisons among the layer means for D2

layer	D2 MEAN	Number
2	6.0516667E-6	1
4	4.0916667E-6	2
6	4.305E-6	3

Dependent Variable: D2

i/j	1	2	3
1		0.0437	0.0786
2	0.0437		0.9591
3	0.0786	0.9591	

Reproduced with permission of the copyright owner. Further reproduction prohibited without permission.

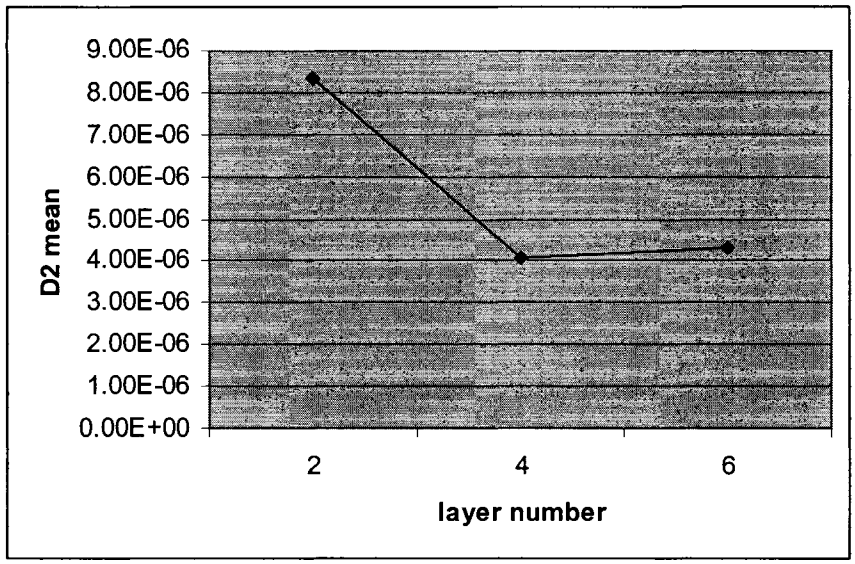

Figure 6.49. Plot of the mean of D2 against layer number

Table 6.6. Pair-wise comparisons among the loading time means for D2

time	D2 MEAN	Number
12	7.7158333E-6	1
36	3.6833333E-6	2
60	3.0491667E-6	3

Dependent Variable: D2

i/j	1	2	3
1		<.0001	<.0001
2	<.0001		0.6945
3	<.0001	0.6945	

Reproduced with permission of the copyright owner. Further reproduction prohibited without permission.

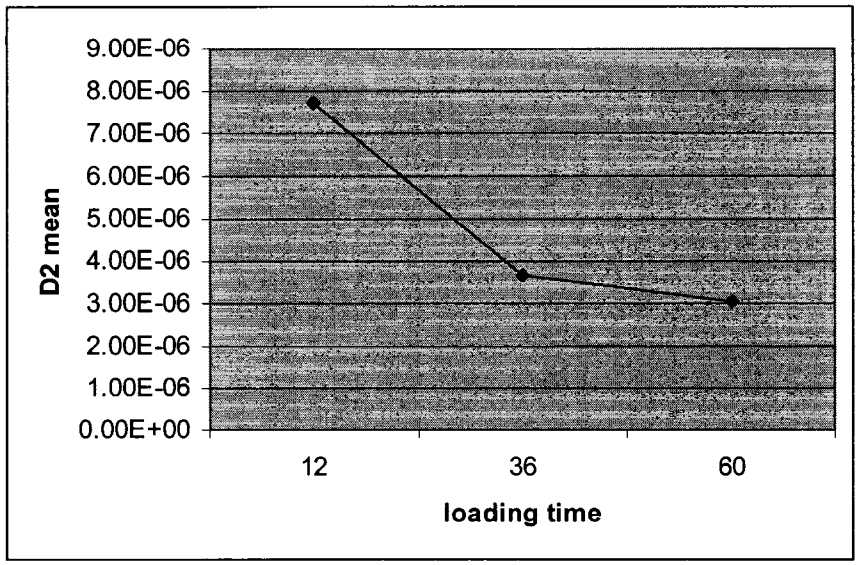

Figure 6.50. Plot of the mean of D2 against loading time

In order to determine the effect of layer type on diffusivity where all four types are present, an analysis of variance on D1 and D2 was performed using the data for four layers in Table 6.1. It is seen from the p values in Table 6.7 that membrane or layer type, loading time, and dextran molecular weight have no effect on diffusivity through the core of the microcapsule.

Table 6.7. Analysis of variance for D1 of data set two

Source	DF	Type III SS	Mean Square	F Value	Pr > F
type	3	2.801755E-11	9.339182E-12	0.76	0.5325
time	2	1.301381E-10	6.506906E-11	5.30	0.0171
mw	1	5.258039E-11	5.258039E-11	4.28	0.0551

From the p values in Table 6.8, it is seen that molecular weight and loading time have significant effects on diffusivity in the wall membrane (D2). From the p values in Table 6.9, it is seen that the diffusivity in the wall membrane is larger for 12 hours of loading time than for 36 or 60 hours. Diffusivity for 36 hours of loading time is not

Reproduced with permission of the copyright owner. Further reproduction prohibited without permission.

significantly different from that for 60 hours. These results are shown graphically in Figure 6.51.

Table 6.8 Analysis of variance for D2 of data set two

Source	DF	Type III SS	Mean Square	F Value	Pr > F
type	3	4101.318716	1367.106239	0.92	0.4525
time	2	3848.150373	1924.075187	1.30	0.3003
mw	1	2014.163475	2014.163475	1.36	0.2608

Table 6.9. Pair-wise comparisons among the D2 means of data set two for loading time

time	D2 MEAN	Number
12	8.345E-6	1
36	3.3045588E-6	2
60	3.36875E-6	3

Dependent Variable: D2

i/j	1	2	3
1		0.0354	0.0301
2	0.0354		0.9993
3	0.0301	0.9993	

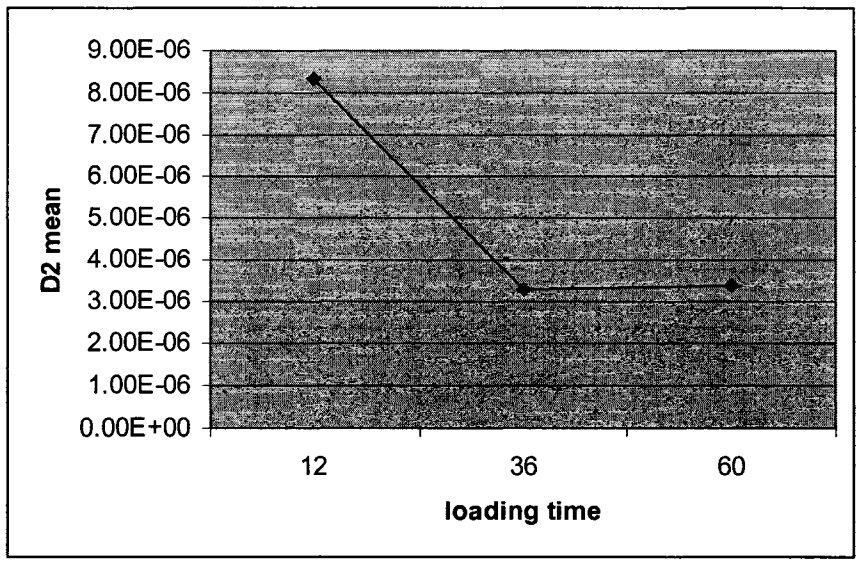

Figure 6.51. Plot of the mean of D2 of data set two against loading time

Reproduced with permission of the copyright owner. Further reproduction prohibited without permission.

It is seen from Table 6.10 that the diffusivity through the wall membrane is smaller for 77000 dextran molecular weight than for 4000 molecular weight. The decrease in diffusivity with an increase in molecular weight is shown graphically in Figure 6.52.

Table 6.10. Mean diffusivity in the membrane wall for 4000 and 77000 dextran molecular weights

mw	D2 MEAN	Pr > |t|
4000	6.5291667E-6	0.0551
77000	3.4830392E-6	

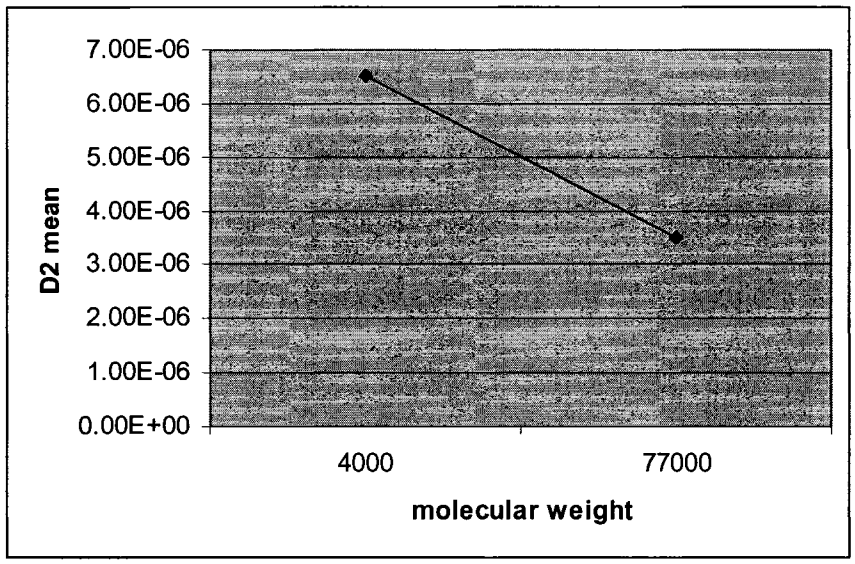

Figure 6.52. Plot of the mean of D2 of data set two against weight

6.4 Conclusion

From the analysis of variance in Tables 6.2 and 6.3, it is seen that only layer thickness had an effect on diffusivity in the core. The diffusivity for four layers was almost half of that for two layers of polyelectrolytes in the core. In the case of diffusivity in the microcapsule wall, both time and layer thickness had an effect (Tables 6.4 and 6.5).

Reproduced with permission of the copyright owner. Further reproduction prohibited without permission.

In this case, diffusivity was larger for two layers of wall membrane thickness than for four or six layers and it was also larger for 12 hours than for 36 or 60 hours of loading time. There was no significant change in diffusivity beyond four layers or beyond 36 hours of loading time. From Tables 6.8 – 6.10, it is interesting to see that for four layers of wall membrane thickness molecular weight had an effect on diffusivity through the wall membrane with the high molecular weight diffusing more slowly than the low molecular weight. In all analyses, membrane type had no marginal effect on diffusivity when considered over all loading times, membrane thickness, and molecular weight.

6.5 Future Work

In the future work, it would be of interest to modify the diffusion model to include only the release stage and apply it to data where dextran is initially encapsulated in the core. In this case, one may gain a clearer insight about the nature of diffusivity inside the core and wall membrane of the microcapsules.

Reproduced with permission of the copyright owner. Further reproduction prohibited without permission.

REFERENCES

[Antipov 2002] Antipov, A.; Vieira, Euridice;Ibarz, Gemma; Sukhorukov, Gleb; Daihne, Lars; Gao, Changyou; Donath, Edwin; Moehwald, Helmuth. "Controlled and sustained release properities of polyelectrolyte multilayer capsules." *International Patent Application (2002).*

[Balakrishnan 1985] Balakrishnan, V. "Anomalous diffusion in one dimension." *Physica A 132, p569.*

[Barkai2000] Barkai, E., R. Metzler and J. Klafter. "From continous time random walks to the fractional Fokker-Planck equation." *Physical Review E 61, p132.*

[Benichou 2004] Benichou, A; A. Aserin; N. Garti. Double emulsions stabilized with hybrds of natural polymers for entrapment and slow release of active matters. *Advances in colloid and interface science. 108-109 p29-41.*

[Chen 2006] Chen, H.; Wei Ouyang; Bisi Lawuyi; Satya Prakash. "Genipin Cross-Linked Alginate-Chitosan Microcapsules: Membrane Characterization and Optimization of Cross-Linking Reaction." *Biomacromolecules,* V7 (7), p2091 -2098.

[Collins 2003] Collins, J.; Yung-Chieh Tan. "Optimization of Shear Driven Droplet Generation in a Microfluidic Device." *Proceedings of IMECE 2003.*

[Dai 1995] Dai, W. "A Parallel Algorithm for Direct Solution of Large Scale Tridiagonal Linear Systems." *Proceedings of the Seventh SIAM Conference on Parallel Processing for Scientific Computing, February 15-17, 1995*

[Decher 1997] Decher, G. "Fuzzy Nanoassemblies: toward Layered Polymeric Multicomposites." *Since 117, p1232-1237.*

[Dorian 1996] Dorian, R. E.; K. C. Cochrum. "Microcapsule Generating System Containing an Air Knife and Method of Encapsulating." *US Patent 5,521,079*

[Dorian 1996] Dorian, R. E.; S. A. Jemtrud; K. C. Cochrum. "Multiple layer alginate coating of biological tissue for transplantation." *US Patent 5,578,314*

Reproduced with permission of the copyright owner. Further reproduction prohibited without permission.

[Gao 2005] Gao, L.; E. Wang; Z. Kang; Y. Song; B. Mao; L. Xu. "Layer-by-Layer assembly of polyoxometalates into microcapsules." *Journal of Physical Chemistry B, V109(35), p16587-16592.*

[Gao 2006] Gao, C.; Z. Feng; Z. Wang; J. Shen. "Method for assembling microcapsule layer-by-layer based on interaction of covalent bond." *Faming Zhuanli Shenqing Gongkai Shuomingshu, p12.*

[Ghan 2004] Ghan, R.; Tatsiana Shutava; Dinesh Kommireddy; Yuri Lvov. "Polyelectrolyte Microcapsules as Reactors for Synthesizing Bio-polymers," *60th Southwest regional meeting of the American Chemical Society.*

[Hong 1993] Hong, D.; K. Lowack; J. Schmitt; G. Decher . "Layer-by-layer Deposited Multilayer Assemblies of Polyelectrolytes and Proteins: From Ultrathin Films to Protein Arrays." *Program Colloid Polymer Science 93, p98-102.*

[Ijichi 1997] Ijichi, K.; H. Yoshizawa; U. Yoshizawa; Y. Hatate; Y. Kawano. "Multi-layered Gelatin/acacia Microcapsules by Complex Coacervation Method." *Journal of Chemical Engineering of Japan. V 30 n 5 p793-798.*

[Kim 2004] Kim, B.; O. I. Vinogradova. "PH-Controlled Swelling of Polyelectrolyte Multilayer Microcapsules." *Journal of Physical Chemistry B, V108(24), p8161-8165.*

[Khopade 2002] Khopade, A.J.;F.Caruso. "Stepwise Self-assembled Poly(amidoamine) Dendrimer and Poly(styrenesulfonate) Microcapsules as Sustained Delivery Vehicles." *Biomacromolecules, V3(6), p1154-1162.*

[Kwok 2002] Kwok, W.; C. Kiparissides; P. Yuet; T. J. Harris; M. F. A. Goosen. "Mathematical Modeling of Protein Diffusion in Microcapsules: a Comparison with Experimental Results." *Canadian Journal of Chemical Engineering, V69(1), p361-70.*

[Lahmani 1996] Lahmani, P.; L. "Simoneau. Sun filter microcapsules." *US Patent 4,904,524 30*

[Lampton 1997] Lampton, M. "Detection of airglow lines from EURD European Space Agency." *European Space Agency, (Special Publication), 413, February, 1998, p837-839*

[Levy 1997] Levy, M.; A. Huc; M. Andry; C. Buffevant. "Process of Manufacture of Biodegradable Microcapsules Having Walls Composed of Crosslinked Atelocollagen and Polyholosides." *US Patent 5,395,620*

[Lister 1998] Lister, John R.; Stone, Howard A. "Capillary Breakup of a Viscous Thread Surrounded by another Viscous Fluid." *Physics of Fluids (1998), V10(11), p 2758-2764.*

Reproduced with permission of the copyright owner. Further reproduction prohibited without permission.

[Liu 2005] Liu, X.; C. Gao; J. Shen; H. Mohwald. "Multilayer Microcapsules as Anti-cancer Drug Delivery Vehicle: Deposition, sustained release, and in vitro bioactivity." *Macromolecular Bioscience, V5(12), p1209-1219.*

[Lu 2005] Lu, Z.; M. D. Prouty; Z. Guo; V. Golub; C. S.S.R. Challa; Y. M. Lvov. "Magnetic Switch of Permeability for Polyelectrolyte Microcapsules Embedded with Co@au Nanoparticles." *Langmuir,V 21(5), p2042-2050.*

[Lvov 2001] Lvov, Y.; F. Caruso. "Biocolloids with Ordered Urease Multiayer Shells as Enzymatic Reactors." *Analytical Chemistry 73, p4212-4217.*

[Lvov 1993] Lvov, Y.; G. Decher; H. Moehwald. Assembly, "Structural Characterization and Thermal Behavior of Layer-by-layer Deposited Ultrathin Films." *Langmuir 9,p481-486.*

[Lyon 2002] Lyon. 2002. 3rd World Congress on Emulsion.

[Ma 2005] Ma, X; W. Yu; W. Xie. "Method for Preparing Microcapsule Containing Immobilized Yeast Cells." *Faming zhuanli shenqing gongkai shuomingshu.*

[Manca 2003] Manca, D.; M. Rovaglio. "Modeling the Controlled Release of Microencapsulated Drugs: Theory and Experimental Validation." *Chemical Engineering Science, V58(7), p1337-1351.*

[Meister 1969] Meister, B. J.; Scheele, George F. "Prediction of jet length in immiscible liquid systems." *American Institute of Chemical Engineers Journal (1969) V15(5), 689-99.*

[Metzler 1999] Metzler, R., E. Barkai and J. Klafter. "Anomalous diffusion and relaxation close to thermal equilibrium: a fractional Fokker- Planck equation approach." *Physical Review Letters 82, p3563.*

[Metzler 2000] Metzler, R. and J. Klafter. "The random walk's guide to anomalous diffusion: a fractional dynamics approach." *Physical Report V339, p1.*

[McDonald 2000] McDonald, J. C.; Duffy, David C.; Anderson, Janelle R.; Chiu, Daniel T.; Wu, Hongkai; Schueller, Olivier J.A.; Whitesides, Geoge M. "Fabrication of Microfluidic Systems in Poly(dimethylsiloxane)." *Electrophoresis (2000),V 21(1), p27-40.*

[McShane 2005] McShane, M. J. "Biosensor Applications of Polyelectrolyte Nanofilms and Microcapsules." *American Chemical Society, V93, p214.*

[Ozisik 1993] Ozisik, M. N. "Heat Conduction." A Wiley-Interscience publication.

Reproduced with permission of the copyright owner. Further reproduction prohibited without permission.

[Orive 2006] Orive, G.; R. M. Hernandez; A. R. Gascon; J. L. Pedraz. "Encapsulation of Cells in Alginate Gels." *Methods in Biotechnology, 22(Immobilization of Enzymes and Cells(2nd Edition)), p345-355.*

[Pargaonkar 2005] Pargaonkar, N.; Y. Lvov; N. Li; J. H. Steenekamp; M. de Villiers. "Controlled release of dexamethasone from microcapsules produced by polyelectrolyte layer-by-layer nanoassembly." *Pharmaceutical Research, V22(5), p826-835.*

[Prevot 2003] Prevot, M.; Ana L. Cordeiro; Gleb B. Sukhorukov; Yuri Lvov; Ronald S. Besser; Helmuth Moehwald. "Design of a Microfluidic System to investigate the Mechanical Properties of Layer-by-layer Fabricated Capsules." *Macromolecular Materials and Engineering, V288(12), p915-918.*

[Prouty 2004] Prouty, M.; Z. Lu; Z. Guo; C. Kumar; Y. Lvov. "Permeability Changes in CoAu Embedded Polyelectrolyte Microcapsules Using an Alternating Magnetic Field." *American Chemical Society, D. C 69FWAQ*

[Polk 1994] Polk, A.E.; Amsden, Brian; Scarratt, David J.;Gonzal, Angelito; Okhamafe, Augustine O.; and Goosen, Mattheus F. A. "Oral Delivery in Aquaculture: Controlled Release of Proteins from Chitosanalginate Microcapsules." *Elsevier Applied Science V13 n4 p311-323.*

[Radtchenko 2000] Radtchenko, I. L.; Sukhorukov, Gleb B.; Leporatti, Stefano; Khomutov, Gennady B.; Donath, Edwin; Mohwald, Helmuth. "Assemblly of Alternated multivalent Ion/Polyelectrolyte Layers on Colloidal Particles. Stability of the Multilayers and Encapsulation of Macromolecules into Polyelectrolyte Capsules." *Journal of Colloid and Interface Science (2000), V230(2), p272-280.*

[Ragaza 1999] Ragaza A.R.;A. Q. Hurtado. "Seasonal Variations in Alginate Yield and Viscosity of Sargassum Carpophyllum." *J. Botanica Marina V42, 1999, p327-331*

[Ray 2005] Ray, A. K.; Z. Gao. "Generation of Tailored Microparticles by Photopolymerization of Monodisperse Droplets." *AlChE Annual Meeting, p2685.*

[Rilling 1997] Rilling, P.; T. Walter; R. Pommersheim; W. Vogt. "Encapsulation of cytochrome C by multilayer microcapsules." *Journal of Membrane Science, V129 n2 p 283-287.*

[Scalas 2004] Scalas, E., R. Gorenflo and F. Mainardi. "Uncoupled Continuous-time Random Walks:Solution and Llimiting Behaviour of the Master Equation." *Physical Review. E 69, 011107.*

[Schneider 1988] Schneider W. R. and W. Wyss. "Fractional Diffusion and Wave Equations." *Journal of Mathematical Physics V30, p134.*

Reproduced with permission of the copyright owner. Further reproduction prohibited without permission.

[Schroder 1998] Schroder, V.; Behrend, Olaf; Schubert, Helmar. "Effect of Dynamic Interfacial Tension on the Emulsification Process Using Microporous, Ceramic Membranes." *Journal of Colloid and Interface Science (1998), V 202(2), p334-340.*

[Setterstrom 1982] Setterstrom, J. A.; Tice, T. R.; Lewis, D. H. and Meyers, W. E. "Controlled Release of Antibiotics from Biodegradable Microcapsules for Wound Infection Control." *U.S. Army Institute of Dental Research. Conference June, 1982.*

[Shigemi 1994] Shigemi, K.; Yoshikawa, Rie. "Preparation of Controlled-release Microcapsules." *Japan Kokai Tokyo Koho (1994).*

[Skelland 1989] Skelland, A.H.P.; Walker, Perry G. "The Effects of Surface Active Agents on Jet Breakup in Liquid-liquid Systems." *Canadian Journal of Chemical Engineering (1989), V67(5), p762-770.*

[Stoltz 2004] Stoltz, J.H.; Huang, Q.; Jin, X.; Gaillard, E.T.; Knight, B.L.; Pack, F.D.; Jayadev, S.; Blanchard, K.T. "Gene Expression Profiling Reveals Multiple Toxicity Endpoints Induced by Hepatotoxicants." *Mutation Research 549, p147-167.*

[Sukhorukov 2000] Sukhorukov, G.B.; E. Donath, S. Moya, A.S. Susha, A. Voigt, J. Hatmann, H. Mohwald. "Microcapsulation by Means of Step-wise Adsorption of Polyelectrolytes." *Journal of Microencapsulation V17(2), p177-185.*

[Sun 2003] Sun, T.;M. L. Chan; Y. Zhou; X. Xu; J. Zhang; X. Lao; X. Wang; C. Quek; J. Chen; K. Leong; H. Yu. "Use of Ultrothin Shell Microcapsules of Hepatocytes in Bioartificial Liver-assist Device." *Tissue Engineering. 9, S65-S75.*

[Sun 2002] Sun, D; Y. Chen; J. Yang; J. Su; A. Sun. "Theoretical Calculation and Experimental Study of Membrane Thickness of Alginate-(poly-L-lysine)-alginate Microcapsules." *Shengwu Yixue Gongchengxue Zazhi. V19(4), p645-647.*

[Takagishi 1994] Takagishi, T.; Kono, K. "Release Control of Drugs from Microcapsules in Response to External Stimuli." *Microcapsulation in Space(1993), 80-3.*

[Takiguchi 2004] Takiguchi, H.; Nagano-ken. "Droplet Discharging Device and Manufacturing Method of Microcapsule." *Europe Patent 1,462,158*

[Tan 2004] Tan, Y.; Fisher, Jeffrey S.; Lee, Alan I.; Cristini, Vittorio; Lee, Abraham Phillip. "Design of Microfluidic Channel Geometries for the Control of Droplet Volume, Chemical Concentration, and Sorting." *Lab on a Chip (2004), V4(4), p292-298.*

[Thomas 1941] Thomas, J. W. (James William), "Numerical partial differential equations."

Reproduced with permission of the copyright owner. Further reproduction prohibited without permission.

[Tong 2006] Tong, W.; Haiqing Song; Changyou Gao; Helmuth Mohwald. "Equilibrium Distribution of Permeants in Polyeletrolyte Microcapsules Filled with Negatively Charged Polyelectrolyte: The Influence of Ionic Strength and Solvent Polarity." *Journal of Physical Chemistry, B C April, V110 (26), p12905 -12909.*

[Thorson 2001] Thorson, T.; Roberts, Richard W.; Arnold, Frances H.; Quake, Stephen R. "Dynamic Pattern Formation in a Vesicle-Generating Microfluidic Device." *Physical Review Letters (2001), V86(18), p4163-4166.*

[Thwar 2005] Thwar, P.; Burns, Mark A.; Linderman, Jennifer J. "On-chip Generation and Manipulation of Emulsion Droplets for Microfluidic Single Cell Assay Devices." *AIChE 2005 Annual Meeting and Fall Showcase, Oct 30-Nov 4, 2005.*

[Webster 2001] Webster, D. R.; Longmire, E. K. "Jet Pinch-off and Drop Formation in Immiscible Liquid-liquid systems." *Experiments in Fluids (2001), V30(1), 47-56.*

[Wheatley 1991] Wheatley. Coated alginate microspheres. "Factors Iinfluencing the Controlled Delivery of Macromolecules." *Journal of Applied Polymer Science, V43(11), p 2123-2135.*

[Windhab 2005] Windhab, E. "Method and Device for the Production of Storage Stable Multi-micro-capsules Comprising Adjustable Synergistically Active Functional Content Components." *International Patent Application, p52.*

[Windhab 2005] Windhab, E.; M. Zimmermann. "Storage Stable Multi-microcapsules Having Adjustable Synergistically Active Functional Content Components." *International Patent Application, p33.*

[Yamamoto 1996] Yamamoto, Y. ; M.V. Sefton. "Surface Grafting onto Vinyl Amine Copolymer: Approach for Double Layered Microcapsules." *Transactions of the Annual Meeting of the Society for Biomaterials in conjunction with the International Biomaterials Symposium. V1 p 638.*

[Yang 2005] Yang, Xiaoling; Han, Xiao; Zhu, Yihua. "(PAH/PSS) Microcapsules Templated on Silica Core: Encapsulation of Anticancer Drup DOX and Controlled Release Study." *Physicochemistry Engineering V264, n1-3, p49-54, ISSN 0927-7757*

[Yu 2006] Yu, W.; X. Liu; X. Li; W. Qi; D. Ren; X. Ma. "Effect of pH of Chitosan Solution on Properties of Sodium Alginate-chitosan Microcapsules with Cells." *Gaodeng Xuexiao Huaxue Xuebao/Chemical Journal of Chinese Universities, V 27, n1, p 182-186.*

[Zhao 2006] Zhao, W.; B. Zheng; D. T. Haynie. "A Molecular Dynamics Study of the Physical Basis of Stability of Polypeptide Multilayer Nanofilms." *American Chemical Society, V22(15), p6668-6675.*

Reproduced with permission of the copyright owner. Further reproduction prohibited without permission.